UNIVERSITÀ
DEGLI STUDI
FIRENZE

DOTTORATO DI RICERCA
INTERNATIONAL DOCTORATE IN STRUCTURAL BIOLOGY

CICLO XXXIV

COORDINATOR Prof. Lucia Banci

Protein expression and characterization for systems involved in the biogenesis of iron sulfur proteins

Settore Scientifico Disciplinare CHIM/03

PhD student
Dott. Giovanni Saudino

Tutor
Prof. Lucia Banci

Coordinator
Prof. Lucia Banci

November 2018 – October 2021

This thesis has been approved by the University of Florence, the University of Frankfurt and the Utrecht University

Universiteit Utrecht

Summary

Abstract

Iron-sulfur clusters are essential cofactors found in all kingdoms of life; they had unique functional roles throughout evolution. These clusters, which are the second major form of complex iron cofactors in biology, are ubiquitous in all organisms, playing a key role in several biological pathways. Mutations on the protein involved in the iron-sulfur clusters biosynthesis pathway are associated with a group of multiple mitochondrial dysfunction syndromes (MMDS). These severe diseases could give infantile encephalopathy, lactic acidosis, leukodystrophy and death in early childhood. In human cells, cluster biosynthesis involves three different types of machinery: ISC (iron-sulfur cluster assembly machinery) located in the mitochondria, CIA (cytosolic iron-sulfur cluster assembly machinery) located in the cytosol and ISC export machinery located in the mitochondria inner membrane. The aim of the thesis was the deep investigation of the third step of the ISC assembly machinery. Indeed, using NMR, UV-vis and CD-vis spectroscopies in combination with size exclusion chromatography and multi-angle light scattering we assessed the key role of NFU1, ISCA1, ISCA2, FDX2 and LIAS in the above-mentioned machinery. Moreover, clinical BOLA3 Cys59Tyr mutation involved in the MMDS diseases has investigated at the atomistic and molecular levels. The gained data elucidated fundamental molecular details in the [4Fe-4S] cluster maturation and transfer to apo recipient proteins along the third step of ISC assembly machinery.

1. Introduction

Metal ions are fundamental cofactors with different roles in the organisms forming coordination compounds with biomolecules. All living systems are dependent on metal-based chemistry for fundamental processes, thus suggesting the importance of metal ions on the evolution of life. Indeed, metals have been exploited in prebiotic chemistry and in the earliest phases of protocellular evolution[1]. During the first billion years of life on the Earth, the environment was anaerobic and iron and sulfur were abundant, and the organisms start to synthetize iron-sulfur clusters as protein cofactors[2]. Iron-sulfur clusters are essential cofactors found in all kingdoms of life and participate in a broad range of electron transfer, biosynthetic processes and important non-redox catalytic and regulatory functions[3]. These clusters, that are the second major form of complex iron cofactors in biology, are ubiquitous in all organisms, playing a key role in several biological pathways. The amount of available free iron ions in the cell is extremely controlled and maintained in low concentration[4]. Otherwise, the free metal ions presence could produce toxic reactive oxygen species. For this reason, all the organisms develop and evolve a large number of proteins that are able to coordinate a safe, powerful and specific biogenesis of the iron-sulfur cofactors[5].

1.1 Iron sulfur clusters structure and function

The composition of iron-sulfur metal sites is relatively simple[6]. They are made of iron atoms bonded with sulfide atoms creating three main forms of clusters (**Figure 1**)[7,8], which are the rhomboid [2Fe-2S] (**Figure 1B**) cluster, the cuboidal [3Fe-4S] cluster (**Figure 1C**), and the cubane [4Fe-4S] cluster (**Figure 1D**), all containing iron ions ($Fe^{2+/3+}$) and inorganic sulfide (S^{2-}), with cysteines generally completing tetrahedral S coordination at each Fe site. Occasionally, aspartate, histidine (e.g., Rieske proteins) or serine residues (lypoil synthase) can replace the thiolate group in the iron sulfur cluster coordination[9,10]. After S^{2-} is incorporated into the cluster, it does not undergo redox transitions, while, Fe^{3+} in the cluster may be reduced to Fe^{2+} and vice versa. In this way, the iron sulfur clusters achieve the ability to accept or donate single electrons to carry out complex enzymatic reactions[11]. These clusters have thus versatile electrochemical properties with

reduction potentials ranging from over 400 mV to below –400 mV[12]. A [2Fe-2S] cluster bound to the proteins can be present in two oxidation states $[2Fe\text{-}2S]^{2+}$ and $[2Fe\text{-}2S]^{+}$. On the contrary, a [4Fe-4S] cluster can exist in three oxidation states, i.e. $[4Fe\text{-}4S]^{3+}$, $[4Fe\text{-}4S]^{2+}$, $[4Fe\text{-}4S]^{+}$ [13]. A [3Fe-4S] cluster is available in two oxidation states; for the $[3Fe\text{-}4S]^{+}$ redox state, all the three iron ions are in 3+ oxidation state[14].

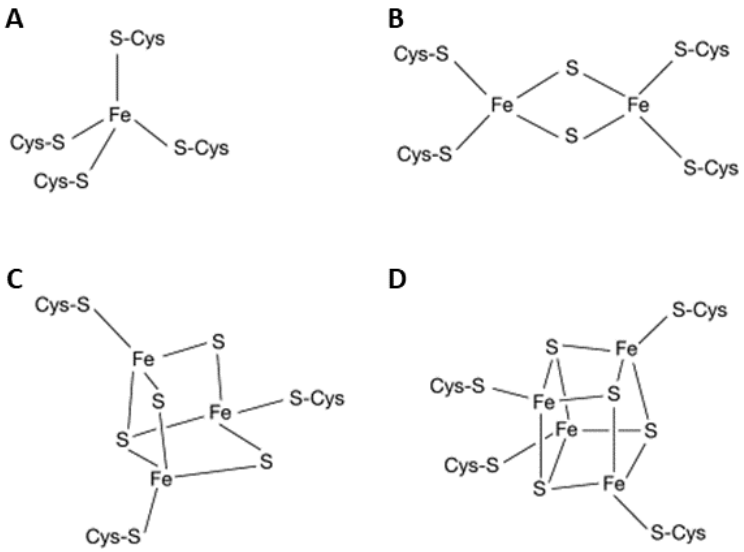

Figure 1. Schematic representation of iron sulfur cluster geometry bound to cysteines residues: **A**)Fe^{3+}; **B**) [2Fe-2S] cluster; **C**) [3Fe-3S] cluster; **D**) [4Fe-4S] cluster.

Iron-sulfur clusters are found in a wide variety of metalloproteins, such as the ferredoxins, NADH dehydrogenase, hydrogenases, coenzyme Q-cytochrome c reductase, succinate-coenzyme Q reductase and nitrogenase. These iron sulfur proteins are involved in several cellular processes, such as cellular respiration, photosynthesis, radical chain reactions, DNA synthesis and repair for genome maintenance, protein translation, RNA modifications, and antiviral defense strategies[3,15,16]. Furthermore, iron sulfur clusters can operate as a sulfur donor for other sulfur-containing protein cofactors such as biotin and lipoic acid[17,18]. Finally, iron sulfur clusters may help stabilizing protein domains, thereby regulating the dynamic interaction with other proteins as proposed for nuclear DNA polymerases[19]. Concluding, it is totally evident that biosynthesis of iron sulfur clusters is fundamental for the proper functioning of the human cells.

1.2 Mitochondrial ISC assembly machinery

In eukaryotic cells, the iron sulfur cluster biosynthesis involves three different machineries: ISC (iron-sulfur cluster) assembly machinery located in the mitochondria (**Figure 2**), CIA (cytosolic iron-sulfur cluster) assembly machinery that generates cytosolic and nuclear iron sulfur cluster protein located in the cytosol[5] and ISC export machinery based on a protein transporter placed in the mitochondrial inner membrane, which has been shown to have a key role for the maturation of the cytosolic and nuclear proteins[20]. The mitochondrial ISC assembly machinery is highly conserved in all eukaryotes, which during evolution was inherited from bacteria by endosymbiosis, and it is the crucial cellular component required for the maturation of mitochondrial and cytosolic/nuclear iron sulfur cluster proteins[2122]. The ISC machinery is the starting point for the *de novo* iron sulfur cluster assembly in all cellular compartments; in humans, it involves 17 different proteins, but the way in which they cooperate is still not well understood. This machinery can be divided into three fundamental steps (**Figure 2**):

- 1st step: A [2Fe-2S] cluster is assembled on the ISCU2 scaffold protein via a large protein complex formed by NFS1, ISD11, FXN, ACP and FDX2[23]. Fe^{2+} ions are imported in the mitochondrial matrix by the intermembrane transporters mitoferrin-1 and mitoferrin-2 making available free iron source[24]. The sulfide ions are provided by the conversion of two cysteines in alanine by the subcomplex composed by NFS1, ISD11 and ACP proteins[25].

- 2nd step: [2Fe-2S] cluster is released from ISCU2 to specific proteins. Two different processes could occur: ISCU2 transfers directly the [2Fe-2S] cluster to GLRX5 or directly inserts it into the target enzymes[26]. These processes are assisted by the HSPA9 chaperone and Hsc20 co-chaperone required for the safe trafficking of the [2Fe-2S] cluster from ISCU2 to the targeting proteins. Then, GLRX5 is able to maturate apo targeting proteins that demanded [2Fe-2S] cofactors[27,28] and it is also essential for the distribution of [2Fe-2S] cluster to the proteins involved in the final step of the ISC assembly machinery for the maturation of [4Fe-4S] target[29].

- 3rd step: ISCA1, ISCA2 and IBA57 are involved in the [4Fe-4S] cluster formation and trafficking. In this step, GLRX5 donates two [2Fe-2S] clusters to the ISCA1-ISCA2

complex that performs the reductive coupling of two [2Fe-2S] clusters to assembles a [4Fe-4S] cluster[29,30] using two electrons given by the reduced form of FDX2. The molecular role of IBA57 in the [4Fe-4S] cluster synthesis is still ambiguous, although *in vivo* data suggest that IBA57 is strictly required for the synthesis[30,31]. Finally, the assembled [4Fe-4S] cluster is released to NFU1 that is needed for cluster insertion into some targeting mitochondrial proteins[32,33]. How the [4Fe-4S] cluster is transferred to these apo targeting proteins is still not defined.

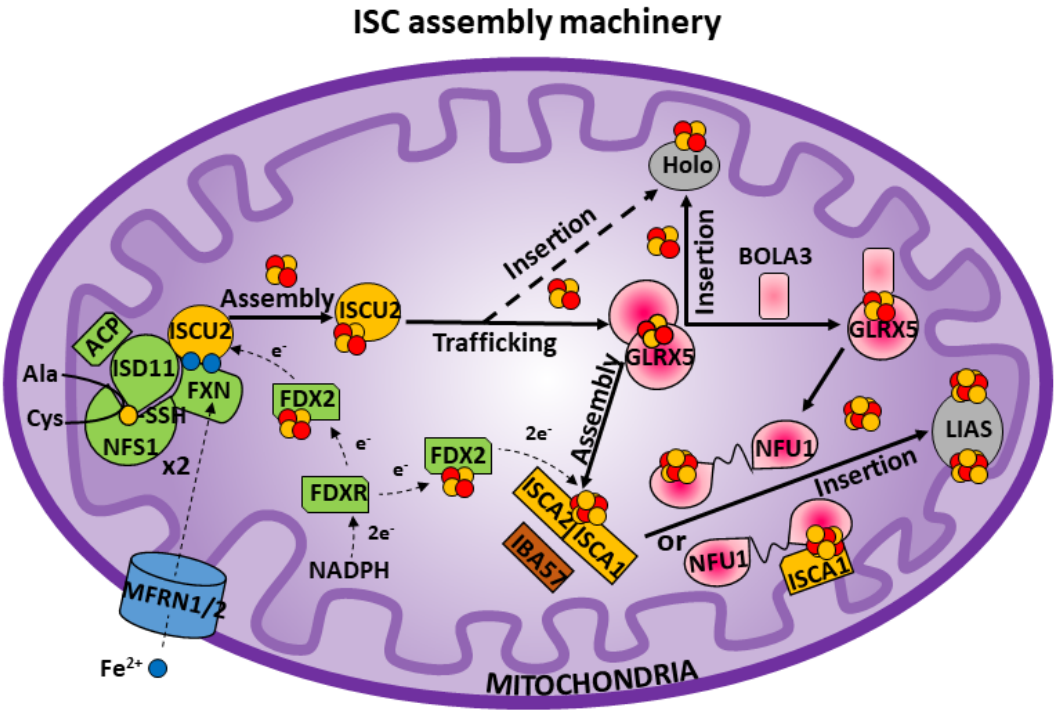

Figure 2. A model of the iron sulfur cluster assembly machinery required for the *de novo* synthesis of [4Fe-4S] and [2Fe-2S] clusters.

A parallel and secondary pathway where BOLA3 complexed with GLRX5 can act in [2Fe-2S] cluster trafficking and/or insertion process was also suggested[34]. This hetero complex in its [2Fe-2S] bound state was shown to be able to transfer the cluster to both apo FDX1 and FDX2 [35,36], as well as to apo NFU1 that assembles a [4Fe-4S] cluster acting as a dimer[37]. The maturation pathway

of mitochondrial targeting proteins dependent by BOLA3-GLRX5 hetero complex is also supported by *in vivo* studies that demonstrate the physiological role of the BOLA3 as a late actor of the ISC assembly machinery[38,39].

1.3 The actors of the late step of the ISC assembly machinery

The third and final step of the ISC assembly machinery, which consists on the mechanisms that lead to the [4Fe-4S] cluster synthesis, trafficking and insertion into apo recipient proteins, is poorly understood and explored. The main protagonists of the late step of the ISC assembly machinery are well established and are ISCA1, ISCA2, IBA57, FDX2, BOLA3 and NFU1 (**Figure 3**). According to their role in [4Fe-4S] protein maturation, mutations on these proteins cause a severe malfunction on the [4Fe-4S] requiring mitochondrial enzymes. In this scenario, ISCA1(**Figure 3A**) and ISCA2 are proteins highly conserved from bacteria to eukaryotic cells and are essential for [4Fe-4S] cluster biosynthesis[27,40,41]. Specifically, ISCA1 and ISCA2 are two highly homologous members of the A-type protein family that are characterized by three highly conserved cysteine residues organized in a C-X_n-C-G-C sequence motif[42]. *In vivo* studies, performed in *S. cerevisiae* on the Isa1 and Isa2 (yeast homologues of human ISCA1 and ISCA2), provide strong evidence of the crucial role in the iron metabolism of these two proteins, specifically on the [4Fe-4S] cluster biosynthesis[40]. Depletion of the Isa1 and Isa2 genes reduce the aconitase and succinate dehydrogenase activities and their [4Fe-4S] cluster content. Further data have demonstrated that the maturation of [2Fe-2S] proteins was unaffected in the absence of the Isa proteins, although that of proteins containing [4Fe-4S] clusters was dependent on their function[43]. In human cells, knockdown of ISCA1 and ISCA2 genes impair the maturation of several mitochondrial [4Fe-4S] cluster proteins, like complexes I and II of the respiratory chain and aconitase[44]. Brancaccio et al. through NMR experiments demonstrated that the two ISCAs proteins are able to synthetize a [4Fe-4S] starting from two [2Fe-2S] clusters given by GLRX5[27,32]. Summarizing, these data definitively prove the ISCA1 and ISCA2 function in the late step of the ISC assembly machinery assembling a [4Fe-4S] cluster.

Although, the ISCA1 and ISCA2 role in the [4Fe-4S] cluster assembly is quite defined, the mechanism underlying the conversion of [2Fe-2S] into [4Fe-4S] clusters is poorly define. In this

step of the ISC assembly machinery, an electron donor is necessary in order to synthetize the [4Fe-4S] cluster starting from two [2Fe-2S] clusters. Recently, it was discovered that the protein involved in the electron transfer necessary for this process is FDX2 (**Figure 3B**)[30,45]. Ferredoxins are small iron-sulfur proteins that use the redox properties of their [2Fe-2S] or [4Fe-4S] cofactors in order to transfer electrons in a wide variety of biochemical reactions. Human mitochondria possess two ferredoxins, FDX1 and FDX2 both containing a [2Fe-2S] cluster[46]. FDX1 is recognized as a versatile electron donator involved in several reactions such as steroid hormone biosynthesis and vitamin D metabolism[47]. It is already known that in the first step of the ISC machinery, FDX2 is a more efficient reductant compared with FDX1; indeed the latter is overexpressed only in specific tissues. It was proposed that FDX2 gives the electrons required to reduce two [2Fe-2S] clusters to form a [4Fe-4S] cluster. The mechanism as well as the essential role of IBA57 in this process are still unclear and further studies are considered necessary.

After the [4Fe-4S] cluster formation, NFU1(**Figure 3C**), the final striker of the third step of the ISC assembly machinery, is required[32,33]. There are two different NFU1 isoforms expressed by human cells with distinct subcellular localizations, the one involved in ISC assembly machinery is isoform I that loose the first 58 N-terminal residues after the mitochondrial internalization. *S. cerevisiae* lacking Nfu1 are partially deficient in the [4Fe-4S] enzymes aconitase, succinate dehydrogenase and lipoic acid synthase. Nfu1 depleted cells do not show any defects in enzymes dependent on [2Fe-2S] clusters, suggesting that Nfu1 acts only in the [4Fe-4S] cluster transfer pathway[38]. The human NFU1 is involved in the maturation of apo targeting proteins preferring respiratory complexes I and II, and lipoyl synthase[17]. A recent structural characterization of human NFU1 displayed that the apo protein is monomeric in solution and adopts a dumbbell-shaped structure with well-structured N and C-domains connected by a highly flexible linker[38,48]. SAXS analysis coupled with NMR analysis define that [4Fe-4S] NFU1 consists of a trimer of dimers, where the cluster is bridged by the cysteine residues of the C-terminal domains of two apo-NFU1 subunits forming a dimer, while the N-terminal domains of three of these dimers form a trimeric conformation[48]. However, it was demonstrated that [4Fe-4S] NFU1 physiologically acts as a dimer bridged by the [4Fe-4S] cluster bound with the highly conserved cysteines of two C-terminal domains[38,49]. From functional point of view, it is described that NFU1 can act in different manner activating different pathways modulated by the [4Fe-4S] clusters cellular request. First, NFU1 can receives the cluster by the ISCA1-ISCA2 heterocomplex as it is already described for bacteria and

yeasts[40,44], acting in dimeric state as a maturation agent for some apo targeting proteins. Additionally, on the basis of genetic and biochemical techniques it has been proposed that the assembly of a [4Fe-4S] cluster on NFU1 requires the coordinate action of three proteins, which are ISCU2, ISCA1 and FDX2[49]. Specifically, the [2Fe-2S] cluster bound forms of ISCA1 and ISCU2 interact and donate their cluster to dimeric NFU1, which then reductively couple into a [4Fe-4S] cluster upon the delivery of two electrons by FDX2. This mechanism is supported by the interactions observed *in vivo* between NFU1 and ISCU2, between NFU1 and ISCA1, between NFU1 and FDX2 and between two NFU1 molecules[49], as well as by *in vitro* NMR and SAXS studies that showed NFU1 and ISCU2 form a complex in which the cluster binding region of ISCU2 interacts with the C-domain of NFU1[50]. This postulated [4Fe-4S] cluster assembly mechanism bypasses the ISCA1-ISCA2 complex, thus not explaining the role of ISCA2 in the ISC assembly machinery. Finally, another possible pathway involves the [2Fe-2S] GLRX5-BOLA3 complex that is able to promote the assembly of a [4Fe-4S] cluster on dimeric NFU1, again with no requirement of the ISCA1-ISCA2 complex[37]. This alternative pathway have been proposed to be activated exclusively under cellular oxidative conditions[37]. These different postulated models depict the NFU1 function in the [4Fe-4S] cluster assembly and trafficking even if the physiological preferred pathway is still ambiguous. Finally, in the third step of the ISC assembly machinery NFU1, alone or complexed, is required for the cluster transfer to the apo targeting proteins. This mechanism is still not well defined and it demands characterization. Lipoyl synthase (LIAS hereafter) (**Figure 4D**) is one of the most important [4Fe-4S] cluster recipient apo proteins. It is a member of the radical S-(5'-Adenosyl)-L-Methionine (SAM) superfamily of enzymes that uses two [4Fe-4S] clusters to catalyse the final step of the biosynthesis of the lipoyl cofactor [51]. LIAS attaches two sulfhydryl groups to C6 and C8 of an octanoyl chain[51]. The appended sulfur atoms derive from an auxiliary [4Fe–4S] cluster that is degraded during the enzymatic turnover, and this degraded cluster is called auxiliary cluster (FeS_{aux} hereafter)[52,53]. The second [4Fe-4S] clusters (FeS_{RS} hereafter) performs a reductive cleavage of a SAM molecule to obtain methionine and a 5'-deoxyadenosyl radical (5-dA•) that is necessary to generate a radical on the octanoyl chain[18]. The FeS_{RS} cluster is bound to a CX_3CX_2C motif, i.e. three iron ions are covalently bound to three Cys residues of the motif (Cys 137,Cys 141 and Cys 144 in LIAS) and the fourth iron ion, termed as catalytic iron ion, is exposed to the SAM binding. The FeS_{aux} cluster is bound through a

conserved CX_4CX_5C motif (Cys 106, Cys 111 and Cys 117 in LIAS) and a serine (Ser 345 in LIAS)[51,54].

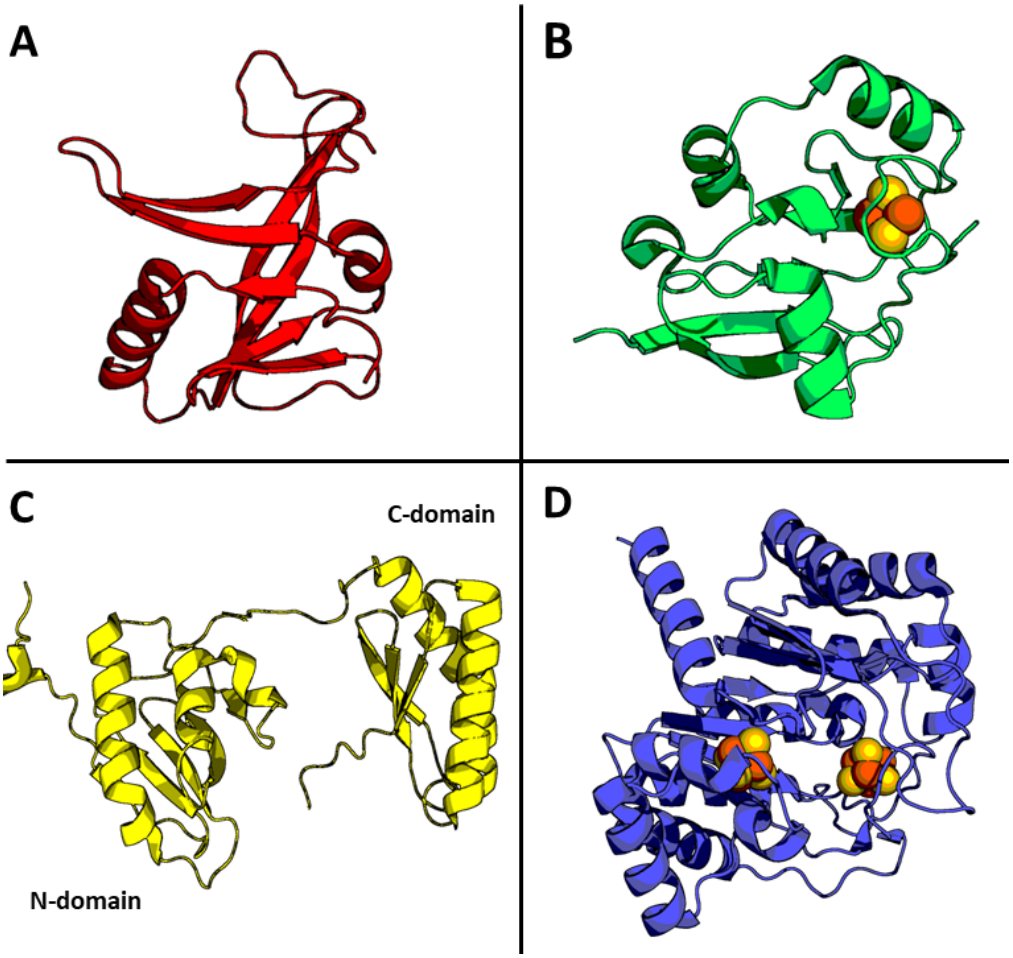

Figure 3 Structures of the proteins involved in the ISC assembly machinery that were mainly studied in the thesis. **A**) apo ISCA1 structure generated by Alphafold software **B**) $[2Fe\text{-}2S]^{2+}$FDX2 structure derived from X-ray diffraction data **C**) apo NFU1 structure derived by in solution NMR data on each isolated domains **D**) M. tuberculosis lipoyl synthase structure derived by X-ray diffraction data.

Recently, it was shown that the iron sulfur cluster carrier protein NfuA from *E. coli* regenerates the auxiliary cluster of *E. coli* lipoyl synthase (LipA) after each turnover. In this way, LipA acts catalytically upon the continuous supply of [4Fe-4S] clusters by NfuA[17]. The latter is the *E. coli* homologous of the human NFU1 that is the late acting protein of the human mitochondrial ISC assembly machinery. While the biosynthetic mechanism of the lipoic acid by lipoyl synthase was

deeply investigated in the recent years, the LIAS maturation process is poorly studied and demand characterization.

In conclusion, elucidating the molecular events leading to the [4Fe-4S] cluster synthesis, trafficking and delivery to apo recipient mitochondrial proteins is fundamental in order to fully characterized the third step of the ISC assembly machinery.

1.4 MMDS: diseases related to the dysfunction of the late steps of the mitochondrial ISC assembly machinery

Due to the essential role of iron sulfur cluster proteins in the human cells, their mutations are related with an increasingly number of rare and severe human diseases (**Table 1**). Iron sulfur clusters, as described in the paragraph 1.2, are involved in uncounted fundamental cellular mechanisms like DNA metabolism, electron transport chain and lipoic acid maturation. Recently, it was discovered that the DNA binding affinity of DNA processing enzymes are modulated by the redox process of a [4Fe-4S] cluster[55]. Iron sulfur cluster enzymes are also required for the DNA translation and repair systems, indeed malfunction related to these proteins cause genome instability and high cancer propension[56]. However, rare neurodegenerative diseases are the most related to iron sulfur cluster protein mutations. In this scenario, the most common inherited iron-related disorder is Friedreich's ataxia, caused by a triplet expansion in intron 1 of the frataxin gene[57,58]. Frataxin deficiency is characterised by accumulation of iron in the mitochondrial matrix causing progressive degeneration of the nervous system leading to ataxia and compromises the heart conditions[59]. Besides, some kind of myopathy (disease of the muscle in which the muscle fibres do not function properly resulting in muscular weakness) are related to mutation on the IscU and FDX2 genes. ISCU myopathy is characterized by severe exercise intolerance, tachycardia, and pain in active muscles due to decreased mitochondrial iron sulfur clusters enzyme activities. This myopathy disease is caused by homozygous splice mutation in intron 4 of the IscU gene resulting in decreased ISCU2 levels. Furthermore, FDX2 related myopathy is associated to a mutation that abolish the ATG initiation codon, resulting in low expression levels of FXD2, and decreased activities of respiratory complexes I–III and mitochondrial aconitase[60,61]. Symptoms are similar but less severe respect to the ISCU myopathy.

Proteins	Affected steps	Diseases	Mutations
NFS1	[2Fe-2S] assembles	Infantile complex II/III deficiency	Missense mutation c.251G>A, p.Arg72Gln
Frataxin	[2Fe-2S] assembles	Friedreich' ataxia	FXN gene suppression, due to expansion of the intronic GAA repeat
FDX2	Fe-S biogenesis electron donor	Mitochondrial muscle myopathy	Homozygous mutation c.1A>T
GLRX5	[2Fe-2S] cluster carrier	Sideroblastic anemia	Non correct splicing
ISCU2	[2Fe-2S] assembles	ISCU myopathy	Missense mutation c.149G>A, p.G50E
BOLA3	[2Fe-2S] cluster and [4Fe-4S] cluster delivery	MMDS2	Homozygous missense mutation c.200T>A in exon 3, p.167N
NFU1	[4Fe-4S] cluster delivery	MMDS1	Homozygosity for c.622G>T (p.Gly208Cys), or compound heterozygosity for c.622G>T
ISCA1	[4Fe-4S] cluster assembles	MMDS5	homozygous missense mutation c.29T>G p.V10G
ISCA2	[4Fe-4S] cluster assembles	MMDS4	Homozygous missense mutation c.229G>A, c.334A>G
IBA57	[4Fe-4S] cluster assembles	MMDS3	Homozygous mutation c.941A>C, p.Gln314Pro
Mitoferrin 1	Mitochondrial iron importer	Variant erythropoietic protoporphyria	Aberrant splicing of MFRN1 transcript

Table 1: Human diseases related to iron sulfur cluster proteins mutations.

The iron sulfur cluster proteins related to human diseases that are more linked with this thesis work are the multiple mitochondrial dysfunction syndromes, named MMDS. These diseases are severe syndromes including mainly malfunctions on the different subunits of the electron transport chain. They are typically characterized by infantile encephalopathy, lactic acidosis, leukodystrophy and leads to death in their first year of life [62,63]. Clinical and biochemical investigations on patients revealed that these symptoms are related to single point mutations on NFU1, BOLA3, IBA57, ISCA1 or ISCA2 genes. These mutations are characterized by deficiency of respiratory complex I and III, pyruvate dehydrogenase (PDH), a-ketogluterate dehydrogenase (KGDH), and lipoate synthase[62,64,65] that are all proteins that need [4Fe-4S] cluster for their function. Typically, symptoms associated to these neurodegenerative MMDS disease are brain dysfunction, seizures, hypotonia, delayed development of mental and movement abilities, difficulties in growing a gaining normal and expected weight and lactic acidosis. Each different MMDS, associated with mutations on different ISC assembly machinery genes, present some or all symptoms described above leading always in a dramatic clinical picture. By elucidating these very severe syndromes, it resulted clear that the study focused on the ISC assembly machinery is required. Analysing and elucidating the steps and the molecular interactions of the ISC assembly machinery might be fundamental to deeply understand the mutation phenotypes. In this way, it might be possible to rationalize new genetic or pharmacological approach for these severe syndromes.

1.4.1 MMDS2: BOLA3 mutations related diseases

BOLA3 is a member of the BolA-like protein family that is highly conserved from prokaryotes to eukaryotes. Recently, it has been suggested that BOLA-type proteins are important partners of monothiol glutaredoxins[66]. In human cells there are three different BOLA proteins: mitochondrial BOLA1 and BOLA3, and the cytosolic BOLA2. BOLA3 is involved in the third step of the ISC assembly machinery being able to bridge a [2Fe-2S] cluster with GLRX5 forming an hetero complex[37]. An *in vitro* study showed that BOLA3 helps GLRX5 in the delivery of two [2Fe-2S] clusters to NFU1 in order to assemble a [4Fe-4S] cluster on NFU1[37]. These results are supported by biochemical analysis performed on yeasts cells where BOLA3 knockdown cause a strong defect in lipoyl synthase (LIAS) assembly and protein lipoylation as well as a weak defect in SDH

activity[67]. Similarly, NFU1 is involved in the lipoic acid maturation pathway[17,67]. All these data suggest an important BOLA3 role in the iron sulfur clusters delivery and assembly[37,38,64]. Due to the important role of BOLA3 in the maturation of mitochondrial [4Fe-4S] proteins, variants in BOLA3 cause MMDS type 2 characterized by infantile encephalopathy, leukodystrophy, lactic acidosis, non-ketotic hyperglycinemia and death in early childhood[64,67,68] . A single base-pair duplication c.123dupA was identified in BOLA3, causing a frame shift that produces a premature stop codon (p.Glu42Argfs∗13) leading to combined deficiency of the 2-oxoacid dehydrogenases, associated with a defect in lipoate synthesis and in complexes I, II, and III of the mitochondrial respiratory chain[64]. Additionally, nonketotic hyperglycinemia, a disorder of glycine metabolism defined by deficient enzyme activity of the glycine cleavage enzyme system, is associated with homozygous c.136C>T(p.R46X) mutation on the BOLA3 gene that leads to truncating and inactive protein[64,67]. Lately, a novel phenotype for MMDS2 with complete clinical recovery and partial resolution of magnetic resonance imaging abnormality was observed in a patient[69]. Whole genome sequencing identified compound heterozygous variants in BOLA3: one previously reported (c.136C > T, p.Arg46* [64,67]) and one novel variant (c.176G > A, p.Cys59Tyr). These heterozygous variants determine a much milder phenotype with respect to homozygous c.136C > T (p.Arg46*) variants reported by Baker et al. in three unrelated patients[67]. The unique discrepancy is the different life span: while the phenotypes at 18 months are equivalent, the grown patient with the heterozygous variants (after 8 years old) regained normal neurological and cognitive function.

1.6 Aim of the thesis

My PhD thesis was focused on the investigation of the molecular mechanisms responsible of the assembly of some mitochondrial [4Fe-4S] cluster proteins. In mitochondria, a machinery composed by at least 17 proteins is responsible of the latter process, which occurs along three major steps. The third step of this machinery is the topic of my thesis; it involves the formation of a [4Fe-4S] cluster starting from [2Fe-2S] clusters and their subsequent insertion into recipient apo proteins. Although all the proteins involved in this last step have been identified, the mechanisms through which these processes occur are not yet elucidated, and thus a complete and detailed molecular picture of the third step of the machinery is needed. This characterization is also essential as several mitochondrial diseases (called Multiple Mitochondrial Dysfunctions Syndrome, MMDS) are associated to the proteins involved in this step. These are: NFU1, ISCA1, ISCA2, IBA57, FDX2, GLRX5 and BOLA3. Previous studies reported that: (i) GLRX5, the [2Fe-2S] metallochaperone of the mitochondrial matrix, donates two [2Fe-2S] clusters to the ISCA1-ISCA2 complex[29]; (ii) Ferredoxin-2 (FDX2) supplies the two electrons required for the reductive coupling of two [2Fe-2S] clusters to form a [4Fe-4S] cluster[30]; iii) IBA57 is required in the latter process, although its role is not clear yet[2]; (iii) NFU1 is required for the cluster delivery to the apo recipient proteins, such as the respiratory complexes I and II and lipoyl synthase (LIAS)[17]. *In vitro* studies described also a parallel pathway where BOLA3, forming an hetero complex with GLRX5, transfers two [2Fe-2S] clusters to NFU1 in order to assembles a [4Fe-4S] cluster bypassing the ISCAs dependent pathway[37]. Initially, my work was focused on the *in vitro* structural and functional characterization of the [4Fe-4S] cluster assembly and transfer involving NFU1, ISCA1 and ISCA2. The current prevailing model, largely based on studies in *S. cerevisiae*, proposes that NFU1 receives a [4Fe-4S] cluster assembled on the ISCAs proteins system and then transfers it to selected apo target proteins with the assistance of BOLA3[38]. In this scenario, a ISCA1, ISCA2 and NFU1 structural and functional characterization, performed exploiting NMR and SEC chromatography techniques, can clarify the steps leading to the formation and transfer of the [4Fe-4S] cluster. The collected data define a detailed molecular model of the succession of events performed in a coordinated manner by ISCA1, ISCA2 and NFU1 to make available [4Fe-4S] clusters for mitochondrial apo recipient proteins. This interaction was also investigated by SAXS, thus obtaining structural models of the different identified hetero-complexes. The molecular

mechanism of lipoyl synthase (LIAS) maturation was also studied, through diamagnetic/paramagnetic NMR and SEC-MALS analysis, thus understanding the molecular steps that lead to the production of mature LIAS. The LIAS and NFU1 interaction pattern were defined at atomic level and the functional role of the newly identified [4Fe-4S] NFU1-ISCA1 hetero-complex in the LIAS maturation understood. The role of FDX2 in the reductive coupling of two [2Fe-2S] clusters to form a [4Fe-4S] cluster was also investigated. Very recently, it was indeed discovered that the protein involved in the electron transfer necessary for the [4Fe-4S] cluster assembly is FDX2 that is able to donate electrons through the oxidation of the [2Fe-2S] cluster bound on the protein[30,45]. The data obtained up to now by us showed that the isolated ISCA1 and ISCA2 proteins do not interact with FDX2, suggesting that the electron transfer process requires IBA57 and/or the formation of the ISCA1-ISCA2 heterocomplex. Finally, a heterozygous variant of BOLA3 gene (c.176G>A, p.Cys59Tyr) was characterized. This mutation is associated with a novel phenotype of MMDS type 2[69]. The tyrosine substitution affects an highly conserved amino acid, the Cys59 residue that has been identified as a ligand of the [2Fe-2S] cluster bound in the BOLA3-GLRX5 complex[34]. Our data indicated that the mutation does not modify the overall structure of BOLA3, it structurally perturbs the iron-sulfur cluster binding region but without abolishing $[2Fe\text{-}2S]^{2+}$ cluster-binding on the hetero-complex, and it promotes the formation of an aberrant apo C59Y BOLA3-GLRX5 complex structurally different from that formed by the wild-type proteins. Overall my PhD studied contributed to characterize at a molecular level the mitochondrial [4Fe-4S] cluster assembling and transfer providing detailed molecular snapshots able to elucidate how the third step of the mitochondrial machinery works.

2. Results

2.1 ISCA1 orchestrates ISCA2 and NFU1 in the maturation of mitochondrial [4Fe-4S] proteins

Dafne Suraci [1,2,†], **Giovanni Saudino** [1,2,†], Veronica Nasta[1,2], Simone Ciofi-Baffoni[1,2,*] Lucia Banci [1,2*]

[1]Magnetic Resonance Center CERM, University of Florence, Via Luigi Sacconi 6, 50019, Sesto Fiorentino, Florence, Italy.

[2]Department of Chemistry, University of Florence, Via della Lastruccia 3, 50019 Sesto Fiorentino, Florence, Italy.

[†]Equally contributed authors.

Published: 10.1016/j.jmb.2021.166924

Abstract

The third step of the ISC assembly machinery is still under investigation because, even if the involved proteins have been identified, the different molecular interactions in the pathway still need to be elucidated. This third step requires: (a) GLRX5, the [2Fe-2S] metallochaperone that gives two $[2Fe\text{-}2S]^{2+}$ clusters to the ISCA1-ISCA2 complex[27]; (b) FDX2, which supplies the two electrons required for the reductive coupling of two $[2Fe\text{-}2S]^{2+}$ clusters to form a $[4Fe\text{-}4S]^{2+}$ cluster[30,70]; (c) NFU1, that is necessary for the cluster transfer to the apo targeting proteins. Previous studies established that ISCA2 and NFU1 are the ISCA1 partners in the third step of the ISC pathway[33]. Within this perspective, this work aimed at elucidating the ISCA1, ISCA2 and NFU1 role in the process of [4Fe-4S] cluster formation, through their structural and functional characterization via NMR and SEC chromatography experiments,. The data showed that ISCA1 is complexed with NFU1 or ISCA2 or with both, although the preferential arrangement is not clear. The results of the apo proteins interaction experiments suggested that the interacting surface on ISCA1 could be the same in the formation of either complexes. Consequently, that surface is no longer accessible for further protein-protein recognition, and ISCA1 is redistributed to form a complex with both proteins separately. These data support a model in which two parallel cluster transfer pathways are operative: the first involves the ISCA1-ISCA2 complex, which is responsible for assembling a [4Fe-4S] cluster targeted to several mitochondrial iron sulfur cluster proteins, while the second involves NFU1-ISCA1 complex, which is responsible for assembling a [4Fe-4S] cluster targeted to a subset of mitochondrial iron sulfur cluster proteins. On the other hand, the NMR experiments on the holo-complexes lead to a different interpretation. In fact, by titrating ^{15}N apo NFU1 with [4Fe-4S] ISCA1-^{15}N ISCA2, it resulted that the final ^{1}H-^{15}N HSQC map of the mixture is essentially superimposable to ^{1}H-^{15}N HSQC map of the apo ^{15}N apo NFU1, apo ISCA1-^{15}N ISCA2 mixture, indicating that the final interaction network is highly similar. However, the ^{1}H 1D paramagnetic spectra acquired on the [4F-4S] NFU1- ISCA1-^{15}N ISCA2 mixture showed that the cluster is shifted from ISCA1-ISCA2 hetero-complex to ISCA1-NFU1 hetero-complex, suggesting that the cysteines of ISCA1 and NFU1 together bind the cluster even though ISCA2 still interacts with ISCA1 forming a trimeric complex. ISCA1 is the key player of the [4Fe-4S] protein maturation process being able indeed to both individually and collectively interact with ISCA2 and NFU1. We can propose a model of the ISC assembly machinery late step where:

- The [4Fe-4S] cluster is assembled on the ISCA1-ISCA2 heterodimer by reductively coupling two [2Fe-2S] clusters donated by GLRX5[27].
- [4Fe-4S] ISCA1-ISCA2 complex can transfer the cluster to client proteins independently from NFU1.
- ISCA1, by its specific recognition with NFU1, mediates the [4Fe-4S] cluster shift from ISCA1-ISCA2 to ISCA1-NFU1 forming ternary ISCA1-ISCA2-NFU1 complex;
- The formed [4Fe-4S] ISCA1-NFU1 complex can then specifically direct the [4Fe-4S] cluster to mitochondrial client proteins.

ISCA1 resulted to be the crucial protein activating all [4Fe-4S] protein maturation pathways, i.e. ISCAs-dependent and [4Fe-4S] NFU1-dependent ones, satisfying the *in vivo* studies reported in the literature.

Research Article

ISCA1 Orchestrates ISCA2 and NFU1 in the Maturation of Human Mitochondrial [4Fe-4S] Proteins

Dafne Suraci † **Giovanni Saudino** † **Veronica Nasta, Simone Ciofi-Baffoni** * **and Lucia Banci** *

Magnetic Resonance Center CERM, *University of Florence, Via Luigi Sacconi 6, 50019 Sesto Fiorentino, Florence, Italy*
Department of Chemistry, *University of Florence, Via della Lastruccia 3, 50019 Sesto Fiorentino, Florence, Italy*

Correspondence to Simone Ciofi-Baffoni and Lucia Banci: Magnetic Resonance Center CERM, University of Florence, Via Luigi Sacconi 6, 50019 Sesto Fiorentino, Florence, Italy. Fax: +39 055 4574923. *ciofi@cerm.unifi.it (S. Ciofi-Baffoni), banci@cerm.unifi.it (L. Banci)*
https://doi.org/10.1016/j.jmb.2021.166924
Edited by M. Guss

Abstract

The late-acting steps of the pathway responsible for the maturation of mitochondrial [4Fe-4S] proteins are still elusive. Three proteins ISCA1, ISCA2 and NFU1 were shown to be implicated in the assembly of [4Fe-4S] clusters and their transfer into mitochondrial apo proteins. We present here a NMR-based study showing a detailed molecular model of the succession of events performed in a coordinated manner by ISCA1, ISCA2 and NFU1 to make [4Fe-4S] clusters available to mitochondrial apo proteins. We show that ISCA1 is the key player of the [4Fe-4S] protein maturation process because of its ability to interact with both NFU1 and ISCA2, which, instead do not interact each other. ISCA1 works as the promoter of the interaction between ISCA2 and NFU1 being able to determine the formation of a transient ISCA1-ISCA2-NFU1 ternary complex. We also show that ISCA1, thanks to its specific interaction with the C-terminal cluster-binding domain of NFU1, drives [4Fe-4S] cluster transfer from the site where the cluster is assembled on the ISCA1-ISCA2 complex to a cluster binding site formed by ISCA1 and NFU1 in the ternary ISCA1-ISCA2-NFU1 complex. Such mechanism guarantees that the [4Fe-4S] cluster can be safely moved from where it is assembled on the ISCA1-ISCA2 complex to NFU1, thereby resulting the [4Fe-4S] cluster available for the mitochondrial apo proteins specifically requiring NFU1 for their maturation.

Introduction

In eukaryotes, mitochondria are the primary site for the biosynthesis of Fe-S clusters. Within the mitochondrial matrix, the biosynthesis of Fe-S clusters and their insertion into apo proteins is assisted by several proteins that are highly conserved from bacteria to mammals.[1,2] Among these proteins, three of them, ISCA1, ISCA2 and NFU1, were shown to be implicated in the assembly of [4Fe-4S] clusters and their insertion into mitochondrial apo proteins.[3–10] ISCA1 and ISCA2 are two highly homologous members of the A-type evolutionarily conserved protein family, which is characterized by three highly conserved cysteine residues organized in a C-X_n-C-G-C sequence motif (n is usually 63–65, but is increased by a 21-residue insert in some eukaryotic proteins).[11] This motif has been shown to be able to bind both [2Fe-2S] and [4Fe-4S] cluster types.[12–18] In humans, a ISCA1-ISCA2 complex was identified *in vivo*[19] and in its heterodimeric state was shown

to act *in vitro* as a platform to assemble a $[4Fe\text{-}4S]^{2+}$ cluster.[14,20] The process, hereafter named ISCAs-dependent pathway, requires: (i) GLRX5, the [2Fe-2S] metallochaperone of the mitochondrial matrix that donates two $[2Fe\text{-}2S]^{2+}$ clusters to the ISCA1-ISCA2 complex; (ii) ferredoxin-2 (FDX2), which supplies the two electrons required for the reductive coupling of two $[2Fe\text{-}2S]^{2+}$ clusters to form a $[4Fe\text{-}4S]^{2+}$ cluster; (iii) IBA57, whose molecular role in the process is still not defined (Figure 1 (A)).[14,20–23] Concerning the role of IBA57 in the latter process, it was found that ISCA2 and IBA57 form a [2Fe-2S] ISCA2-IBA57 complex, suggesting that IBA57 might work with ISCA2 in the [4Fe-4S] cluster assembly process.[24–26] This stringent IBA57-ISCA2 functional association was also documented *in vivo* by the finding that ISCA2, but not ISCA1, interacts with IBA57.[19] In marked contrast to the just mentioned [4Fe-4S] cluster assembly process, some *in vivo* data provided evidence that only human ISCA1 is essential for mitochondrial [4Fe-4S] proteins in skeletal muscle or primary neuronal cells under defined physiological conditions, while ISCA2 is dispensable.[19] These data, however, contrast with what was found in HeLa cells in which similar phenotypes were observed for ISCA1, ISCA2 and IBA57 knockdowns, supporting that the three proteins function together in the biosynthesis of mitochondrial [4Fe-4S] clusters,[4] as well as they contrast with the finding that pathogenic mutations in either ISCA1, ISCA2, or IBA57 genes are associated with similar disease phenotypes that include neurodegenerative defects, suggesting that each encoded protein is crucial in neurons.[27–29] Thus, the latter mentioned *in vivo* data support that the ISCAs-dependent pathway described above is operative in mitochondria.

The other player of the ISCA1-ISCA2 pathway is NFU1, a universally present protein composed by globular N-terminal and C-terminal domains (N- and C-domains, hereafter) connected by a flexible linker.[30–32] Human NFU1 contains a conserved CXXC motif located in the C-domain, shown to be involved in [4Fe-4S] cluster binding.[10,31,33] NFU1 was proposed to act downstream the ISCA1-ISCA2 complex.[34] This model was based on studies

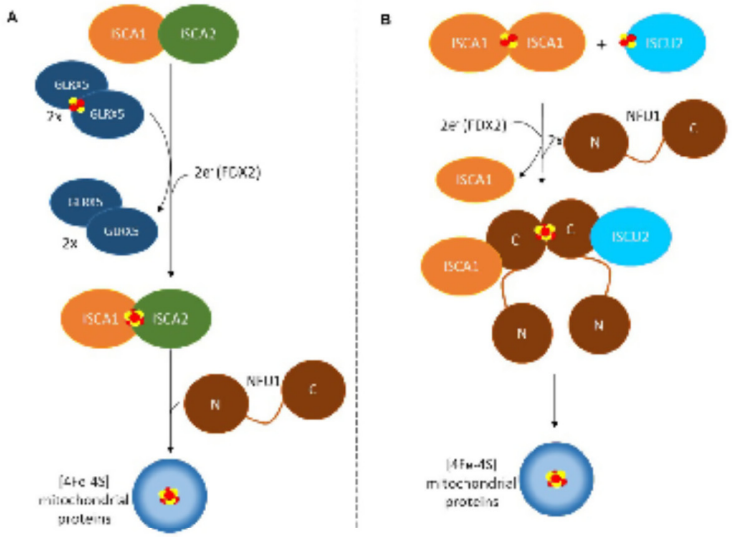

Figure 1. Proposed models of [4Fe-4S] cluster assembly and transfer to mitochondrial targets. (A) The ISCAs-dependent pathway requires ISCA1 and ISCA2 to assemble a $[4Fe\text{-}4S]^{2+}$ cluster on the ISCA1-ISCA2 complex by receiving two $[2Fe\text{-}2S]^{2+}$ clusters from GLRX5 and two electrons ($2e^-$) from FDX2.[14, 21] IBA57 is required to activate this process, but, since its molecular role is still undefined, it was not shown in the figure. Then, the $[4Fe\text{-}4S]^{2+}$ ISCA1-ISCA2 complex was proposed to transfer the cluster to specific protein targets with the assistance of NFU1.[7, 35] The N and C letters of NFU1 indicate the N-terminal and C-terminal domains, respectively. **(B)** In the ISCA1-dependent pathway, two [2Fe-2S] clusters, each ligated by ISCA1 and ISCU2, are transferred to dimeric NFU1 and assembled into a $[4Fe\text{-}4S]^{2+}$ cluster by a reductive coupling mediated by FDX2, which provide two electrons ($2e^-$).[38] A complex, formed by dimeric NFU1, monomeric ISCA1 and ISCU2, has been proposed to transfer the assembled $[4Fe\text{-}4S]^{2+}$ cluster to specific protein targets.

in *Saccharomyces cerevisiae*[35] and suggested that NFU1 receives the [4Fe-4S] cluster assembled on the ISCAs complex and then transfers it to selected apo proteins (Figure 1(A)). Supporting this model, it was found that yeast Nfu1 specifically interacts *in vivo* with the yeast homologues of both human ISCA1 and ISCA2.[35] On the other hand, human ISCA1 and ISCA2 were found to have distinct interacting partners. Indeed, while a specific interaction between ISCA1 and NFU1 was observed *in vivo* by immunoprecipitation experiments, NFU1 did not co-immunoprecipitate with ISCA2.[19] In addition, the ISCAs-NFU1-dependent pathway might be not unique, since other alternative [4Fe-4S] cluster assembling pathways have been recently described. By employing genetic and biochemical techniques, it has been shown that the assembly of a [4Fe-4S] cluster on NFU1 requires the coordinate action of three proteins, which are ISCU2, the scaffold protein able to *de novo* assemble a $[2Fe\text{-}2S]^{2+}$ cluster,[36,37] ISCA1 and FDX2.[38] It was postulated a model (hereafter named ISCA1-dependent pathway) where the $[2Fe\text{-}2S]^{2+}$ cluster-bound forms of ISCA1 and ISCU2 interact with dimeric NFU1 to donate their clusters, which then reductively couple into a $[4Fe\text{-}4S]^{2+}$ cluster upon the provision of two electrons by FDX2 (Figure 1(B)). This mechanism is supported by the interactions observed *in vivo* between NFU1 and ISCU2, between NFU1 and ISCA1, between NFU1 and FDX2 and between two NFU1 molecules,[38] as well as by *in vitro* NMR and SAXS studies that showed that NFU1 and ISCU2 form a complex in which the cluster binding region of ISCU2 interacts with the C-domain of NFU1.[39] Then, in the ISCA1-dependent pathway, a multi-protein complex composed by ISCA1, ISCU2, FDX2 and dimeric [4Fe-4S]-NFU1 was proposed to interact with mitochondrial apo proteins and to transfer to them the assembled $[4Fe\text{-}4S]^{2+}$ cluster (Figure 1(B)).[38] This proposed $[4Fe\text{-}4S]^{2+}$ cluster assembly mechanism bypasses the ISCA1-ISCA2 complex. Another alternative mechanism of $[4Fe\text{-}4S]^{2+}$ cluster assembly, which is possibly activated under oxidative cellular conditions only,[35] was proposed based on a NMR study. It was shown indeed that the [2Fe-2S] GLRX5-BOLA3 complex[40,41] is able to promote the assembly of a $[4Fe\text{-}4S]^{2+}$ cluster on dimeric NFU1 with no requirement of the ISCA1-ISCA2 complex.[33]

In summary, the data available up to now in the literature do not still depict a molecular view of how ISCA1, ISCA2 and NFU1 proteins cooperate in the maturation of mitochondrial [4Fe-4S] proteins. In order to shed light on this matter, we report here a NMR-based study investigating the ISCA1, ISCA2 and NFU1 patterns of interactions and cluster transfer processes. Our data define a detailed molecular model of the succession of events performed in a coordinated manner by ISCA1, ISCA2 and NFU1 to make available [4Fe-4S] clusters for mitochondrial apo proteins. This model provides a general view of the late-acting steps of the maturation of mitochondrial [4Fe-4S] proteins.

Results

Interaction network among ISCA1, ISCA2 and NFU1 in their apo forms

Protein-protein interaction studies were characterized through NMR spectroscopy and analytical size exclusion chromatography, by titrating two or three proteins, which are ISCA1, ISCA2 and NFU1, in their apo forms with different mixing sequences. The used protein constructs were: (i) the mitochondrial isoform of human NFU1 having, in the mature state, a molecular mass of ~22 kDa, as obtained upon removal of the N-terminal mitochondrial targeting sequence of 58 residues[10]; (ii) human ISCA2 without the predicted N-terminal mitochondrial targeting sequence of 43 residues and thus having a molecular mass of ~12 kDa[13]; (iii) human ISCA1 in its full-length form (molecular mass of ~14 kDa) as its mitochondrial presequence is not removed upon its mitochondrial import.[27]

First, we investigated protein–protein interactions occurring between couples of proteins. When apo ^{15}N ISCA2 was stepwise titrated with apo ^{15}N NFU1 up to a 1:1 protein ratio (calculated considering monomeric protein concentrations), no chemical shift changes were observed along the ^{1}H-^{15}N HSQC NMR experiments and the ^{1}H-^{15}N HSQC map of the final 1:1 mixture is the sum of the ^{1}H-^{15}N HSQC maps of the two isolated proteins (Figure 2(A)), indicating that the two proteins do not interact each other. Analytical size exclusion chromatography data confirmed this result as no peaks, with apparent molar mass higher than those of the two isolated ISCA2 and NFU1 proteins (running, respectively, as a homodimer and a monomer with a low percentage of homodimer[14,33]) were observed in the final 1:1 mixture (Figure 2(B)).

When apo ^{15}N ISCA2 was stepwise titrated with apo ISCA1 up to a 1:1 protein ratio (calculated considering monomeric protein concentrations), chemical shift changes were observed in the ^{1}H-^{15}N HSQC maps of apo ^{15}N ISCA2 in a slow exchange regime on the NMR time scale, which means that signals of apo ISCA2 decreased in intensity and those of a new species, assigned to the apo ISCA1-ISCA2 complex, appeared and increased in intensity along the titration (Figure 2(C)). Once the 1:1 ISCA1-ISCA2 ratio was reached, the signals of apo ISCA2 completely disappeared and the signals of the apo ISCA1-ISCA2 complex reached their maximal intensity, indicating that the complex is fully formed at the 1:1 stoichiometric ratio. Analytical size exclusion

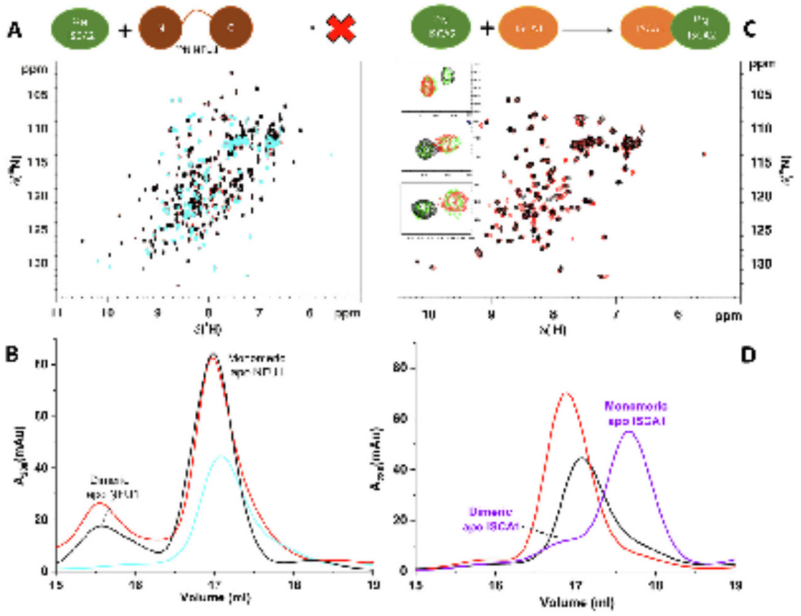

Figure 2. Apo ISCA2 interacts with apo ISCA1 and not with apo NFU1. A schematic cartoon depicting the NMR titration related to each panel is reported. **(A)** Overlay of the ^{1}H-^{15}N HSQC spectrum acquired on a 1:1 apo ^{15}N ISCA2-apo ^{15}N NFU1 mixture (red) with the ^{1}H-^{15}N HSQC spectra acquired on isolated apo ^{15}N ISCA2 (cyan) and on isolated apo ^{15}N NFU1 (black). **(B)** Analytical size exclusion chromatography of apo ISCA2 (cyan), apo NFU1 (black) and a 1:1 apo ISCA2-apo NFU1 mixture (red). **(C)** Overlay of the ^{1}H-^{15}N HSQC spectrum acquired on a 1:1 apo ^{15}N ISCA2-apo ISCA1 mixture (red) with the ^{1}H-^{15}N HSQC spectrum acquired on isolated apo ^{15}N ISCA2 (black). In the inset, overlays of three different regions of ^{1}H-^{15}N HSQC spectra, acquired on isolated apo ^{15}N ISCA2 (black) and on apo ^{15}N ISCA2-apo ISCA1 mixtures at 1:1 (red) and 1:0.5 (green) ratios, are shown. **(D)** Analytical size exclusion chromatography of apo ISCA2 (black), apo ISCA1 (violet) and a 1:1 apo ISCA2-apo ISCA1 mixture (red).

chromatography of apo ISCA1 showed that the protein is essentially monomeric with a small fraction of dimer (Figure 2(D)) and that of the final 1:1 mixture showed: (i) a single peak with an apparent molar mass of ~24 kDa, which is close to the molecular weight calculated for a dimeric apo ISCA1-ISCA2 complex (26 kDa) and which contains both ISCA1 and ISCA2 proteins, as detected by SDS-PAGE (Figure S1), (ii) that the monomeric state of apo ISCA1 is no longer present in the mixture (Figure 2(D)). Considering the concentration at which the complex is fully formed in the NMR and SEC-MALS experiments, the dissociation constant for the apo ISCA1-ISCA2 complex could be estimated to be lower than 50 μM. Overall, the NMR and analytical size exclusion chromatography data indicated the formation of a heterodimeric apo ISCA1-ISCA2 complex. The meaningful ($1\sigma\ \Delta\delta_{avg}$(HN) > 0.05 ppm) ^{1}H and ^{15}N chemical shift changes between apo ISCA2 alone and in the 1:1 protein mixture (Figure S2) are localized in a well-defined region of the protein, which matches with the subunit-subunit interface in dimeric apo ISCA2.[14] The same results were previously found using a shorter ISCA1 construct without its predicted mitochondrial presequence of 1–23 amino acids,[14] thus indicating that the latter stretch does not affect complex formation and does not take part as active contributor to complex formation.

Apo ISCA1 forms a heterocomplex also with apo NFU1. Indeed, when apo ^{15}N NFU1 was stepwise titrated with apo ISCA1 up to a 1:1 protein ratio (calculated considering monomeric protein concentrations), chemical shift changes were observed on the ^{1}H-^{15}N HSQC maps of apo NFU1 in an intermediate exchange regime on the NMR time scale (Figure 3(A)). Indeed, a lot of resonances of the C-domain of NFU1 shift and concomitantly broaden beyond detection upon additions of apo ISCA1 (Figures 3(A) and S3(A)), due to the complex formation. This analysis cannot allow to exactly quantify the amount of complex formed at the final point of the titration,

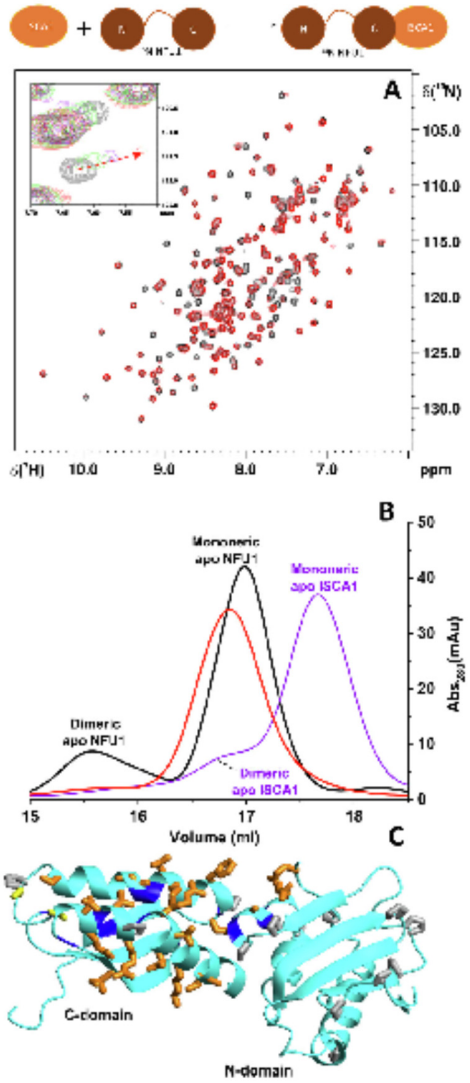

Figure 3. Apo ISCA1 interacts with the C-domain of apo NFU1. (A) A schematic cartoon depicting the NMR titration related to this panel is reported. Overlay of the ^{1}H-^{15}N HSQC spectrum acquired on a 1:1 apo ^{15}N NFU1-apo ISCA1 mixture (red) with the ^{1}H-^{15}N HSQC spectrum acquired on isolated apo ^{15}N NFU1 (black). In the inset, overlay of a region of the ^{1}H-^{15}N HSQC spectra of mixtures obtained by adding apo ISCA1 at increasing concentration to apo ^{15}N NFU1. **(B)** Analytical size exclusion chromatography of apo ISCA1 (violet), apo NFU1 (black) and a 1:1 apo NFU1-apo ISCA1 mixture (red). **(C)** Meaningful chemical shift changes for the backbone NHs of apo ^{15}N NFU1 upon the addition of 1 equivalent of apo ISCA1 are mapped on a structural model of monomeric apo NFU1 in a closed conformation.[39] In orange are the sidechains of the solvent exposed (>50%) residues showing chemical shift changes (line broadening beyond detection effects and/or meaningful chemical shift changes). The protein stretches in blue represent residues showing chemical shift changes but with a solvent exposure below 50%. The sidechains of the proline and cysteine residues are shown in gray and yellow, respectively.

even though the detection of chemical shift variations and broadening upon apo ISCA1 additions indicates the formation of the complex with the concomitant reduction of free monomeric apo NFU1. On the other hand, in the analytical size exclusion chromatography of the final 1:1 apo NFU1-apo ISCA1 mixture, a single peak, which contains both proteins (as detected by SDS-PAGE, Figure S1), is present with an elution volume smaller than those of the two isolated proteins, while the peaks of the isolated monomeric apo ISCA1 and dimeric apo NFU1 are absent (Figure 3(B)). Thus, the single peak containing both NFU1 and ISCA1 identifies exclusively the heterodimeric complex, which is fully formed at the 1:1 apo NFU1-apo ISCA1 ratio. SEC-MALS indicated that this single peak has a molar mass of 29.2 ± 0.5 kDa (Figure S3(B)). This value is intermediate between those of the isolated proteins (apo ISCA1: 14 kDa, apo NFU1: 22 kDa) and that expected for a heterodimeric apo NFU1-ISCA1 complex (36 kDa). Considering the complex concentration in the NMR and SEC-MALS experiments where the complex formation was fully reached, a dissociation constant for the apo NFU1-ISCA1 complex lower than 50 μM can be estimated. Overall, both NMR and SEC-MALS data showed that a heterodimeric ISCA1-NFU1 complex is fully formed via a specific recognition between ISCA1 and the C-domain of NFU1. On the other hand, also a few resonances of the N-domain of NFU1 were affected by apo ISCA1 additions (residues 54–58, Figure S3(A)). These residues are located at the interacting interface between the N- and C-domains of apo NFU1 when it is in its closed conformation.[33] This closed conformation is in equilibrium with an open conformation where the N- and C-domains freely move in solution.[31,33] Considering these structural properties and the effect of ISCA1 addition on the NH signals of residues 54–58, we can propose that the ISCA1-NFU1 complex formation induces structural rearrangements at the interaction interface between the N- and C-domains of NFU1, possibly affecting the open-closed conformational equilibrium. This ISCA1-driven effect on the open-closed conformational equilibrium of NFU1 might also explain the lower than expected molar mass of the ISCA1-NFU1 complex as estimated by SEC-MALS data analysis. By mapping the meaningful chemical shift changes (both broadening beyond detection effects and chemical shift changes with 1σ $\Delta_{avg}(HN) > 0.03$ ppm) on the closed conformation of apo NFU1, we see that (i) the two helices of the C-domain are largely affected by the protein–protein interaction, while the β-sheet of the C-domain is essentially unaffected, and (ii) only the first short helix of the N-domain in close contact with the C-domain is affected by the protein-protein interaction (Figure 3(C). The two helices of the C-domain encase the cluster binding CXXC motif of NFU1, indicating that ISCA1 in the complex is positioned close to the cluster binding region, although the CXXC motif is not largely involved in protein–protein recognition.

The apo complexes, ISCA1-^{15}N NFU1 and ISCA1-^{15}N ISCA2, were then titrated with apo ISCA2 and apo ^{15}N NFU1, respectively, and the resulting mixtures were again analyzed by NMR. In the first titration, the comparison of the ^{1}H-^{15}N HSQC map of the final mixture, having a 1:1 ratio between apo ISCA1-^{15}N NFU1 complex and apo ISCA2, with the maps of apo ^{15}N NFU1 alone and in the complex with ISCA1, indicated that NFU1 remains complexed with ISCA1, thus ISCA2 not being able to extract ISCA1 from the ISCA1-NFU1 complex to form an isolated ISCA1-ISCA2 complex. Indeed, the signals of NFU1 complexed with ISCA1 were not affected by the addition of apo ISCA2 and the signals of isolated apo NFU1 were not detected, thus indicating that free apo NFU1 was not released in solution, as it would have expected in the case of the formation of an isolated ISCA1-ISCA2 complex (Figure 4(A)). In the second titration, when apo ISCA1-^{15}N ISCA2 complex is titrated with apo ^{15}N NFU1 up to a 1:1 ratio, ISCA2 remains complexed with ISCA1, thus NFU1 not being able to extract ISCA1 from the ISCA1-ISCA2 complex to form an isolated ISCA1-NFU1 complex. Indeed, the signals of ISCA2 complexed with ISCA1 were not affected by the addition of apo NFU1 and the signals of isolated apo ISCA2 were not detected (Figure 4(B)), thus indicating that free apo ISCA2 was not released in solution, as it would have been expected in the case of the formation of an isolated ISCA1-NFU1 complex. However, the backbone NH signals of ^{15}N NFU1 changed upon its addition to the ISCA1-ISCA2 complex and, in the final apo ISCA1-apo ^{15}N ISCA2-apo ^{15}N NFU1 1:1:1 mixture, they overlap with those of the apo ISCA1-^{15}N NFU1 complex, while they differ from those of apo ^{15}N NFU1 alone (Figure 4(C)). Overall, from these data we can conclude that (i) apo NFU1 interacts with the apo ISCA1-ISCA2 complex via the C-domain of NFU1 similarly to what happens in the apo NFU1-ISCA1 complex; (ii) apo ISCA1 is the protein mediating the interaction between apo NFU1 and apo ISCA2, being the latter two not interacting each other, in agreement with what observed when the two proteins are mixed (as described above). Thus, these data indicated that ISCA1, interacting with both ISCA2 and NFU1, mediates the formation of a ternary complex.

To further corroborate this model, apo ISCA1 was stepwise added to a 1:1 mixture containing the two not-interacting apo ^{15}N ISCA2 and apo ^{15}N NFU1 proteins. The ^{1}H-^{15}N HSQC maps showed the occurrence of the interaction of apo ISCA1 with both apo ISCA2 and apo NFU1. In the final mixture, the NH signals of apo NFU1 overlap with those of apo NFU1 complexed with apo ISCA1,

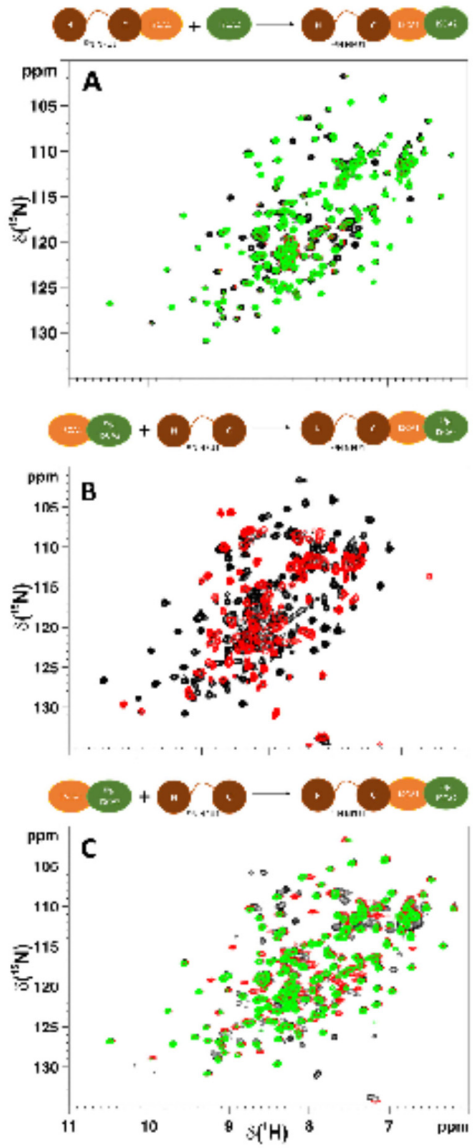

Figure 4. Apo ISCA1-ISCA2 heterodimeric complex interacts with the C-domain of apo NFU1. A schematic cartoon depicting the NMR titration related to each panel is reported. **(A)** Overlay of the ^{1}H-^{15}N HSQC spectrum acquired on a mixture containing apo ^{15}N NFU1-ISCA1 complex and apo ISCA2 at 1:1 ratio (green) with the ^{1}H-^{15}N HSQC spectra acquired on isolated apo ^{15}N NFU1 (black) and on apo ^{15}N NFU1-ISCA1 complex (red). **(B)** Overlay of the ^{1}H-^{15}N HSQC spectrum acquired on a mixture containing apo ^{15}N ISCA2-ISCA1 complex and apo ^{15}N NFU1 at 1:1 ratio (black) with the ^{1}H-^{15}N HSQC spectrum acquired on apo ^{15}N ISCA2-ISCA1 complex (red). **(C)** Overlay of the ^{1}H-^{15}N HSQC spectrum acquired on a mixture containing apo ^{15}N ISCA2-ISCA1 complex and apo ^{15}N NFU1 at 1:1 ratio (black) with the ^{1}H-^{15}N HSQC spectra acquired on isolated apo ^{15}N NFU1 (red) and on apo ^{15}N NFU1-ISCA1 complex (green).

and not with those of isolated apo NFU1 (Figure S4 (A)), and the NH signals of apo ISCA2 overlap with those of apo ISCA2 complexed with apo ISCA1, and not with those of isolated apo ISCA2 (Figure S4(B)). The observed chemical shift changes are concurrent on both proteins along the titration and the chemical shift changes on both ^{15}N ISCA2/^{15}N NFU1 apo proteins are complete once one equivalent of apo ISCA1 was added to the 1:1 ISCA2/NFU1 apo mixture. Consistently, additions up to two equivalents of apo ISCA1 to the mixture did not significantly affect the ^{1}H-^{15}N HSQC map. These results conclusively indicated that apo ISCA1 interacts with both apo ISCA2 and apo NFU1, promoting the formation of a ternary complex that involves the two not interacting proteins apo ISCA2 and apo NFU1. The latter titration also allowed to estimate a dissociation constant for the apo ternary complex lower than 500 μM on the basis of the complex concentration reached once the complex was fully formed. On the other hand, analytical size exclusion chromatography of the final mixture did not show the presence of a peak with an elution volume smaller than those of the two isolated ISCA1-ISCA2 and ISCA1-NFU1 apo complexes, as it would be expected for the presence of a ternary complex. This result can be interpreted considering that the ternary complex is readily released at the lower protein concentrations used in the analytical size exclusion chromatography with respect to the higher protein concentrations used in the NMR experiments, suggesting its transient nature.

Protein-protein interaction studies between [4Fe-4S] ISCA1-ISCA2 and apo NFU1

Anaerobic purification of ISCA1 and ISCA2 led to a mixture of apo and $[2Fe\text{-}2S]^{2+}$ cluster-bound forms (see Materials and Methods for details). While chemical reconstitution of anaerobically purified ISCA2 led to the formation of a $[4Fe\text{-}4S]^{2+}$ cluster-bound dimeric form,[14] chemical reconstitution of anaerobically purified ISCA1 does not lead to the formation of a [4Fe-4S] cluster-bound form. Indeed, UV–visible spectrum of chemically reconstituted ISCA1 maintains, with a ~20% increase, the bands of the anaerobically purified ISCA1 at 325, 420 nm and a shoulder at 460 nm (Figure S5(A)), typical of Cys-bound $[2Fe\text{-}2S]^{2+}$ clusters.[42–44] The only difference is the presence of a band at ~650 nm in the chemically reconstituted protein (Figure S5(A)), which is indicative of the presence of some Fe^{3+}-containing aggregates, that were not fully removed by the PD-10 desalting column performed at the end of chemical reconstitution protocol.[42] The CD-visible spectrum of chemically reconstituted ISCA1 showed both positive and negative bands with well-defined peaks accompanied by shoulders and inflections, which are typical of $[2Fe\text{-}2S]^{2+}$ protein-bound clusters (Figure S5 (B)).[42,45] The CD-visible spectrum of chemically reconstituted ISCA1 showed the same bands detected in anaerobically purified $[2Fe\text{-}2S]^{2+}$ ISCA1 (Figure S5(B)) and is also very similar to CD-visible spectrum of the $[2Fe\text{-}2S]^{2+}$ form of *Azotobacter vinelandii* NifIscA.[12] No formation of a [4Fe-4S] cluster-bound ISCA1 species was confirmed by the 1D ^{1}H paramagnetic NMR spectrum of chemically reconstituted ISCA1, which has indeed the same signals of anaerobically purified $[2Fe\text{-}2S]^{2+}$ ISCA1, which are typical of $[2Fe\text{-}2S]^{2+}$ protein-bound clusters (Figure S5(D) and S5(E)). On the other hand, chemical reconstitution of the 1:1 ISCA1-ISCA2 heterodimer (see Materials and Methods for details) led to the formation of a [4Fe-4S] cluster-bound, heterodimeric species ([4Fe-4S] ISCA1-ISCA2, hereafter), as shown by paramagnetic ^{1}H 1D NMR and UV–visible/CD-visible spectra. The UV–visible spectrum of the chemically reconstituted ISCA1-ISCA2 complex differs from that of anaerobically purified ISCA1, as it shows only a broad band at 420 nm characteristic of Cys-bound [4Fe-4S] clusters (Figure S5(A)).[42,46] The CD-visible spectrum of the chemically reconstituted ISCA1-ISCA2 complex exhibits negligible CD intensity compared to the signals of anaerobically purified ISCA1 (Figure S5(B)), consistent with [4Fe-4S] cluster formation in the ISCA1-ISCA2 complex.[42] In agreement with the latter conclusion, the CD-visible spectrum of the chemically reconstituted ISCA1-ISCA2 complex is also very similar to that of the $[4Fe\text{-}4S]^{2+}$ form of *Azotobacter vinelandii* IscA and differs from that of the $[2Fe\text{-}2S]^{2+}$ form of *A. vinelandii* IscA.[12] The 1D ^{1}H paramagnetic NMR spectrum of [4Fe-4S] ISCA1-ISCA2 (Figure 5(A)) has down-field shifted signals originating from βCH_2 of the Cys ligands and is similar to that of homodimeric [4Fe-4S] ISCA2,[14] while it differs from that of $[2Fe\text{-}2S]^{2+}$ cluster-bound species of both ISCA1 and ISCA2 (compare Figure 5 (A) with 1D ^{1}H paramagnetic NMR spectra of $[2Fe\text{-}2S]^{2+}$ ISCA1 and $[2Fe\text{-}2S]^{2+}$ ISCA2 reported in Figure S5(D) and in Brancaccio *et al.*[14] respectively). In conclusion, all the spectroscopic data indicated that ISCA1 binds a [4Fe-4S] cluster only when it is in the ISCA1-ISCA2 heterodimeric complex.

Analytical size exclusion chromatography of the [4Fe-4S] ISCA1-ISCA2 complex showed the presence of a single peak containing both ISCA1 and ISCA2 proteins, as detected by SDS-PAGE (Figure S1), and eluting at a volume very similar to that of the dimeric ISCA2 with no presence of monomeric ISCA1, consistent with the complete formation of a dimeric hetero-complex (Figure 5 (B)). The ^{1}H-^{15}N HSQC spectra of the 1:1 ISCA1-^{15}N ISCA2 mixture before and after chemical reconstitution showed that the chemical shifts of most of the backbone NH signals did not vary, consistent with ISCA2 being still complexed with ISCA1 upon chemical reconstitution.

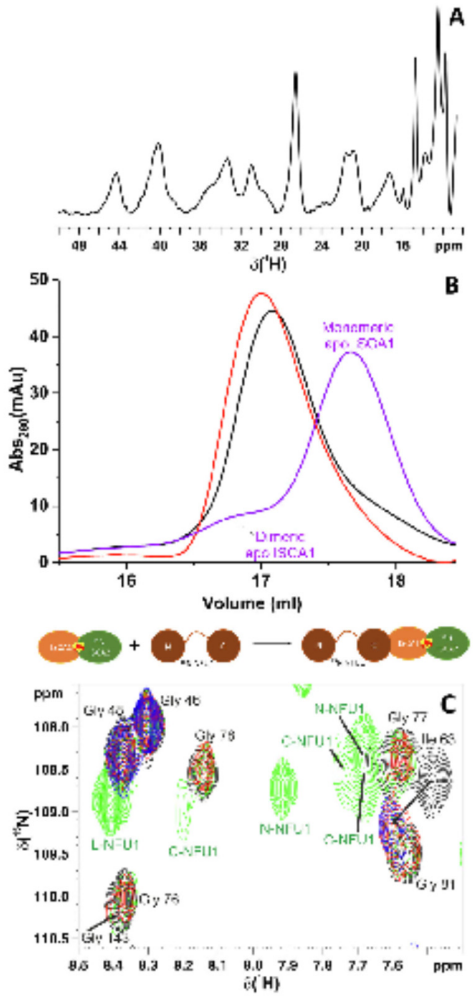

Figure 5. The ISCA1-ISCA2 heterodimer binds a [4Fe-4S] cluster. (A) 1D ^{1}H paramagnetic NMR spectrum at 283 K of [4Fe-4S] ISCA1-ISCA2, obtained by chemically reconstituting a 1:1 mixture of anaerobically purified ISCA1 and ISCA2. **(B)** Analytical size exclusion chromatography of [4Fe-4S] ISCA1-ISCA2 (red), apo ISCA2 (black) and apo ISCA1 (violet). **(C)** A schematic cartoon depicting the NMR titration related to this panel is reported. Overlay of the ^{1}H-^{15}N HSQC spectra acquired on isolated apo ^{15}N ISCA2 (black), on apo ^{15}N ISCA2-ISCA1 complex (red), on [4Fe-4S] ^{15}N ISCA2-ISCA1 complex (blue) and on a mixture containing [4Fe-4S] ^{15}N ISCA2-ISCA1 complex and apo ^{15}N NFU1 at 1:1 ratio (green). The backbone NH signals of ISCA2 residues (Gly 46, Gly 48, Ile 63, Gly 76, Gly 77, Gly 78, Gly 81 and Gly 143) are shown, and those of the N-domain, the linker and the C-domain of NFU1 are indicated as N-, L- and C-NFU1, respectively.

However, the residues of ISCA2 surrounding the cluster binding cysteines (Cys 79, Cys 144 and Cys 146), such as Gly 76, Gly 77, Gly 78, Gly 81, Gly 143 and Gly 147, broaden beyond detection upon chemical reconstitution (in Figure 5(C) compare Gly residues in red with those in blue), due to the binding of the paramagnetic [4Fe-4S] cluster. This indicates that the C-X_{64}-C-G-C

conserved sequence motif of ISCA2 is involved in [4Fe-4S] cluster binding in the ISCA1-ISCA2 complex.

When the [4Fe-4S] ISCA1-^{15}N ISCA2 complex was stepwise titrated with apo ^{15}N NFU1 up to a 1:1 ratio, the backbone NH signals of ISCA2 did not show chemical shift changes, with the exception of the residues close to the Cys cluster ligands, whose backbone NH signals, at the end of the titration, became detectable again in the ^{1}H-^{15}N HSQC map at the chemical shift values of the apo ISCA1-ISCA2 complex (in Figure 5(C) compare Gly residues in green with those in blue and red). On the contrary, many spectral changes (mostly line broadening effects) were observed for the backbone NH signals of the C-domain of NFU1, and the affected residues are located on the same interacting region mapped in the ISCA1-NFU1 and ISCA1-ISCA2-NFU1 apo complexes. Overall, these NMR data indicate that: (i) NFU1 interacts with the [4Fe-4S] ISCA1-ISCA2 complex via its C-domain similarly to what found in the apo ternary complex, thus with ISCA1 in the complex with ISCA2 mediating the interaction with NFU1 and promoting the formation of a ternary complex; (ii) the cluster is no longer bound to ISCA2, possibly being shared by ISCA1 and NFU1 in the ternary ISCA1-ISCA2-NFU1 complex.

To further support this model, [4Fe-4S] ISCA1-^{15}N ISCA2 complex was titrated with a ^{15}N labelled construct of apo NFU1 comprising only the C-domain, up to the 1:1 ratio. The spectral changes observed in the ^{1}H-^{15}N HSQC NMR map of the final mixture were the same as those observed in the titration with full-length NFU1, both on ISCA2 (no spectral changes observed as ISCA2 still remains complexed with ISCA1, Figure S6) and on NFU1 (the observed changes map on the same region of C-domain of NFU1 interacting with ISCA1, as identified in the apo ISCA1-apo NFU1 1:1 mixture, compare inset of Figure S6 with Figure 3(C)). These data corroborate the proposed model that ISCA1 promotes the formation of a ternary complex between NFU1, via its the C-domain, and [4Fe-4S] ISCA1-ISCA2.

The still remaining question to be addressed is which kind of cluster is present in the ISCA1-ISCA2-NFU1 ternary complex and its redox state as well as which among the three proteins coordinate it. The paramagnetic 1D ^{1}H NMR spectrum of the 1:1 mixture of [4Fe-4S] ISCA1-ISCA2 and apo NFU1 showed the presence of two hyperfine-shifted signals at 19.3 and 12.9 ppm and two close signals at around 10.5 ppm (Figure 6(A)), all having an anti-Curie (i.e. the chemical shift of hyperfine-shifted signals increases as the temperature is increased) temperature dependence (Figure S7). The chemical shift values of these signals, their anti-Curie temperature dependence and their linewidths are typical of βCH_2 signals of Cys residues bound to a $[4Fe\text{-}4S]^{2+}$ cluster with an S = 0 electronic ground state, with the paramagnetism arising from excited states of the electron spin ladder, whose population is increased with temperature.[47,48] In particular, the anti-Curie temperature dependence of the paramagnetic signals allows to establish that the cluster bound to the complex is in an oxidized $[4Fe\text{-}4S]^{2+}$ state, because an anti-Curie temperature dependence is typically observed for the cysteine hyperfine-shifted resonances in oxidized $[4Fe\text{-}4S]^{2+}$ ferredoxins.[48–51] The paramagnetic 1D ^{1}H NMR spectrum of the 1:1 [4Fe-4S] ISCA1-ISCA2/apo NFU1 mixture is completely different with respect to that of the [4Fe-4S] ISCA1-ISCA2 complex while it is closer, although not superimposable, to that of dimeric $[4Fe\text{-}4S]^{2+}$ NFU1 (compare Figure 6(A) with Figures 6(B) and 5(A)). These comparisons indicated that the $[4Fe\text{-}4S]^{2+}$ cluster coordination in the ternary ISCA1-ISCA2-NFU1 complex differs from both of those observed in the ISCA1-ISCA2 complex and in dimeric NFU1, although it is more similar to the latter case. The ^{1}H-^{15}N HSQC NMR data described above (Figure 5(C)), showing that ISCA2 is not involved in cluster binding in the ternary complex, suggested that the $[4Fe\text{-}4S]^{2+}$ cluster in the ternary complex is bridged between NFU1 and ISCA1. In order to validate this model, the heterodimeric ISCA1-NFU1 complex, obtained by mixing anaerobically purified ISCA1 and apo ^{15}N NFU1, was chemically reconstituted. Its paramagnetic 1D ^{1}H NMR spectrum (Figure 6(C)) showed the presence of the same anti-Curie, hyperfine-shifted signals observed when the $[4Fe\text{-}4S]^{2+}$ cluster is bound to the ternary ISCA1-ISCA2-NFU1 complex. This data provides strong hints to the model that the $[4Fe\text{-}4S]^{2+}$ cluster is shared by ISCA1 and NFU1 in the ternary complex. In addition, the latter data showed that the ISCA1-NFU1 complex can bind the $[4Fe\text{-}4S]^{2+}$ cluster, independently of the presence of ISCA2. To provide conclusive proofs that the $[4Fe\text{-}4S]^{2+}$ cluster is shared by ISCA1 and NFU1 in the ternary complex, 1D ^{1}H paramagnetic NMR data were acquired on $[4Fe\text{-}4S]^{2+}$ ^{15}N NFU1 titrated with apo ISCA1 (Figure 6(D)). Once the 1:1 $[4Fe\text{-}4S]^{2+}$ NFU1-apo ISCA1 ratio was reached, the 1D ^{1}H paramagnetic NMR spectrum displayed the same hyperfine-shifted signals observed when the $[4Fe\text{-}4S]^{2+}$ cluster is bound to the ternary ISCA1-ISCA2-NFU1 complex (compare Figure 6(A) with Figure 6(D)), conclusively proving that the $[4Fe\text{-}4S]^{2+}$ cluster is shared by ISCA1 and NFU1 in the ternary ISCA1-ISCA2-NFU1 complex.

Discussion

The late-acting steps of the maturation of mitochondrial [4Fe-4S] proteins, consisting of the assembly and insertion of [4Fe-4S] clusters into

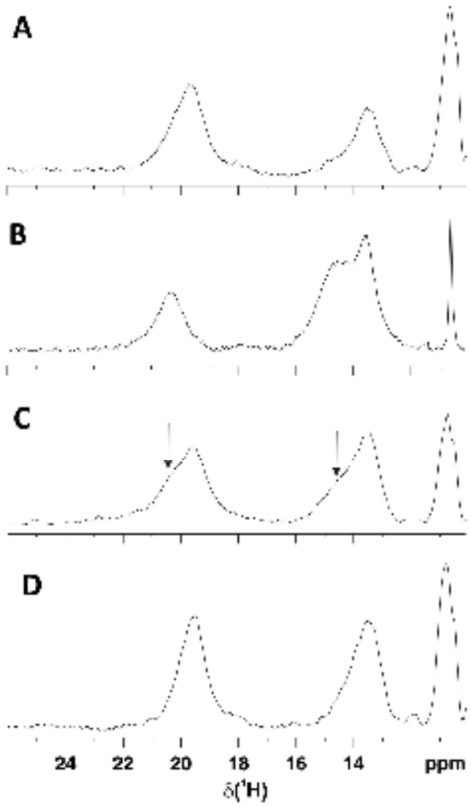

Figure 6. A [4Fe-4S]$^{2+}$ cluster is bound to the ternary ISCA1-ISCA2-NFU1 complex. 1D ^{1}H paramagnetic NMR spectra acquired on **(A)** a mixture containing [4Fe-4S] ISCA1-ISCA2 complex and apo NFU1 at 1:1 ratio, **(B)** dimeric [4Fe-4S]$^{2+}$ NFU1, **(C)** a chemically reconstituted mixture of anaerobically purified ISCA1 and apo NFU1 at 1:1 ratio, **(D)** a 1:1 dimeric [4Fe-4S]$^{2+}$ NFU1-apo ISCA1 mixture. The arrows in panel C indicate signals with the same chemical shift values of [4Fe-4S]$^{2+}$ NFU1 (compare them with signals of panel B), indicating that upon the chemical reconstitution, a small fraction of dimeric [4Fe-4S]$^{2+}$ NFU1 is formed.

mitochondrial apo proteins, are not yet fully understood. The available genetic, biochemical and proteomic data do not yet provide a definitive picture on how the proteins that are essential for the assembly and insertion of the [4Fe-4S] clusters into the final proteins operate. Depending on the type of human cells or of the eukaryotic organisms, genetic and biochemical data pointed out at different mechanisms where either ISCA1 only,[19,38] or both ISCA1 and ISCA2,[3,4,52] are essential for the mitochondrial [4Fe-4S] protein biogenesis *in vivo* (Figure 1). Recently, an *in vitro* biochemical study mimicking physiological conditions strongly supported the model that both human ISCA1 and ISCA2, with the assistance of IBA57, are required to assemble a [4Fe-4S] cluster.[21] A significant discrepancy was also observed in the proteomic data. Indeed, human NFU1 was found to interact with ISCA1, but not with ISCA2,[19] while yeast NFU1 interacts with both yeast ISCA1 and ISCA2.[35]

The here presented NMR-based study provides a molecular model for the succession of events orchestrated by ISCA1, ISCA2 and NFU1 to make [4Fe-4S] clusters available to mitochondrial apo proteins. We have shown that ISCA1 is the key player, being able to interact either individually with ISCA2 or NFU1 or with both proteins, promoting the formation of a transient ISCA1-ISCA2-NFU1 ternary complex. ISCA1 works as

the promoter of the interaction between ISCA2 and NFU1 that otherwise do not interact each other. The interaction between ISCA1 and NFU1 involves the C-domain of NFU1, while the N-domain of NFU1 does not take part to the protein–protein recognition. Specifically, the two helices of the C-domain of NFU1 encasing the cluster binding CXXC motif are involved in the recognition with ISCA1. We also found that the [4Fe-4S] cluster bound form of the ISCA1-ISCA2 complex, which is the physiological mitochondrial [4Fe-4S] cluster assembler,[14,20,21] interacts with apo NFU1. Upon this interaction, the cluster is not transferred from the ISCA1-ISCA2 complex to NFU1 to form dimeric $[4Fe\text{-}4S]^{2+}$ NFU1. On the contrary, a ternary ISCA1-ISCA2-NFU1 complex, the same formed by the interaction among the three apo proteins, is formed. In the ternary complex, the cluster is transferred from a bridged ISCA1-ISCA2 coordination to a bridged ISCA1-NFU1 coordination, thus leaving ISCA2 no more involved in cluster binding. The same cluster coordination mode is also present in a ISCA1-NFU1 complex isolated in different ways (Figure 6(C) and (D)), suggesting that ISCA2 might not be required in the following step of cluster release to the mitochondrial [4Fe-4S] proteins. On the basis of these overall findings, the pathway of the maturation of mitochondrial [4Fe-4S] proteins (Figure 7) can thus be outlined as it follows: (i) the $[4Fe\text{-}4S]^{2+}$ cluster is assembled on the ISCA1-ISCA2 heterodimer by reductively coupling two $[2Fe\text{-}2S]^{2+}$ clusters donated by GLRX5, being the two required electrons provided by FDX2[14,20,21]; (ii) $[4Fe\text{-}4S]^{2+}$ ISCA1-ISCA2 complex can transfer the cluster to proteins that do not require NFU1 for their maturation, such as aconitase[6,7,21]; (iii) ISCA1, through its specific recognition with the C-domain of NFU1, mediates the $[4Fe\text{-}4S]^{2+}$ cluster transfer from the ISCA1-ISCA2 cluster binding site to the ISCA1-NFU1 cluster binding site upon the formation of a transient, ternary ISCA1-ISCA2-NFU1 complex; (iv) the latter complex, coordinating the $[4Fe\text{-}4S]^{2+}$ cluster via ISCA1 and NFU1, specifically directs the $[4Fe\text{-}4S]^{2+}$ cluster to mitochondrial proteins that require NFU1 for their maturation, that are the respiratory complexes I and II and the radical SAM protein lipoyl synthase[6,7,53–55]; (v) upon ISCA2 release from the ternary complex (consistent with the transient nature of the ternary complex, which might then be a transient intermediate in the pathway), the $[4Fe\text{-}4S]^{2+}$ NFU1-ISCA1 adduct can also be able to transfer the $[4Fe\text{-}4S]^{2+}$ cluster to mitochondrial proteins. Along this pathway (Figure 7), the cluster can be safely moved from

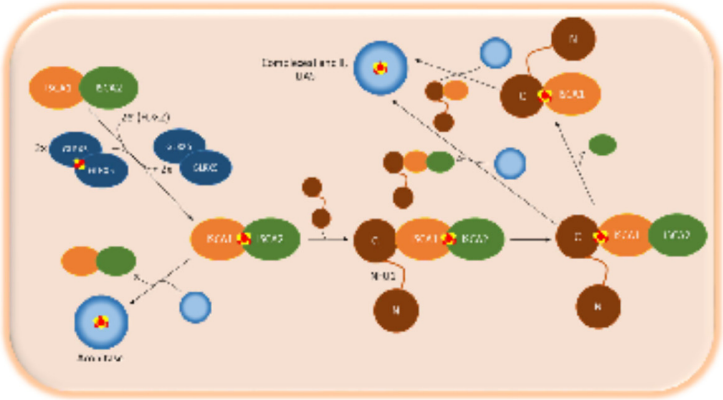

Figure 7. Iron-sulfur cluster assembly pathways for the maturation of mitochondrial [4Fe-4S] proteins. The ISCAs-dependent pathway requires ISCA1 and ISCA2 to mature [4Fe-4S] mitochondrial proteins: 1) the ISCA1-ISCA2 complex receives two $[2Fe\text{-}2S]^{2+}$ clusters from GLRX5[14] and two electrons ($2e^-$) from FDX2[21] to assemble a $[4Fe\text{-}4S]^{2+}$ cluster by means of IBA57, whose molecular role is still undefined and for this reason is not shown in the figure; 2) the $[4Fe\text{-}4S]^{2+}$ ISCA1-ISCA2 complex can transfer the cluster to aconitase maturing it or can specifically interact with the C-domain of apo NFU1 forming a transient ternary $[4Fe\text{-}4S]^{2+}$ NFU1-ISCA1-ISCA2 complex; 3) the $[4Fe\text{-}4S]^{2+}$ cluster is moved within the ternary complex from a bridged ISCA1-ISCA2 coordination to a bridged ISCA1-NFU1 coordination; 4) the $[4Fe\text{-}4S]^{2+}$ ISCA1-ISCA2-NFU1 complex might transfer the cluster to mature respiratory complexes I and II and lipoyl synthase (LIAS), with the help of other accessory proteins when required (not shown in the Figure); 5) upon ISCA2 release by the transient ternary complex, a $[4Fe\text{-}4S]^{2+}$ NFU1-ISCA1 adduct is formed and it might be another species directing the $[4Fe\text{-}4S]^{2+}$ cluster to mitochondrial proteins. The N and C letters of NFU1 indicate the N-terminal and C-terminal domains, respectively.

where it is assembled on the ISCA1-ISCA2 complex towards the final proteins in a selective manner, with no risk of being released free in the mitochondrial matrix where it might damage the cellular environment. This pathway is in agreement with the *in vivo* proteomics data showing that ISCA2 interacts with ISCA1, but not with NFU1, and that ISCA1 interacts with both ISCA2 and NFU1 proteins.[19] In conclusion, our results support the physiological relevance of the ISCAs-dependent pathway shown in Figure 1(A). We have indeed defined for the first time the molecular function of the *in vivo*-detected ISCA1-ISCA2-NFU1 interactions: the ISCA1-ISCA2 interaction produces a complex, which, in its [4Fe-4S] bound form, is able to interact with apo NFU1 to form a ternary complex where the cluster is shared by ISCA1 and NFU1 to be ready for being inserted into mitochondrial proteins requiring NFU1 for their maturation.

Materials and Methods

Protein expression and purification

pDONR221 plasmid containing full-length ISCA1 gene (UniProt: Q9BUE6) was purchased by Genscript. Gateway cloning technology (Invitrogen) was then applied to clone full-length ISCA1 gene into pDEST-HisMBP plasmid to express N-terminal 6His-tag-MBP-ISCA1 protein. The latter plasmid was transformed in *Escherichia coli* BL21-Gold(DE3) (Agilent) competent cells. Cells were cultivated at 37 °C in LB media adding ampicillin (100 μg/mL), 4 mL of Solution Q (40 mM HCl, 50 mg/l $FeCl_2$ $4H_2O$, 184 mg/l $CaCl_2$ $2H_2O$, 64 mg/l H_3BO_3, 18 mg/l $CoCl_2$ $6H_2O$, 4 mg/l $CuCl_2$ $2H_2O$, 340 mg/l $ZnCl_2$, 355 mg/l Na_2MoO_4 $2H_2O$, 40 mg/l $MnCl_2$ $4H_2O$) and 250 μM of $FeCl_3$ per liter of sterile LB until OD_{600} reached 0.8–1. Protein expression was induced with 0.2 mM IPTG at 18 °C for 16 h. The cells were harvested by centrifugation at 5000 rpm for 20 min (JA-10, Beckman Coulter) and then resuspended in binding buffer (50 mM Tris-HCl, 500 mM NaCl, 15 mM Imidazole, pH 8.0). The cells were lysed by sonication at 4 °C. The N-terminal 6His-tag-MBP-ISCA1 protein was purified from the lysate using a HisTrap HP column (GE Healthcare) and then the 6His-MBP tag was cleaved by tobacco etch virus protease treatment over-night at room temperature in binding buffer. HisTrap column followed by amylose resin column were performed to separate the digested ISCA1 from MBP-6His tag and from undigested 6His-tag-MBP-ISCA1 protein. The final yield of ISCA1 was ~15 mg/L of LB culture. Apo ISCA1 was obtained performing all the purification steps under aerobic conditions, while a mixture of apo and $[2Fe\text{-}2S]^{2+}$ ISCA1 was purified under anaerobic conditions (named as anaerobically purified ISCA1). The anaerobically purified ISCA1 protein was characterized by UV- and CD-visible absorption and 1D ^1H paramagnetic NMR spectroscopies, analytical size exclusion chromatography (Figure S5), and iron and acid-labile sulfide content. Protein quantification was carried out with the Bradford protein assay, using BSA as a standard. Non-heme iron and acid-labile sulfide content was determined as described previously.[56] In the UV–visible absorption spectrum of anaerobically purified ISCA1, the extinction coefficients at 325 and 420 nm (ranging from 4200 to 5700 and from 2100 to 3900 M^{-1} cm^{-1} depending on protein preparation, respectively) are far from the lower end of the range of values that are considered typical for [2Fe-2S] clusters (11000 and 8000 M^{-1} cm^{-1}, respectively),[57] indicating a partial [2Fe-2S] cluster occupancy in the homodimer. Iron and acid-labile sulfide analyses of anaerobically purified ISCA1 samples indicate ~0.3 $[2Fe\text{-}2S]^{2+}$ cluster per homodimer (Fe, 0.6 ± 0.1; acid-labile S, 0.5 ± 0.1 per mol of homodimer; Fe and S measurements are the averages of three independent samples).

The production of human ISCA2, and of full-length and C-domain NFU1 in their apo and Fe-S cluster-bound forms were obtained as previously described in literature.[13,33] As previously reported,[14] the purification under anaerobic conditions of ISCA2 resulted in a dimer, which is composed by a mixture of apo and $[2Fe\text{-}2S]^{2+}$ cluster-bound dimeric species with a $[2Fe\text{-}2S]^{2+}$ cluster occupancy of 0.1–0.2 cluster per homodimer.

Production of Fe-S cluster-bound species

A 1:1 mixture of ISCA1 and ISCA2 was produced by stepwise titrating anaerobically purified ^{15}N ISCA2 with anaerobically purified ISCA1 and monitoring changes in the ^1H-^{15}N HSQC NMR maps. Chemical shift changes occur in a slow exchange regime on the NMR time scale, which were completed once the 1:1 protein ratio was reached, indicating that an ISCA1-ISCA2 hetero-complex is fully formed at this stoichiometric ratio. The ISCA1-ISCA2 complex was then chemically reconstituted to obtain the [4Fe-4S] cluster-bound hetero-complex. Chemical reconstitution was anaerobically performed in 50 mM Tris-HCl, 100 mM NaCl and 5 mM DTT buffer at pH 8.0 adding eight equivalents of $FeCl_3$ and Na_2S to a protein solution of ~40–80 μM. The reaction was incubated for 16 h at room temperature. Anaerobic conditions were obtained performing the chemical reconstitution in glove-box (MBraun Labstar 130) with less than 2 ppm of oxygen and by using all buffers degassed. The excess of $FeCl_3$ and Na_2S as well as Fe-S aggregates/precipitates were removed by PD-10 desalting column following a widely used methodology applied in Fe-S protein reconstitution protocols.[42] Anaerobically purified ISCA1 and a 1:1 mixture of anaerobically purified ISCA1 and apo NFU1 were chemically reconstituted following the same procedure. This led to dimeric

$[2Fe\text{-}2S]^{2+}$ and dimeric $[4Fe\text{-}4S]^{2+}$ cluster-bound species, respectively. Iron and acid-labile sulfide analyses indicated an $Fe:S^{2-}$ ratio close to 1:1 for both chemically reconstituted ISCA1-ISCA2 and ISCA1-NFU1 complexes. Moreover, the analytical data on three independent preparations of both latter complexes indicated a 3.5 ± 0.1 Fe and 3.7 ± 0.1 S^{2-} content per heterodimer, consistent with the presence of ~0.9 [4Fe-4S] cluster per heterodimer. Dimeric $[4Fe\text{-}4S]^{2+}$ NFU1 with 90% of cluster loading was produced following the protocol previously reported.[33]

Analytical size exclusion chromatography and SEC-MALS

In the analytical size exclusion chromatography, purified samples were loaded on a Superdex 200 Increase 10/300 GL column attached to an AKTA pure chromatography unit with a continuous flow rate of 0.65 mL/min. The column was calibrated with gel filtration marker calibration kit, 6500–66000 Da (Sigma-Aldrich), to obtain the apparent molecular masses of the detected species. The column was equilibrated with degassed phosphate buffer 50 mM, 150 mM NaCl, 5 mM DTT and pH 7.0. SEC-MALS data were acquired by attaching a Superdex™ 200 Increase 10/300 GL column to a DAWN HELEOS system with a continuous flow rate of 0.6 mL/min using a filtered buffer (50 mM, 150 mM NaCl, 5 mM DTT and pH 7.0). Each experiment was successfully repeated at least three times.

UV- and CD-visible spectroscopy

UV- and CD-visible spectra were performed to characterize the cluster bound to anaerobically purified and chemically reconstituted ISCA1 as well as chemically reconstituted ISCA1-ISCA2 heterodimeric complex. The experiments were performed under anaerobic conditions, preparing the samples in glove-box with less than 5 ppm of oxygen with degassed buffers and using a gas-tight cuvette. UV- and CD-visible spectra were performed at room temperature (25 °C) in 50 mM phosphate buffer, 150 mM NaCl, 5 mM DTT and pH 7.0 on a Cary 50 Eclipse spectrophotometer and JASCO J-810 circular dichroism spectropolarimeter, respectively. Each experiment was successfully repeated three times.

NMR spectroscopy

$^{1}H\text{-}^{15}N$ HSQC spectra were acquired at 298 K in 50 mM phosphate buffer, 150 mM NaCl, 5 mM DTT pH 7.0, 10% (v/v) D_2O. Diamagnetic NMR spectra were recorded on Bruker AVANCE 700, 900 and 950 MHz, processed using the standard Bruker software (Topspin) and analyzed with CARA program.[58] To monitor the possible interaction among ISCA1, ISCA2 and NFU1 in their apo and Fe-S cluster-bound states, ^{15}N labeled protein(s) were stepwise titrated in anaerobic conditions with increasing amounts of unlabeled or ^{15}N-labelled protein(s). Chemical shifts of the backbone NHs observed in the ^{1}H ^{15}N HSQC spectra along the additions of the unlabeled or ^{15}N-labelled protein(s) were compared with chemical shifts of ^{15}N-labelled protein(s) in the initial state(s). The observed chemical shift changes were reported as backbone weighted average chemical shift differences $\Delta\delta_{avg}(HN)$, i.e. $(((\Delta H)^2 + (\Delta N/5)^2)/2)^{1/2}$, where ΔH and ΔN are chemical shift differences for backbone amide ^{1}H and ^{15}N nuclei, respectively. Chemical shift assignment of full-length NFU1 and of the C-domain of NFU1 were available in the Biological Magnetic Resonance Bank (under accession codes BMRB: 26801 [full-length NFU1] and BMRB: 19068 [NFU1 C-domain].[31] Chemical shift assignment of apo ISCA2 was also already available.[14] Each titration was successfully repeated three times.

1D ^{1}H paramagnetic NMR experiments were acquired at 400 MHz with a ^{1}H optimized 5 mm probe at temperatures ranging from 283 K and 298 K, with protein samples in 50 mM phosphate buffer, 150 mM NaCl, 5 mM DTT pH 7.0, 99% (v/v) D_2O. The protein concentration was 0.5–0.8 mM. Water signal was suppressed via fast repetition experiments and water selective irradiation.[59,60] Experiments were typically performed using an overall recycle delay of 90 ms. Squared cosine and exponential multiplications were applied prior to Fourier transformation.[61] Manual baseline correction was performed, using polynomial functions. Each experiment was successfully repeated three times.

CRediT authorship contribution statement

Dafne Suraci: Investigation, Methodology, Validation, Visualization. **Giovanni Saudino:** Investigation, Methodology, Validation, Visualization. **Veronica Nasta:** Investigation, Validation. **Simone Ciofi-Baffoni:** Conceptualization, Supervision, Writing - original draft, Writing - review & editing, Funding acquisition. **Lucia Banci:** Conceptualization, Writing - review & editing, Project administration, Funding acquisition.

Acknowledgements

The authors acknowledge funding from timb3 (grant number 810856) and iNEXT-Discovery, Grant Agreement No. 871037, both funded by the Horizon 2020 programme of the European Commission. Financial support of the Fondazione Cassa di Risparmio di Firenze (CRF2018.0920) is also gratefully acknowledged. Work at CERM is

supported by the Italian Ministry for University and Research (FOE funding) to the Italian Center (CERM, University of Florence) of Instruct-ERIC, a European Research Infrastructure, ESFRI Landmark. This article is based upon work from COST Action CA15133, supported by COST (European Cooperation in Science and Technology).

Declaration of Competing Interest

The authors declare that they have no known competing financial interests or personal relationships that could have appeared to influence the work reported in this paper.

Appendix A. Supplementary material

Supplementary data to this article can be found online at https://doi.org/10.1016/j.jmb.2021.166924.

Received 10 November 2020;
Accepted 1 March 2021;
Available online 10 March 2021

Keywords:
iron-sulfur protein;
iron-sulfur cluster assembly machinery;
mitochondria;
NMR;
protein-protein interaction

† Equally contributed authors.

Abbreviations used:
Fe-S, Iron-sulfur; HSQC, Heteronuclear single quantum coherence; SEC-MALS, Size exclusion chromatography equipped with multiangle light scattering; LB, Luria-Bertani; IPTG, Isopropyl-β-D-1-thiogalactopyranoside; BSA, Bovine serum albumin; DTT, 1,4-dithiothreitol

References

1. Ciofi-Baffoni, S., Nasta, V., Banci, L., (2018). Protein networks in the maturation of human iron-sulfur proteins. *Metallomics*, **10**, 49–72.
2. Andreini, C., Banci, L., Rosato, A., (2016). Exploiting bacterial operons to illuminate human iron-sulfur proteins. *J. Proteome Res*, **15**, 1308–1322.
3. Muhlenhoff, U., Richter, N., Pines, O., Pierik, A.J., Lill, R., (2011). Specialized function of yeast Isa1 and Isa2 proteins in the maturation of mitochondrial [4Fe-4S] proteins. *J. Biol. Chem*, **286**, 41205–41216.
4. Sheftel, A.D., Wilbrecht, C., Stehling, O., Niggemeyer, B., Elsasser, H.P., Muhlenhoff, U., et al., (2012). The human mitochondrial ISCA1, ISCA2, and IBA57 proteins are required for [4Fe-4S] protein maturation. *Mol. Biol. Cell*, **23**, 1157–1166.
5. Schilke, B., Voisine, C., Beinert, H., Craig, E., (1999). Evidence for a conserved system for iron metabolism in the mitochondria of Saccharomyces cerevisiae. *Proc. Natl. Acad. Sci. USA*, **96**, 10206–10211.
6. Cameron, J.M., Janer, A., Levandovskiy, V., MacKay, N., Rouault, T.A., Tong, W.H., et al., (2011). Mutations in iron-sulfur cluster scaffold genes NFU1 and BOLA3 cause a fatal deficiency of multiple respiratory chain and 2-oxoacid dehydrogenase enzymes. *Am. J. Hum. Genet*, **89**, 486–495.
7. Navarro-Sastre, A., Tort, F., Stehling, O., Uzarska, M.A., Arranz, J.A., Del, T.M., et al., (2011). A fatal mitochondrial disease is associated with defective NFU1 function in the maturation of a subset of mitochondrial Fe-S proteins. *Am. J. Hum. Genet*, **89**, 656–667.
8. Kaut, A., Lange, H., Diekert, K., Kispal, G., Lill, R., (2000). Isa1p is a component of the mitochondrial machinery for maturation of cellular iron-sulfur proteins and requires conserved cysteine residues for function. *J. Biol. Chem*, **275**, 15955–15961.
9. Pelzer, W., Muhlenhoff, U., Diekert, K., Siegmund, K., Kispal, G., Lill, R., (2000). Mitochondrial Isa2p plays a crucial role in the maturation of cellular iron-sulfur proteins. *FEBS Letters*, **476**, 134–139.
10. Tong, W.H., Jameson, G.N., Huynh, B.H., Rouault, T.A., (2003). Subcellular compartmentalization of human Nfu, an iron-sulfur cluster scaffold protein, and its ability to assemble a [4Fe-4S] cluster. *Proc. Natl. Acad. Sci. USA*, **100**, 9762–9767.
11. Vinella, D., Brochier-Armanet, C., Loiseau, L., Talla, E., Barras, F., (2009). Iron-sulfur (Fe/S) protein biogenesis: phylogenomic and genetic studies of A-type carriers. *PLoS Genet*, **5**, e1000497
12. Mapolelo, D.T., Zhang, B., Naik, S.G., Huynh, B.H., Johnson, M.K., (2012). Spectroscopic and functional characterization of iron-sulfur cluster-bound forms of Azotobacter vinelandii (Nif)IscA. *Biochemistry*, **51**, 8071–8084.
13. Banci, L., Brancaccio, D., Ciofi-Baffoni, S., Del Conte, R., Gadepalli, R., Mikolajczyk, M., et al., (2014). [2Fe-2S] cluster transfer in iron-sulfur protein biogenesis. *Proc. Natl. Acad. Sci. USA*, **111**, 6203–6208.
14. Brancaccio, D., Gallo, A., Mikolajczyk, M., Zovo, K., Palumaa, P., Novellino, E., et al., (2014). Formation of [4Fe-4S] clusters in the mitochondrial iron-sulfur cluster assembly machinery. *J. Am. Chem Soc*, **136**, 16240–16250.
15. Wu, G., Mansy, S.S., Hemann, C., Hille, R., Surerus, K.K., Cowan, J.A., (2002). Iron-sulfur cluster biosynthesis: characterization of Schizosaccharomyces pombe Isa1. *J. Biol. Inorg. Chem*, **7**, 526–532.
16. Krebs, C., Agar, J.N., Smith, A.D., Frazzon, J., Dean, D.R., Huynh, B.H., et al., (2001). IscA, an alternate scaffold for Fe-S cluster biosynthesis. *Biochemistry*, **40**, 14069–14080.
17. Ollagnier-de-Choudens, S., Mattioli, T., Takahashi, Y., Fontecave, M., (2001). Iron-sulfur cluster assembly: characterization of IscA and evidence for a specific and functional complex with ferredoxin. *J. Biol. Chem*, **276**, 22604–22607.
18. Ollagnier-de Choudens, S., Nachin, L., Sanakis, Y., Loiseau, L., Barras, F., Fontecave, M., (2003). SufA from Erwinia chrysanthemi. Characterization of a scaffold protein required for iron-sulfur cluster. *J. Biol. Chem*, **278**, 17993–18001.
19. Beilschmidt, L.K., Ollagnier de Choudens, S., Fournier, M., Sanakis, I., Hograindleur, M.A., Clemancey, M., et al.,

(2017). ISCA1 is essential for mitochondrial Fe4S4 biogenesis in vivo. *Nature Commun.*, **8**, 15124.
20. Brancaccio, D., Gallo, A., Piccioli, M., Novellino, E., Ciofi-Baffoni, S., Banci, L., (2017). [4Fe-4S] Cluster Assembly in Mitochondria and Its Impairment by Copper. *J. Am. Chem. Soc*, **139**, 719–730.
21. Weiler, B.D., Brück, M.C., Kothe, I., Bill, E., Lill, R., Mühlenhoff, U., (2020). Mitochondrial [4Fe-4S] protein assembly involves reductive [2Fe-2S] cluster fusion on ISCA1-ISCA2 by electron flow from ferredoxin FDX2. *Proc. Natl. Acad. Sci. USA*, **117**, 20555–20565.
22. Talib, E.A., Outten, C.E., (2020). Iron-sulfur cluster biogenesis, trafficking, and signaling: roles for CGFS glutaredoxins and BolA proteins. *Biochim. Biophys. Acta Mol. Cell Res.*, **1868**, **118847**
23. Mapolelo, D.T., Zhang, B., Randeniya, S., Albetel, A.N., Li, H., Couturier, J., et al., (2013). Monothiol glutaredoxins and A-type proteins: partners in Fe-S cluster trafficking. *Dalton Trans*, **42**, 3107–3115.
24. Gourdoupis, S., Nasta, V., Calderone, V., Ciofi-Baffoni, S., Banci, L., (2018). IBA57 recruits ISCA2 to form a [2Fe-2S] cluster-mediated complex. *J. Am. Chem. Soc.*, **140**, 14401–14412.
25. Gourdoupis, S., Nasta, V., Ciofi-Baffoni, S., Banci, L., Calderone, V., (2019). In-house high-energy-remote SAD phasing using the magic triangle: how to tackle the P1 low symmetry using multiple orientations of the same crystal of human IBA57 to increase the multiplicity. *Acta Crystallogr. D Struct. Biol.*, **75**, 317–324.
26. Nasta, V., Da Vela, S., Gourdoupis, S., Ciofi-Baffoni, S., Svergun, D.I., Banci, L., (2019). Structural properties of [2Fe-2S] ISCA2-IBA57: a complex of the mitochondrial iron-sulfur cluster assembly machinery. *Sci Rep.*, **9**, 18986.
27. Torraco, A., Stehling, O., Stümpfig, C., Rösser, R., De Rasmo, D., Fiermonte, G., et al., (2018). ISCA1 mutation in a patient with infantile-onset leukodystrophy causes defects in mitochondrial [4Fe-4S] proteins. *Hum. Mol. Genet.*, **27**, 2739–2754.
28. Alaimo, J.T., Besse, A., Alston, C.L., Pang, K., Appadurai, V., Samanta, M., et al., (2018). Loss-of-function mutations in ISCA2 disrupt 4Fe-4S cluster machinery and cause a fatal leukodystrophy with hyperglycinemia and mtDNA depletion. *Hum. Mutat.*, **39**, 537–549.
29. Lossos, A., Stumpfig, C., Stevanin, G., Gaussen, M., Zimmerman, B.E., Mundwiller, E., et al., (2015). Fe/S protein assembly gene IBA57 mutation causes hereditary spastic paraplegia. *Neurology*, **84**, 659–667.
30. Py, B., Gerez, C., Angelini, S., Planel, R., Vinella, D., Loiseau, L., et al., (2012). Molecular organization, biochemical function, cellular role and evolution of NfuA, an atypical Fe-S carrier. *Mol. Microbiol*, **86**, 155–171.
31. Cai, K., Liu, G., Frederick, R.O., Xiao, R., Montelione, G.T., Markley, J.L., (2016). Structural/functional properties of human NFU1, an intermediate [4Fe-4S] carrier in human mitochondrial iron-sulfur cluster biogenesis. *Structure*, **24**, 2080–2091.
32. Li, J., Ding, S., Cowan, J.A., (2013). Thermodynamic and structural analysis of human NFU conformational chemistry. *Biochemistry*, **52**, 4904–4913.
33. Nasta, V., Suraci, D., Gourdoupis, S., Ciofi-Baffoni, S., Banci, L., (2020). A pathway for assembling [4Fe-4S](2+) clusters in mitochondrial iron-sulfur protein biogenesis. *FEBS J.*, **287**, 2312–2327.
34. Lill, R., Freibert, S.A., (2020). Mechanisms of mitochondrial iron-sulfur protein biogenesis. *Annu. Rev. Biochem.*, **89**, 471–499.
35. Melber, A., Na, U., Vashisht, A., Weiler, B.D., Lill, R., Wohlschlegel, J.A., et al., (2016). Role of Nfu1 and Bol3 in iron-sulfur cluster transfer to mitochondrial clients. *Elife*, **5**, **e15991**
36. Webert, H., Freibert, S.A., Gallo, A., Heidenreich, T., Linne, U., Amlacher, S., et al., (2014). Functional reconstitution of mitochondrial Fe/S cluster synthesis on Isu1 reveals the involvement of ferredoxin. *Nature Commun.*, **5**, 5013.
37. Gervason, S., Larkem, D., Mansour, A.B., Botzanowski, T., Müller, C.S., Pecqueur, L., et al., (2019). Physiologically relevant reconstitution of iron-sulfur cluster biosynthesis uncovers persulfide-processing functions of ferredoxin-2 and frataxin. *Nature Commun.*, **10**, 3566.
38. Jain, A., Singh, A., Maio, N., Rouault, T.A., (2020). Assembly of the [4Fe-4S] cluster of NFU1 requires the coordinated donation of two [2Fe-2S] clusters from the scaffold proteins, ISCU2 and ISCA1. *Hum. Mol. Genet.*, **29**, 3165–3182.
39. Cai, K., Frederick, R.O., Markley, J.L., (2020). ISCU interacts with NFU1, and ISCU[4Fe-4S] transfers its Fe-S cluster to NFU1 leading to the production of holo-NFU1. *J. Struct. Biol.*, **210**, **107491**
40. Sen, S., Rao, B., Wachnowsky, C., Cowan, J.A., (2018). Cluster exchange reactivity of [2Fe-2S] cluster-bridged complexes of BOLA3 with monothiol glutaredoxins. *Metallomics*, **10**, 1282–1290.
41. Nasta, V., Giachetti, A., Ciofi-Baffoni, S., Banci, L., (2017). Structural insights into the molecular function of human (2Fe-2S) BOLA1-GRX5 and (2Fe-2S) BOLA3-GRX5 complexes. *Biochim. Biophys. Acta*, **1861**, 2119–2131.
42. Freibert, S.A., Weiler, B.D., Bill, E., Pierik, A.J., Muhlenhoff, U., Lill, R., (2018). Biochemical reconstitution and spectroscopic analysis of iron-sulfur proteins. *Methods Enzymol*, **599**, 197–226.
43. Camponeschi, F., Prusty, N.R., Heider, S.A.E., Ciofi-Baffoni, S., Banci, L., (2020). GLRX3 acts as a [2Fe-2S] cluster chaperone in the cytosolic iron-sulfur assembly machinery transferring [2Fe-2S] Clusters to NUBP1. *J. Am. Chem. Soc.*, **142**, 10794–10805.
44. Banci, L., Ciofi-Baffoni, S., Mikolajczyk, M., Winkelmann, J., Bill, E., Pandelia, M.E., (2013). Human anamorsin binds [2Fe-2S] clusters with unique electronic properties. *J. Biol. Inorg. Chem*, **18**, 883–893.
45. Banci, L., Camponeschi, F., Ciofi-Baffoni, S., Muzzioli, R., (2015). Elucidating the molecular function of human BOLA2 in GRX3-dependent anamorsin maturation pathway. *J. Am. Chem. Soc*, **137**, 16133–16134.
46. Crack, J.C., den Hengst, C.D., Jakimowicz, P., Subramanian, S., Johnson, M.K., Buttner, M.J., et al., (2009). Characterization of [4Fe-4S]-containing and cluster-free forms of Streptomyces WhiD. *Biochemistry*, **48**, 12252–12264.
47. Bertini, I., Capozzi, F., Luchinat, C., Piccioli, M., (1993). ^{1}H NMR investigation of oxidized and reduced HiPIP from *R. globiformis*. *Eur. J. Biochem.*, **212**, 69–78.
48. Banci, L., Camponeschi, F., Ciofi-Baffoni, S., Piccioli, M., (2018). The NMR contribution to protein-protein networking in Fe-S protein maturation. *J. Biol. Inorg. Chem.*, **23**
49. Cheng, H., Markley, J.L., (1995). NMR spectroscopic studies of paramagnetic proteins: iron-sulfur proteins. *Annu. Rev. biophys. biomol. Struct*, **24**, 209–237.

50. Bertini, I., Briganti, F., Luchinat, C., Scozzafava, A., (1990). ^{1}H NMR studies of the oxidized and partially reduced 2 (4Fe-4S) ferredoxin from *Clostridium pasteurianum*. *Inorg. Chem.*, **29**, 1874–1880.
51. Banci, L., Bertini, I., Luchinat, C., (1990). The ^{1}H NMR parameters of magnetically coupled dimers - the Fe_2S_2 proteins as an example. *Struct. Bonding*, **72**, 113–135.
52. Muhlenhoff, U., Gerl, M.J., Flauger, B., Pirner, H.M., Balser, S., Richhardt, N., et al., (2007). The ISC proteins Isa1 and Isa2 are required for the function but not for the de novo synthesis of the Fe/S clusters of biotin synthase in Saccharomyces cerevisiae. *Eucaryotic Cell*, **6**, 495–504.
53. Lebigot, E., Gaignard, P., Dorboz, I., Slama, A., Rio, M., de Lonlay, P., et al., (2017). Impact of mutations within the [Fe-S] cluster or the lipoic acid biosynthesis pathways on mitochondrial protein expression profiles in fibroblasts from patients. *Mol. Genet. Metab.*, **122**, 85–94.
54. Ahting, U., Mayr, J.A., Vanlander, A.V., Hardy, S.A., Santra, S., Makowski, C., et al., (2015). Clinical, biochemical, and genetic spectrum of seven patients with NFU1 deficiency. *Front. Genet.*, **6**, 123.
55. Culley, M.K., Perk, D., Chan, S.Y., (2020). NFU1, iron-sulfur biogenesis, and pulmonary arterial hypertension: a (metabolic) shift in our thinking. *Am. J. Respir. Cell Mol. Biol.*, **62**, 136–138.
56. Banci, L., Bertini, I., Ciofi-Baffoni, S., Boscaro, F., Chatzi, A., Mikolajczyk, M., et al., (2011). Anamorsin is a 2Fe2S cluster-containing substrate of the Mia40-dependent mitochondrial protein trapping machinery. *Chem. Biol.*, **18**, 794–804.
57. Dailey, H.A., Finnegan, M.G., Johnson, M.K., (1994). Human ferrochelatase is an iron-sulfur protein. *Biochemistry*, **33**, 403–407.
58. Keller, R., (2004). The Computer Aided Resonance Assignment Tutorial. CANTINA Verlag, Goldau.
59. Fernández, C.O., Cricco, J.A., Slutter, C.E., Richards, J.H., Gray, H.B., Vila, A.J., (2001). Axial ligand modulation of the electronic structures of binuclear copper sites: analysis of paramagnetic 1H NMR spectra of Met160Gln Cu(A). *J. Am. Chem. Soc.*, **123**, 11678–11685.
60. Inubushi, T., Becker, E.D., (1983). Efficient detection of paramagnetically shifted NMR resonances by optimizing the WEFT pulse sequence. *J. Magn. Reson.*, **51**, 128–133.
61. Ciofi-Baffoni, S., Gallo, A., Muzzioli, R., Piccioli, M., (2014). The IR-^{15}N-HSQC-AP experiment: a new tool for NMR spectroscopy of paramagnetic molecules. *J. Biomol. NMR*, **58**, 123–128.

Supplementary Materials

ISCA1 orchestrates ISCA2 and NFU1 in the maturation of mitochondrial [4Fe-4S] proteins

Dafne Suraci [1,2,†], **Giovanni Saudino** [1,2,†], Veronica Nasta[1,2], Simone Ciofi-Baffoni[1,2,] Lucia Banci [1,2]

[1]Magnetic Resonance Center CERM, University of Florence, Via Luigi Sacconi 6, 50019, Sesto Fiorentino, Florence, Italy.

[2]Department of Chemistry, University of Florence, Via della Lastruccia 3, 50019 Sesto Fiorentino, Florence, Italy.

[†]Equally contributed authors.

Figure S1. SDS-PAGE of SEC peaks to identify the constituents of the protein complexes. 1. apo ISCA1; 2. apo NFU1; 3. diluted apo NFU1; 4. apo ISCA2; 5. peak of analytical size exclusion chromatography performed on [4Fe-4S] ISCA1-ISCA2 (red peak in Figure 5B); 6. peak of analytical size exclusion chromatography performed on a 1:1 apo NFU1-apo ISCA1 mixture (red peak in Figure 3B); 7. peak of analytical size exclusion chromatography performed on 1:1 apo ISCA2-apo ISCA1 mixture (red peak in Figure 2D).

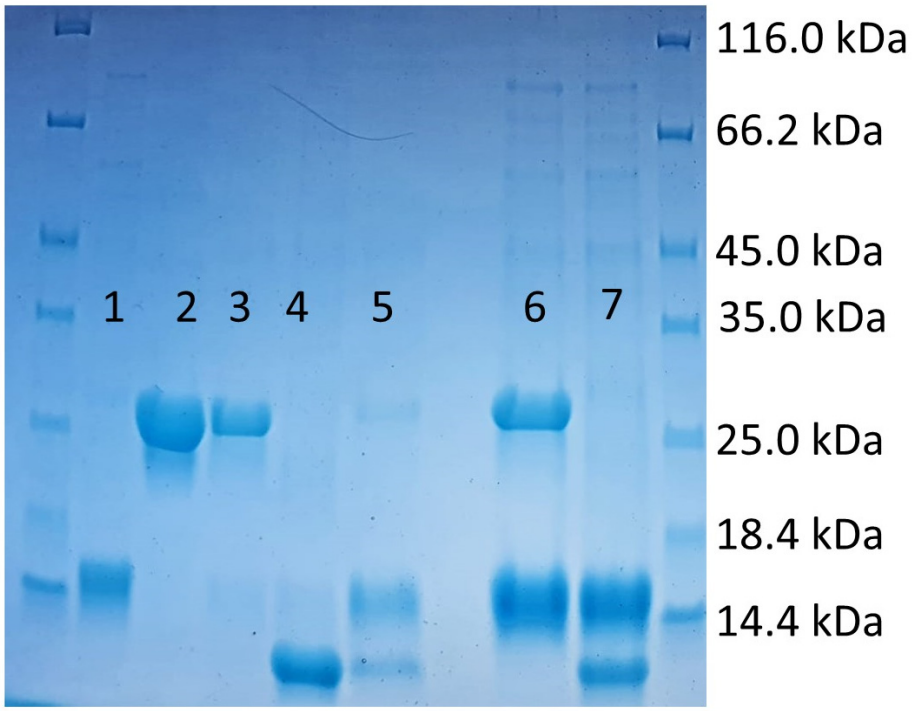

Figure S2. Apo ISCA1 and apo ISCA2 form a heterodimeric complex. Weighted-average chemical shift differences $\Delta\delta_{avg}$ (that is, $([(\delta_{HN})^2 + (\delta_N/5)^2]/2)^{1/2}$, where δ_{HN} and δ_N are chemical shift differences for ^{1}HN and ^{15}N, respectively) between apo ^{15}N-labeled ISCA2 alone and in a 1:1 mixture with unlabeled apo ISCA1. The cyan bars represent proline residues. The blue bars represent residues whose NHs are not detected or too broad to be analyzed. The dotted horizontal line indicates the threshold to consider chemical shift changes as meaningful (1σ $\Delta\delta_{avg} > 0.04$ ppm). In the inset, meaningful chemical shift changes for the backbone NHs of apo ^{15}N-labeled ISCA2 upon the addition of 1 equivalent of unlabeled apo ISCA1 are mapped on the structural model of monomeric ISCA2. In red are the sidechains of the residues showing meaningful chemical shift changes. The protein stretches in blue and cyan represent residues whose NHs are not detected or too broad to be analyzed and proline residues, respectively.

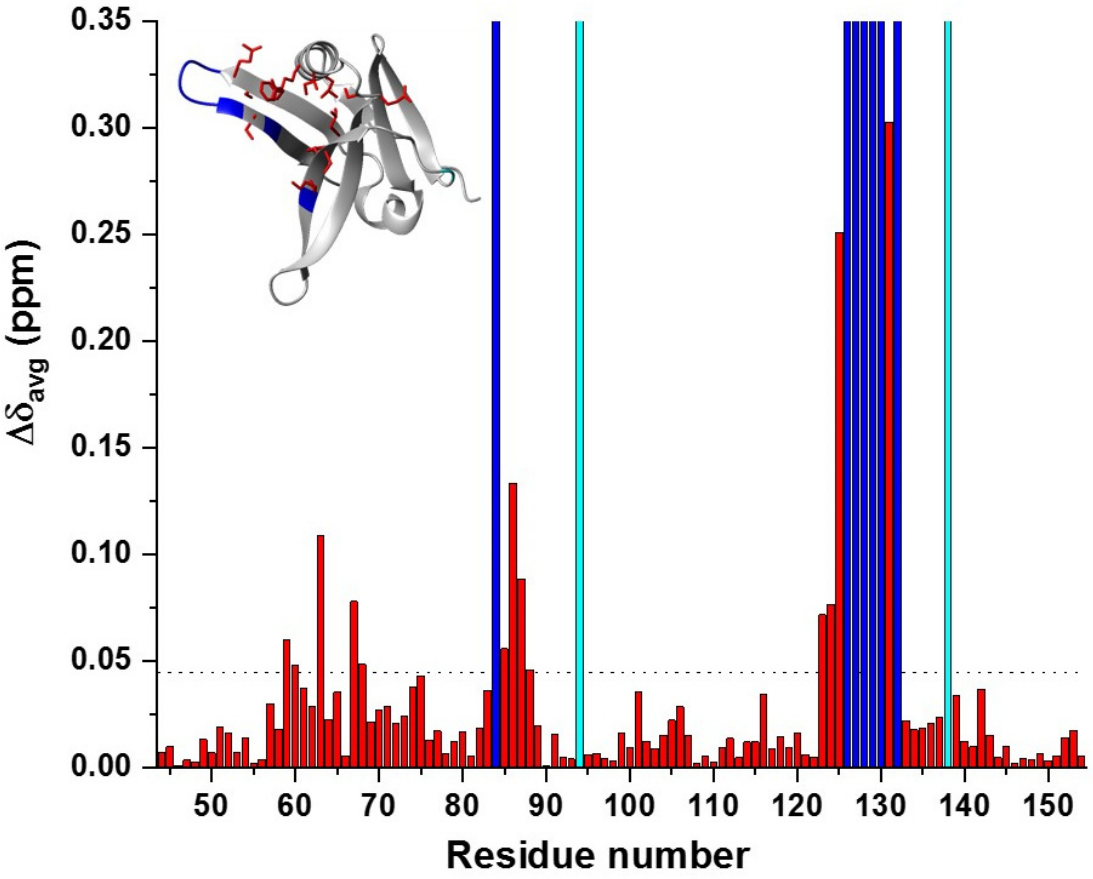

Figure S3. Apo ISCA1 interacts with the C-domain of apo NFU1 forming a heterodimeric complex. (**A**) Weighted-average chemical shift differences $\Delta\delta_{avg}$ (that is, $([(\delta_{HN})^2 + (\delta_N/5)^2]/2)^{1/2}$, where δ_{HN} and δ_N are chemical shift differences for ^{1}HN and ^{15}N, respectively) between apo ^{15}N NFU1 alone and in a 1:1 mixture with apo ISCA1. The cyan bars represent proline residues. The yellow bars represent residues whose NHs broaden beyond detection or are very broad upon additions of apo ISCA1. The dotted horizontal line indicates the threshold to consider chemical shift changes as meaningful ($1\sigma\ \Delta\delta_{avg} > 0.03$ ppm). (**B**) SEC-MALS of a 1:1 apo NFU1-apo ISCA1 mixture.

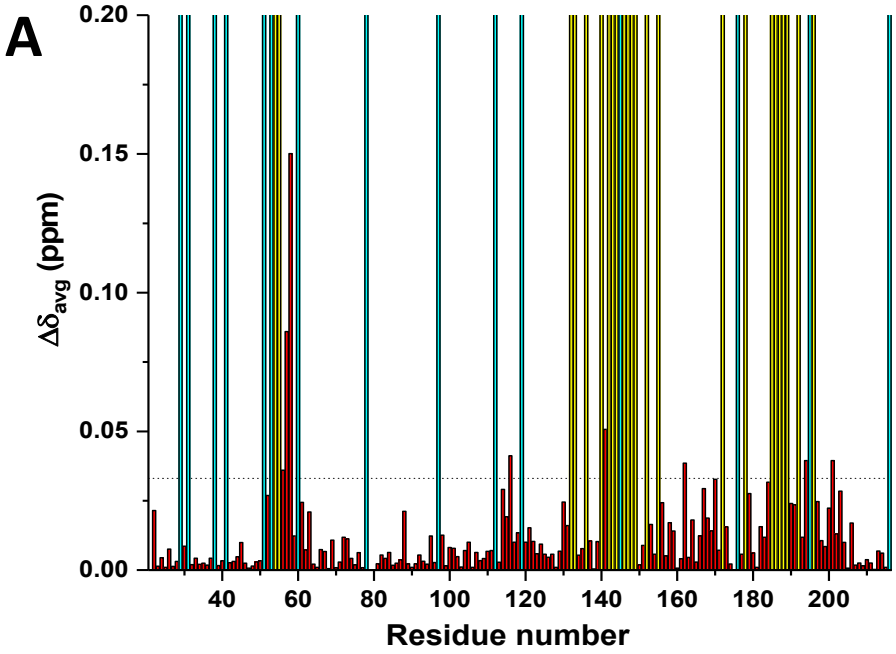

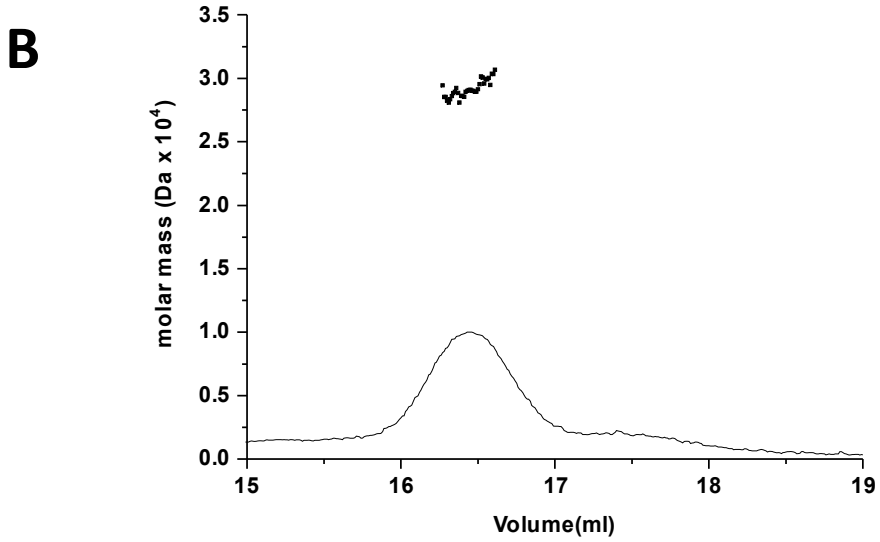

Figure S4. Apo ISCA1 promotes the formation of a ternary complex between apo ISCA2 and apo NFU1. A schematic cartoon depicting the NMR titration related to each panel is reported. (**A**) Overlay of the ^{1}H-^{15}N HSQC spectrum acquired on a 1:1:1 ^{15}N apo ISCA2-apo ^{15}N NFU1-apo ISCA1 mixture (black) with the ^{1}H-^{15}N HSQC spectra acquired on isolated apo ^{15}N NFU1 (red) and on a 1:1 apo ^{15}N NFU1 and apo ISCA1 mixture (green). (**B**) Overlay of the ^{1}H-^{15}N HSQC spectrum acquired on a 1:1:1 apo ^{15}N ISCA2-apo ^{15}N NFU1-apo ISCA1 mixture (black) with the ^{1}H-^{15}N HSQC spectra acquired on isolated apo ^{15}N ISCA2 (cyan) and on a 1:1 apo ^{15}N ISCA2-apo ISCA1 mixture (red). In the inset, an overlay of a region of the here overlapped ^{1}H-^{15}N HSQC spectra is shown. The arrow indicates a backbone NH signal of ISCA2 that monitors the formation of ISCA2 complexed with ISCA1 at the 1:1:1 mixture. The ^{1}H-^{15}N HSQC spectrum of the 1:1 apo ^{15}N NFU1-apo ISCA1 mixture is shown in green to identify in the inset the NH signals of NFU1 complexed with ISCA1.

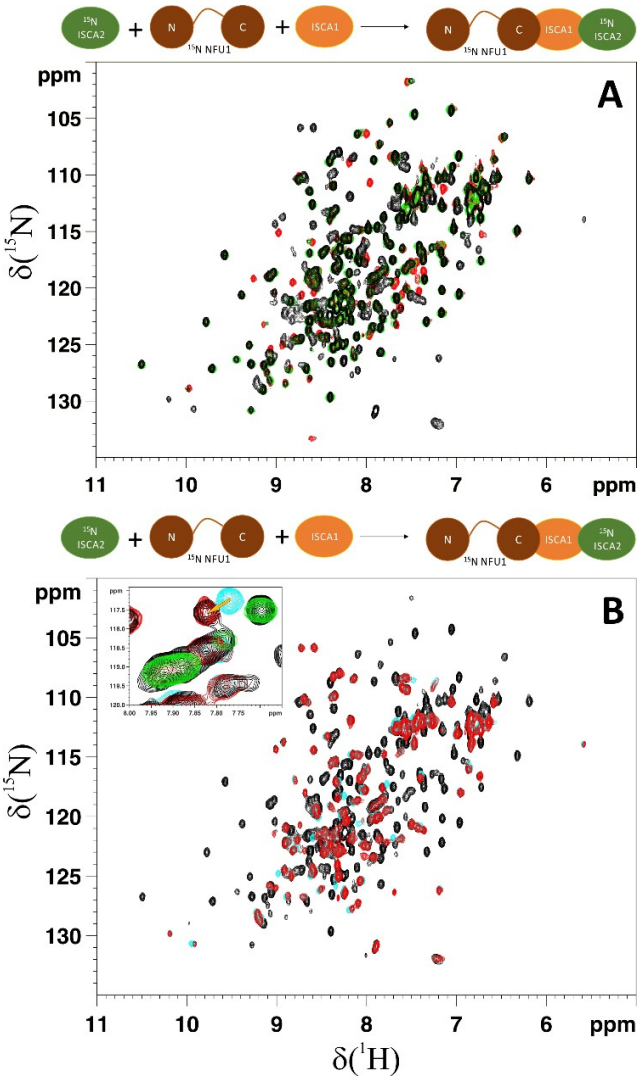

Figure S5. Dimeric ISCA1 binds [2Fe-2S]$^{2+}$ cluster. UV-visible (**A**) and CD-visible (**B**) absorption spectra of "as purified" (black), chemically reconstituted (red) ISCA1 and chemically reconstituted 1:1 ISCA1-ISCA2 mixture (green). (**C**) Analytical gel filtration of "as purified" ISCA1. Paramagnetic 1D ^{1}H NMR spectra of "as purified" (**D**) and chemically reconstituted (**E**) ISCA1 at 298 K. The signal-to-noise ratio of the NMR spectrum is worse in (E) than in (D) because the protein largely precipitates during the acquisition time of the NMR experiment in (E). All data were recorded in 50 mM phosphate buffer pH 7.0, 150 mM NaCl, 5 mM DTT.

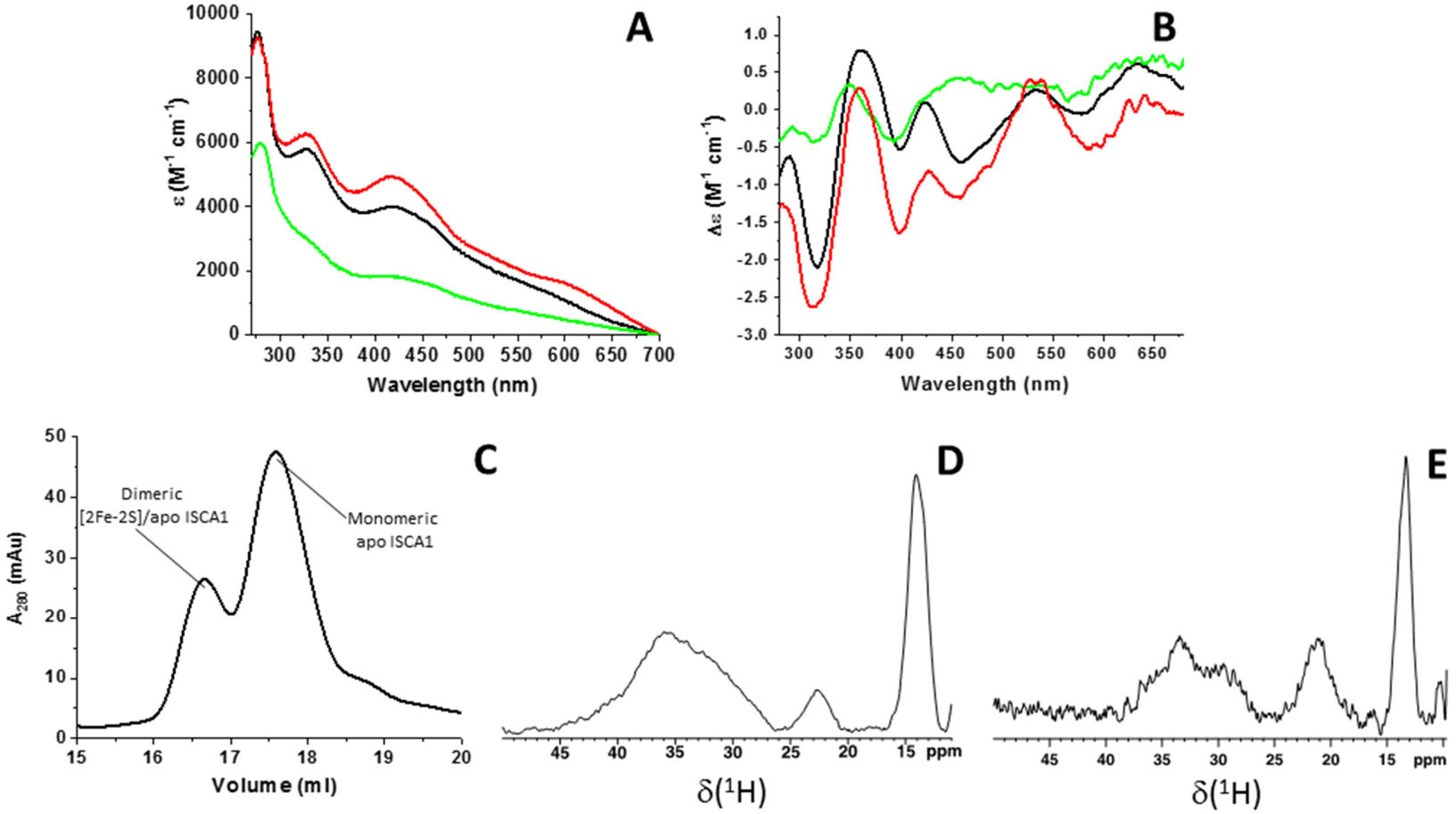

Figure S6. [4Fe-4S] ISCA1-ISCA2 interacts with apo NFU1 via its C-domain. A schematic cartoon depicting the NMR titration related to each panel is reported. (**A**) Overlay of the ^{1}H-^{15}N HSQC spectrum acquired on apo ^{15}N ISCA2-ISCA1 complex (red) with the ^{1}H-^{15}N HSQC spectrum acquired on a 1:1 mixture of [4Fe-4S] ^{15}N ISCA2-ISCA1 complex and C-domain of apo ^{15}N NFU1 (black). (**B**) Overlay of the ^{1}H-^{15}N HSQC spectrum acquired on the C-domain of apo ^{15}N NFU1 (red) with the ^{1}H-^{15}N HSQC spectrum acquired on a 1:1 mixture of [4Fe-4S] ^{15}N ISCA2-ISCA1 complex and C-domain of apo ^{15}N NFU1 (black). The residues of the C-domain of NFU1 whose backbone NH chemical shifts were affected (in terms of line broadening beyond detection effects and/or meaningful chemical shift changes) in the final mixture when compared to those of isolated apo NFU1 are indicated in the ^{1}H-^{15}N HSQC spectrum and are shown in the inset on the structure of the C-domain of NFU1 (PDB ID 2M5O) as orange sidechains. The sidechains of proline residues are shown in gray.

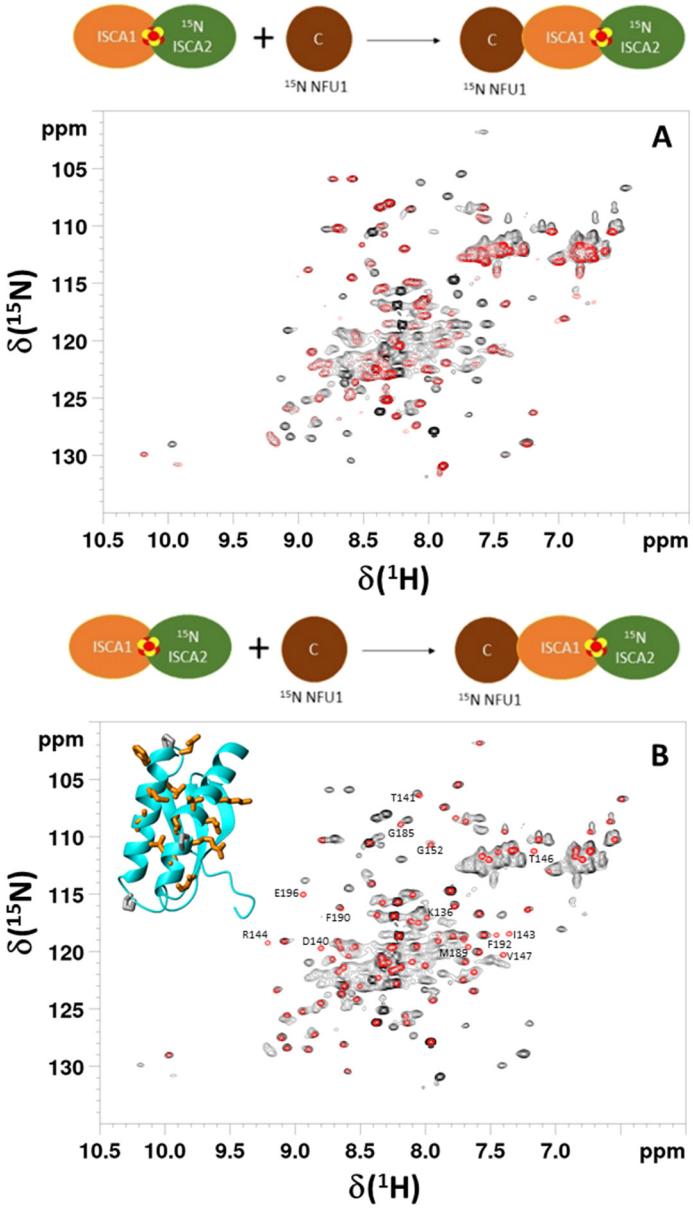

Figure S7. Temperature dependence of hyperfine-shifted signals of cluster ligands in the paramagnetic 1D ^{1}H NMR spectrum acquired on the 1:1 mixture of [4Fe-4S] ISCA1-ISCA2 and apo NFU1. The paramagnetic 1D ^{1}H NMR spectra were recorded on a Bruker NMR spectrometer operating at 400 MHz at 283 K (black) and 298 K (red) in degassed 50 mM phosphate, 150 mM NaCl buffer pH 7.0, and 5 mM DTT.

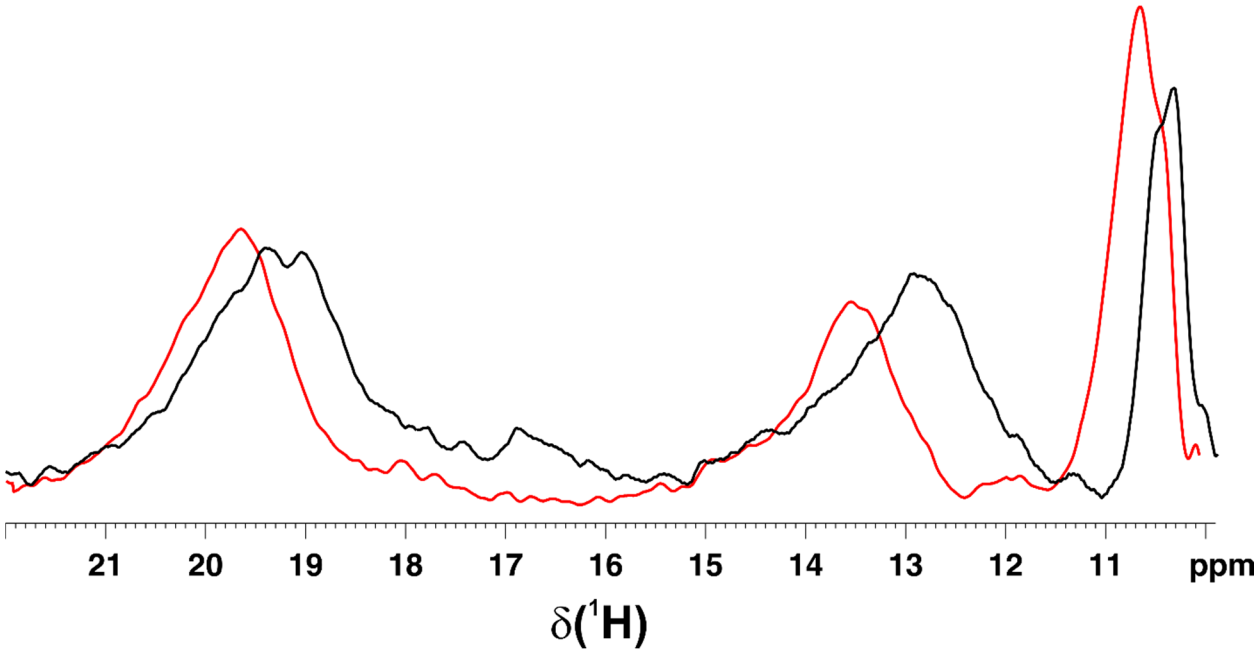

2.2 Molecular Basis of Multiple Mitochondrial Dysfunctions Syndrome 2 Caused by CYS59TYR BOLA3 Mutation

Giovanni Saudino [1,2,†], Dafne Suraci [1,2,†], Veronica Nasta[1,2], Simone Ciofi-Baffoni[1,2,] Lucia Banci [1,2]

[1]Magnetic Resonance Center CERM, University of Florence, Via Luigi Sacconi 6, 50019, Sesto Fiorentino, Florence, Italy.

[2]Department of Chemistry, University of Florence, Via della Lastruccia 3, 50019 Sesto Fiorentino, Florence, Italy.

[†]Equally contributed authors.

Published: 10.3390/ijms22094848

Abstract

Recently, a novel phenotype for MMDS2 with complete clinical recovery and partial resolution of the MRI abnormalities was reported for a patient[69]. Whole genome sequencing on the latter MMDS2 patient identified heterozygous variants in BOLA3: one previously reported (c.136C > T, p.Arg46*, paternally inherited[71,72]) and one novel variant (c.176G > A, p.Cys59Tyr, maternally inherited). These heterozygous variants determined a much milder phenotype with respect to homozygous c.136C > T (p.Arg46*) variants reported by Baker et al. in three unrelated patients[72]. The essential discrepancy is the different life span: while the phenotypes at 18 months are comparable, the grown patients (after 8 years old) regained normal neurological and cognitive functions until a complete clinical recovery only in the heterozygous BOLA3 variants. Cysteine-59 in BOLA3 was shown to be a coordinating ligand of a $[2Fe–2S]^{2+}$ cluster bound to a hetero-dimeric complex formed by BOLA3 and its protein partner GLRX5[66]. Specifically, the $[2Fe–2S]^{2+}$ cluster is bridged between the two proteins being coordinated, from the GLRX5 side, by Cysteine 67 and by the cysteine of a GLRX5-bound glutathione (GSH) molecule, and, from the BOLA3 side, by Cys59 and His96. The aim of this work was to unravel the molecular basis of the Cys59Tyr BOLA3 pathogenic mutation in MMDS2 in order to rationalize its novel and unique phenotype, never documented before in MMDS, i.e., associated with a complete clinical recovery. To do so, we first investigated the structural impact of the Cys59Tyr mutation on BOLA3 by NMR, and then we analysed the mutation impact on BOLA3–GLRX5 complex formation and on the hetero-complex cluster-binding properties, through various spectroscopic techniques, including NMR, UV–vis Circular dichroism, UV–vis and fluorescence spectroscopies, as well as by experimentally-driven molecular docking. The ^{1}H ^{15}N HSQC spectrum of ^{15}N labeled C59Y BOLA3 mutant showed, indeed, a well-folded protein, in agreement with all the cross-peaks having wide dispersions and sharp linewidths. The $^{1}H–^{15}N$ HSQC spectrum of ^{15}N-labeled C59Y BOLA3 showed some differences when compared to that of the wild-type protein, but the same protein fold was maintained. Successively, the Cys59Tyr mutation impact on the GLRX5-BOLA3 complex formation and on the [2Fe-2S] cluster binding and trafficking was investigated. All the observed spectroscopic data were consistent with the presence of a $[2Fe–2S]^{2+}$ cluster bound to the Cys59Tyr BOLA3–GLRX5 complex, as it occurred in the wild-type hetero-complex. However, they also showed that the Cys59Tyr mutation determined a perturbation in the chemical environment of the $[2Fe–2S]^{2+}$ cluster due to the absence of the Cysteine 59 iron sulfur cluster ligand. In order to further examine the potential involvement of Tyr59 in cluster-binding in place of Cys59, we performed fluorescence emission spectroscopy, which has been extensively applied to discriminate between a tyrosine having a protonated or a deprotonated phenolic side-chain group in proteins. The

acquired fluorescence emission data strongly support the idea that Tyr59 is not involved in the [2Fe-2S] cluster coordination. Finally, considering that we have recently shown the transfer of $[2Fe–2S]^{2+}$ clusters bound to BOLA3–GLRX5 to apo NFU1 to form a $[4Fe–4S]^{2+}$ cluster-bound NFU1 dimer[37], we investigated by NMR the effect of the Cys59Tyr mutation on this process. Specifically, by replicating on the Cys59Tyr mutant the $^{1}H–^{15}N$ HSQC NMR experiments previously performed on the wild-type protein[37], we found that, although the [4Fe–4S] cluster assembly on NFU1 was not abolished, a significant lower efficiency was observed for the mutant with respect to the wild-type protein. Specifically, the amount of [4Fe–4S] NFU1 that was formed in the final mixture was 25% (C59Y mutant) vs. 65% (wild type). Concluding, we have shown that the mutation structurally perturbed the iron–sulfur cluster-binding region of BOLA3, but without abolishing $[2Fe–2S]^{2+}$ cluster-binding on the hetero-complex; tyrosine 59 did not replace cysteine 59 as iron–sulfur cluster ligand; and the mutation promoted the formation of an aberrant apo C59Y BOLA3–GLRX5 complex. All these aspects allowed us to rationalize the unique phenotype observed in MMDS2 caused by Cys59Tyr mutation.

International Journal of
Molecular Sciences

Article

Molecular Basis of Multiple Mitochondrial Dysfunctions Syndrome 2 Caused by CYS59TYR BOLA3 Mutation

Giovanni Saudino [1,†], Dafne Suraci [1,†], Veronica Nasta [1], Simone Ciofi-Baffoni [1,2,*] and Lucia Banci [1,2,3,*]

[1] Magnetic Resonance Center (CERM), University of Florence, 50019 Sesto Fiorentino, Italy; saudino@cerm.unifi.it (G.S.); dafne.suraci@gmail.com (D.S.); nasta.veronica@gmail.com (V.N.)
[2] Department of Chemistry "Ugo Schiff", University of Florence, 50019 Sesto Fiorentino, Italy
[3] Consorzio Interuniversitario Risonanze Magnetiche di Metalloproteine (CIRMMP), 50019 Sesto Fiorentino, Italy
* Correspondence: ciofi@cerm.unifi.it (S.C.-B.); banci@cerm.unifi.it (L.B.)
† These authors contributed equally to this work.

Abstract: Multiple mitochondrial dysfunctions syndrome (MMDS) is a rare neurodegenerative disorder associated with mutations in genes with a vital role in the biogenesis of mitochondrial [4Fe–4S] proteins. Mutations in one of these genes encoding for BOLA3 protein lead to MMDS type 2 (MMDS2). Recently, a novel phenotype for MMDS2 with complete clinical recovery was observed in a patient containing a novel variant (c.176G > A, p.Cys59Tyr) in compound heterozygosity. In this work, we aimed to rationalize this unique phenotype observed in MMDS2. To do so, we first investigated the structural impact of the Cys59Tyr mutation on BOLA3 by NMR, and then we analyzed how the mutation affects both the formation of a hetero-complex between BOLA3 and its protein partner GLRX5 and the iron–sulfur cluster-binding properties of the hetero-complex by various spectroscopic techniques and by experimentally driven molecular docking. We show that (1) the mutation structurally perturbed the iron–sulfur cluster-binding region of BOLA3, but without abolishing $[2Fe–2S]^{2+}$ cluster-binding on the hetero-complex; (2) tyrosine 59 did not replace cysteine 59 as iron–sulfur cluster ligand; and (3) the mutation promoted the formation of an aberrant apo C59Y BOLA3–GLRX5 complex. All these aspects allowed us to rationalize the unique phenotype observed in MMDS2 caused by Cys59Tyr mutation.

Keywords: BOLA3; GLRX5; multiple mitochondrial dysfunctions syndrome; iron–sulfur protein; mitochondria; MMDS2

check for updates

Citation: Saudino, G.; Suraci, D.; Nasta, V.; Ciofi-Baffoni, S.; Banci, L. Molecular Basis of Multiple Mitochondrial Dysfunctions Syndrome 2 Caused by CYS59TYR BOLA3 Mutation. *Int. J. Mol. Sci.* 2021, 22, 4848. https://doi.org/10.3390/ijms22094848

Academic Editor: Paola Costantini

Received: 24 March 2021
Accepted: 28 April 2021
Published: 3 May 2021

1. Introduction

Multiple mitochondrial dysfunctions syndrome (MMDS) is a rare, severe autosomal recessive disorder of the energy metabolism with onset in early infancy, characterized by markedly impaired neurological development, weakness, respiratory failure, lactic acidosis, hyperglycinemia, and early fatality [1–4]. Mutations in genes encoding for NFU1, BOLA3, IBA57, ISCA2, and ISCA1 proteins lead to MMDS types 1 to 5, respectively. All these five genes play an essential role in the biogenesis of mitochondrial [4Fe–4S] cluster-binding proteins [5–10], which, in humans, consist of the respiratory chain complexes I and II, aconitase, the lipoic acid synthase, the molybdenum cofactor biosynthesis protein 1, and the electron transfer flavoprotein-ubiquinone oxidoreductase involved in the β-oxidation of lipids [2]. Thus, MMDS types 1–5 induce impairment of cellular respiration and lipoic acid metabolism [5,6,8].

Bi-allelic variants in BOLA3 cause MMDS type 2 with hyperglycinaemia (MMDS2; MIM#614299), typically characterized by infantile encephalopathy, leukodystrophy, lactic acidosis, non-ketotic hyperglycinemia and death in early childhood [5,7,11]. Six missense and six non-sense disease-causing variants in BOLA3 have been identified to date in patients affected by MMDS2 [5,7,11–21]. Recently, a novel phenotype for MMDS2 with

complete clinical recovery and partial resolution of magnetic resonance imaging abnormality was observed in a patient [18]. Whole genome sequencing on the latter MMDS2 patient identified compound heterozygous variants in BOLA3: one previously reported (c.136C > T, p.Arg46*, paternally inherited [7,12]) and one novel variant (c.176G > A, p.Cys59Tyr, maternally inherited). These heterozygous variants determine a much milder phenotype with respect to homozygous c.136C > T (p.Arg46*) variants reported by Baker et al. in three unrelated patients [7]. The essential discrepancy is the different life span: while the phenotypes at 18 months are comparable, the grown patient (after 8 years old) regained normal neurological and cognitive function until a complete clinical recovery only in the heterozygous BOLA3 variants.

Cysteine-59 in BOLA3 was shown to be a coordinating ligand of a $[2Fe–2S]^{2+}$ cluster bound to a hetero-dimeric complex formed by BOLA3 and its protein partner GLRX5 [22]. Specifically, the $[2Fe–2S]^{2+}$ cluster is bridged between the two proteins being coordinated, from the GLRX5 side, by Cys67 and by the cysteine of a GLRX5-bound glutathione (GSH) molecule, and, from the BOLA3 side, by Cys59 and His96. A combination of in vitro and in vivo studies support that BOLA3 complexed with GLRX5 could function in [2Fe–2S] cluster trafficking and/or insertion reactions in the mitochondrial iron–sulfur protein biogenesis [23]. Recently, the BOLA3–GLRX5 complex in its $[2Fe–2S]^{2+}$ bound state was shown to transfer the cluster to both apo human ferredoxins FDX1 and FDX2 with rate constants comparable to other cluster donors to FDX proteins [24,25], as well as to transfer its cluster to apo NFU1 to form a $[4Fe–4S]^{2+}$ cluster-bound NFU1 dimer [26]. However, considering that the yeast homologue of human BOLA3 was shown not to be required for the maturation of mitochondrial [2Fe–2S] proteins [23], the cluster transfer to FDXs is very likely not physiologically relevant. On the contrary, the BOLA3-driven cluster assembly on NFU1 is supported by in vivo studies. NFU1 is the protein of the mitochondrial iron-sulfur cluster (ISC) assembly machinery implicated in inserting the $[4Fe–4S]^{2+}$ cluster into specific mitochondrial client proteins, i.e., lipoic acid synthase and components of respiratory complexes I and II [6,27,28]. Recently, a molecular view of how NFU1 cooperates with ISCA1 and ISCA2 proteins in the maturation of mitochondrial [4Fe–4S] proteins has been defined [29]. MMDS type 1 patients harboring a frame-shift mutation in the NFU1 gene presented with a biochemical phenotype similar to BOLA3-deficient individuals affected by MMDS2 [30–32], suggesting that the two proteins take part to the same cellular pathway, in agreement with the in vitro BOLA3–GLRX5–NFU1-dependent pathway previously reported [26]. Following this molecular picture, the impairment of the latter [4Fe–4S] protein assembly pathway, caused by the pathogenic mutations found in MMDS1 and MMDS2, might explain the cellular functional defects associated to the lack of an efficient biogenesis of lipoic acid synthase and components of respiratory complexes I and II [5]. However, BOLA3 and NFU1 were also implicated at another stage of the mitochondrial ISC machinery that does not involve GLRX5. Indeed, BOLA3 was proposed to drive the transfer of the $[4Fe–4S]^{2+}$ cluster bound to NFU1 into specific mitochondrial target proteins [28]. On the other hand, the interaction between NFU1 and BOLA3 was not clearly detected in vivo [28], and recent in vitro data showed that BOLA3 and NFU1 do not interact each other in both apo and holo forms [24,26]. Thus, these in vitro data suggest that BOLA3 might be not involved at this stage of the mitochondrial ISC assembly machinery, but only when it works in the complex with GLRX5.

The aim of this work was to unravel the molecular basis of the Cys59Tyr BOLA3 pathogenic mutation in MMDS2 in order to comprehend its novel and unique phenotype never documented in MMDS, i.e., associated with a complete clinical recovery. To do so, we first investigated the structural impact of the Cys59Tyr mutation on BOLA3 by NMR, and then we analyzed how the mutation impacts on BOLA3–GLRX5 complex formation and on the hetero-complex cluster-binding properties by various spectroscopic techniques, including NMR, UV–VIS circular dichroism, UV–VIS and fluorescence spectroscopies, as well as by experimentally driven molecular docking. We show that 1) the mutation does not modify the overall structure of BOLA3, but it structurally perturbs the iron–sulfur

(Fe–S) cluster-binding region; 2) the mutation promotes the formation of an aberrant apo C59Y BOLA3–GLRX5 complex structurally different from that formed by the wild-type proteins; 3) although the mutation does not abolish $[2Fe\text{-}2S]^{2+}$ cluster-binding on the hetero-complex, it determines a perturbation in the chemical environment of the $[2Fe\text{–}2S]^{2+}$ cluster due to the lack of the Cys59 Fe–S cluster ligand, which it is not replaced by the tyrosine. All these aspects allowed us to rationalize the unique phenotype observed for the Cys59Tyr BOLA3 pathogenic mutation in MMDS2.

2. Results

2.1. Cys59Tyr Mutation Structurally Perturbed Only the Fe–S Cluster-Binding Region of BOLA3

The pathogenic mutation of cysteine-59 to a tyrosine did not drastically affect the structural properties of BOLA3 protein. The ^{1}H–^{15}N HSQC spectrum of ^{15}N labelled Cys59Tyr BOLA3 mutant (C59Y BOLA3, hereafter) showed, indeed, a well-folded protein, in agreement with all the cross-peaks having wide dispersions and sharp linewidths (Figure 1A). The ^{1}H–^{15}N HSQC spectrum of ^{15}N-labelled C59Y BOLA3 experienced some differences when compared to that of the wild-type protein, but the same protein fold was maintained (Figure 1A). The backbone chemical shift differences between wild-type and C59Y BOLA3 proteins indicated that the Cys59Tyr mutation in BOLA3 affected some residues of the loop containing the mutation and the spatially close, fully conserved His96 (Figure 1B), which is the other [2Fe–2S] cluster ligand of BOLA3 in the BOLA3–GLRX5 hetero-dimeric complex [22]. When, in a previous study [22], Cys59 was mutated to Ala, the residues with significant backbone chemical shift differences were similar (when calculated applying the same chemical shift threshold value of 0.06 on both C59A and C59Y BOLA3 mutants). The only differences consisted of two less residues perturbed in the loop containing the mutation, once Ala 59 was present, and of the loop containing the His96 ligand that was not perturbed by the C59A mutation. This indicates that the introduction of a tyrosine with respect to an alanine perturbed slightly more the local structural environment of the cluster-binding region of BOLA3, in agreement with the bulky steric hindrance of the tyrosine vs. that of the alanine that has a steric hindrance similar to that of the cysteine.

In conclusion, the NMR data showed that the Cys59Tyr mutation did not affect the protein fold, but that only the Fe–S cluster-binding region resulted in being structurally perturbed.

2.2. Cys59Tyr BOLA3 Mutation Modified the Interaction of BOLA3 with Apo GLRX5

BOLA3 is known to form a hetero-dimeric complex with apo GLRX5 with an affinity constant of 1.2×10^{5} M^{-1} [22–25]. To test whether the Cys59Tyr mutation affected the formation of the apo BOLA3–GLRX5 complex, we stepwise added apo GLRX5 to ^{15}N-labelled C59Y BOLA3, or vice versa adding C59Y BOLA3 to apo ^{15}N-labelled GLRX5, and the interaction was followed through ^{1}H–^{15}N HSQC NMR experiments (see the Materials and Methods section for details). Spectral changes occurred on both titrations, and the NMR signals of the free and the bound proteins were in fast and intermediate exchange regimes relative to the NMR time scale (Figure 2). These data indicate that the Cys59Tyr mutation did not impair apo hetero-complex formation. Moreover, the NMR titration data (see the Materials and Methods section for details) showed that the two proteins interacted both in the absence and in the presence of GSH, and that GSH, which bound to the GLRX5 subunit of the hetero-complex, was involved at the protein–protein interface, as it occurred for the wild-type protein.

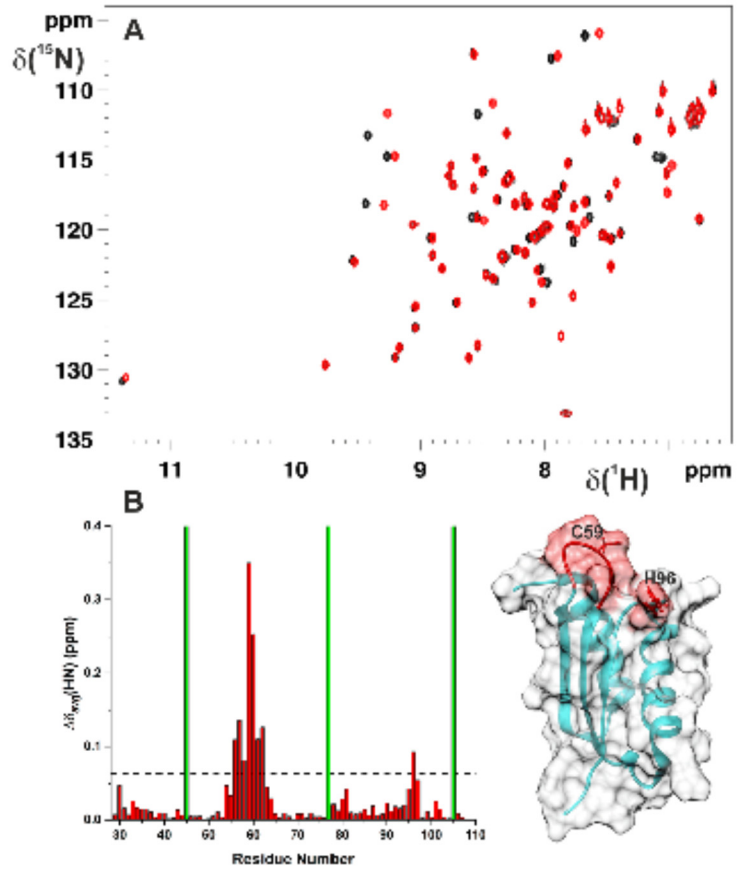

Figure 1. C59Y mutation structurally perturbed only the Fe–S cluster-binding region of BOLA3. (**A**) Overlay of the $^{1}H-^{15}N$ HSQC spectra of ^{15}N-labelled BOLA3 (black) and ^{15}N-labelled C59Y BOLA3 (red). The $^{1}H-^{15}N$ HSQC spectra were acquired at 298 K in 150 mM NaCl, 5 mM GSH, 5 mM DTT, 50 mM phosphate buffer (pH 7.0), and 10% (*v/v*) D_2O. (**B**) Backbone weighted average chemical shift differences ($\Delta\delta_{avg}$(HN)) between BOLA3 and C59Y BOLA3. A chemical shift threshold value of 0.06, indicated as a dashed line, was estimated to define meaningful chemical shift differences (see the Materials and Methods section). The green bars indicate proline residues or unassigned NHs. The meaningful chemical shift differences are mapped in red on the solution structure of BOLA3 (PDB 2NCL). The side-chains of Cys59 and His96 Fe–S cluster ligands are depicted in red sticks.

As following step, chemical shift perturbations and line broadening analyses were performed by comparing the $^{1}H-^{15}N$ HSQC spectra of ^{15}N-labelled BOLA3 and ^{15}N-labelled C59Y BOLA3, respectively, with those recorded in presence of equimolar amounts of apo GLRX5, at two different starting concentrations of ^{15}N-labelled BOLA3 and ^{15}N-labelled C59Y BOLA3 (100 and 800 µM). The observed spectral changes were then mapped on the solution structures of BOLA3 (PDB 2NCL) and on a structural model of C59Y BOLA3, obtained by homology modelling through MODELLER 9.10 software followed by energy minimization in water through AMBER 12.0 program (see the Materials and Methods section for details).

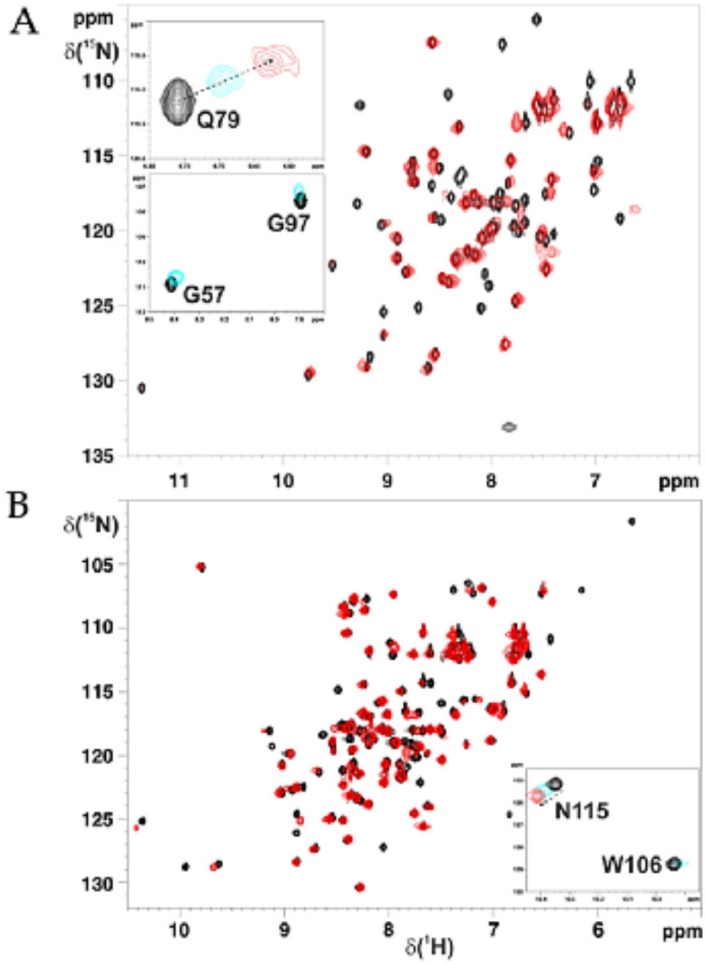

Figure 2. NMR showed apo hetero-complex formation between C59Y BOLA3 and GLRX5. (**A**) Overlay of the $^{1}H-^{15}N$ HSQC spectra of ^{15}N-labelled C59Y BOLA3 (starting protein concentration 800 μM, black) and of a 1:1 ^{15}N-labelled C59Y BOLA3-unlabelled apo GLRX5 mixture (red). In the insets, the overlay of $^{1}H-^{15}N$ HSQC spectra of ^{15}N-labelled C59Y BOLA3 at 0.0 (black), 0.5 (cyano), and 1.0 (red) equivalents of unlabeled apo GLRX5 is reported, showing backbone NHs of residues in fast (Q79) and intermediate (G57 and G97) exchange regimes relative to the NMR time scale. (**B**) Overlay of the $^{1}H-^{15}N$ HSQC spectra of ^{15}N-labelled apo GLRX5 (starting protein concentration 800 μM, black) and of a 1:1 ^{15}N-labelled apo GLRX5-unlabelled C59Y BOLA3 mixture (red). In the inset, the overlay of $^{1}H-^{15}N$ HSQC spectra of ^{15}N-labelled apo GLRX5 at 0.0 (black), 0.5 (cyano), and 1.0 (red) equivalents of unlabeled apo C59Y BOLA3 is reported, showing backbone NH of N115 in a fast exchange regime relative to the NMR time scale and the NH of the indole ring of W106 in an intermediate exchange regime relative to the NMR time scale. The $^{1}H-^{15}N$ HSQC spectra were acquired at 298 K in 150 mM NaCl, 5 mM GSH, 5 mM DTT, 50 mM phosphate buffer (pH 7.0), and 10% (*v*/*v*) D_2O.

In the titrations performed at 100 µM protein concentration, the spectral analyses showed that very similar interacting regions were identified on both BOLA3 proteins, i.e., wild-type and Cys59Tyr mutant (Figure 3A,B, respectively). These regions included helix α_2; strand β_3; the loop connecting the latter two elements, which contains His96 Fe–S cluster ligand; and a few residues following the Cys59 Fe–S cluster ligand (Figure 3A,B). Comparing the chemical shifts of the backbone NH signals that were in fast exchange on the NMR time scale on the $^{1}H-^{15}N$ HSQC spectra of ^{15}N-labelled BOLA3 and ^{15}N-labelled C59Y BOLA3 acquired at the final 1:1 ratio, we found that they had the same values, suggesting that the hetero-complex was formed in both cases at the same level and thus that the Cys59Tyr mutation of BOLA3 did not significantly affect the affinity relative to hetero-complex formation with apo GLRX5. This was confirmed by an NMR titration, where a 1:1 ^{15}N-labelled BOLA3-^{15}N-labelled C59Y BOLA3 mixture was titrated with unlabeled apo GLRX5. Indeed, in the latter experiment, we were able to follow the stepwise interaction of apo GLRX5 concomitantly occurring with both ^{15}N-labelled BOLA3 and ^{15}N-labelled C59Y BOLA3, mixed at a 1:1 ratio. We found that apo GLRX5 interacted at the same extent with both BOLA3 proteins from substoichiometric ratios up to when the final 2:1 ratio was reached, indicating that the added apo GLRX5 was equally partitioned between the two BOLA3 proteins along the additions (Supplementary Figure S1).

The spectral analysis performed at 800 µM starting protein concentration also showed that, in addition to the interacting regions mentioned above in the titrations performed at 100 µM protein concentration, the loop of BOLA3 containing Cys59Tyr mutation was also affected in the C59Y BOLA3–GLRX5 interaction, experiencing all its backbone NHs line broadening beyond detection, while the same loop was not involved in the wild-type BOLA3–GLRX5 interaction (Figure 3C,D). This result indicates that the Cys59Tyr mutation can promote the formation of an aberrant interaction in the hetero-complex characterized by protein–protein contacts that involve the loop region containing the Cys59Tyr mutation and that are not present in the wild-type protein–protein interaction.

Spectral changes were also analyzed on the $^{1}H-^{15}N$ HSQC map of ^{15}N-labelled apo GLRX5 at a starting protein concentration of 800 µM upon the interaction with BOLA3 or C59Y BOLA3 and mapped on the solution structure of GSH-bound GLRX5 (PDB 2WUL) (Figure 4). Similar interaction regions were observed in both wild-type and C59Y BOLA3–GLRX5 titrations. They involved the residues in contact with GSH and with the Cys67 Fe–S cluster ligand of GLRX5, indicating that GLRX5 interacted with both BOLA3 and C59Y BOLA3 proteins via the same Fe–S cluster binding site region (Figure 4). However, a higher number of signals of GLRX5, which specifically display line broadening beyond signal detection, were observed in the Cys59Tyr BOLA3 mutant interaction with respect to the wild-type BOLA3 interaction (Figure 4), similarly to what was observed on the BOLA3 side (Figure 3C,D).

In order to structurally visualize the aberrant protein–protein interaction induced by the Cys59Tyr mutation, we carried out a protein–protein docking modeling to obtain the structural models of apo BOLA3–GLRX5 and apo C59Y BOLA3–GLRX5 complexes, using, as experimental data, the chemical shift perturbations observed on C59Y BOLA3, BOLA3, and apo GLRX5 proteins for the NMR titrations performed at 800 µM starting protein concentration. Structural models of apo BOLA3–GLRX5 and apo C59Y BOLA3–GLRX5 complexes were calculated following the standard protocol of HADDOCK 2.2 docking program [33,34] and considering the GSH Fe–S cluster ligand bound to GLRX5, according to what has been previously reported [22] (see the Materials and Methods section for details). The docking models were clustered on the basis of common contacts following the standard HADDOCK scoring approach [35] (Supplementary Figure S2). From the comparison of the two best models, we found that once the GLRX5 structure in the two hetero-complexes was superimposed, it appeared that C59Y BOLA3 had a different orientation with respect to BOLA3, with the latter hetero-complex being more compact than that with C59Y BOLA3 (Figure 5). Specifically, the loop between the β1 and β2 strands, where Tyr59 of C59Y BOLA3 was located, became closer to the [2Fe–2S] cluster ligands of GLRX5 (Cys67 and

GSH), with respect to what occurred for Cys59 of BOLA3 in the BOLA3–GLRX5 complex. Overall, these NMR-based docking models showed that the Cys to Tyr mutation triggered a close interaction between the C59Y-mutated loop and the Fe–S cluster ligands of GLRX5. This turned out in a significant alteration of the structural arrangement in the apo C59Y BOLA3–GLRX5 complex, which is, indeed, less compact and more elongated with respect to that of the wild-type hetero-complex.

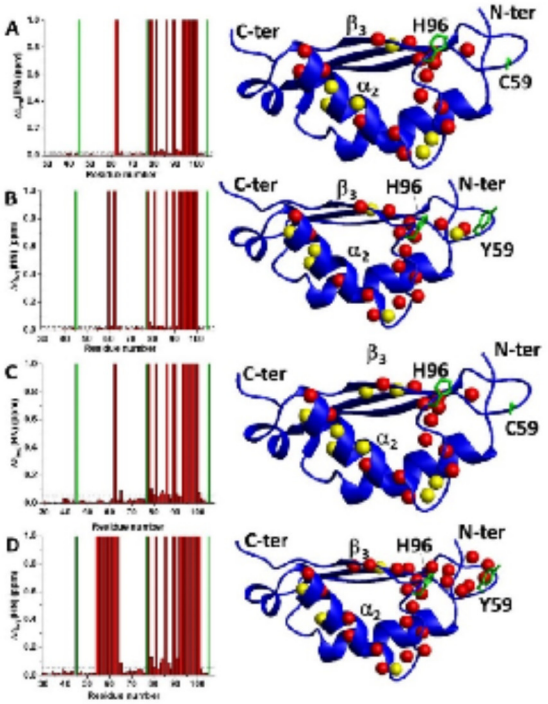

Figure 3. C59Y mutation promoted the formation of an aberrant protein–protein interaction. (**A**) Backbone weighted average chemical shift differences ($\Delta\delta_{avg}$(HN)) on ^{15}N-labelled BOLA3 (100 μM starting protein concentration) upon hetero-complex formation with apo GLRX5 (left panel). Meaningful chemical shift differences are mapped on the solution structure of BOLA3 (PDB 2NCL) (right panel). (**B**) $\Delta\delta_{avg}$(HN) on ^{15}N-labelled C59Y BOLA3 (100 μM starting protein concentration) upon hetero-complex formation with apo GLRX5 (left panel). Meaningful chemical shift differences are mapped on the structural model of C59Y BOLA3 (right panel). (**C**) $\Delta\delta_{avg}$(HN) on ^{15}N-labelled BOLA3 (800 μM starting protein concentration) upon hetero-complex formation with apo GLRX5 (left panel). Meaningful chemical shift differences are mapped on the solution structure of BOLA3 (PDB 2NCL) (right panel). (**D**) $\Delta\delta_{avg}$(HN) on ^{15}N-labelled C59Y BOLA3 (800 μM starting protein concentration) upon hetero-complex formation with apo GLRX5 (left panel). Meaningful chemical shift differences are mapped on the structural model of C59Y BOLA3 (right panel). Red bars with $\Delta\delta_{avg}$(HN) = 1 indicate residues whose backbone NH signals broaden beyond detection. The green bars indicate proline residues or unassigned NHs. Chemical shift threshold values (see the Materials and Methods section) are indicated as dashed lines. On the blue ribbon diagrams, backbone NHs showing line broadening beyond detection are depicted as red spheres, while backbone NHs with chemical shifts above the thresholds are depicted as yellow spheres. Sidechains of Cys59, Tyr59, and His96 are shown as green sticks.

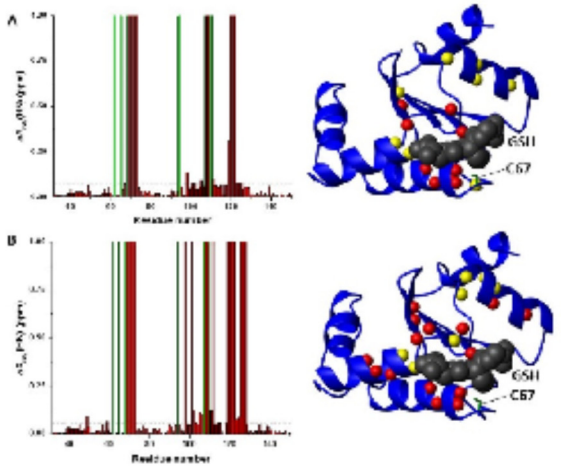

Figure 4. Mapping NMR chemical shift changes on GLRX5 upon apo hetero-complex formation. (**A**) Backbone weighted average chemical shift differences ($\Delta\delta_{avg}$(HN)) on ^{15}N-labelled GLRX5 (800 μM starting protein concentration) upon complex formation with BOLA3 (left panel). Meaningful chemical shift differences were mapped on the solution structure of GSH-bound GLRX5 (PDB 2WUL) (right panel). (**B**) $\Delta\delta_{avg}$(HN) on ^{15}N-labelled GLRX5 (800 μM starting protein concentration) upon hetero-complex formation with C59Y BOLA3 (left panel). Meaningful chemical shift differences were mapped on the solution structure of GSH-bound GLRX5 (PDB 2WUL) (right panel). Red bars with $\Delta\delta_{avg}$(HN) = 1 indicate residues whose backbone NH signals broaden beyond detection. The green bars indicate proline residues or unassigned NHs. Chemical shift threshold values (see the Materials and Methods section) are indicated as dashed lines. On the blue ribbon diagrams, backbone NHs showing line broadening beyond detection are depicted as red spheres, and the backbone NHs with chemical shifts above the thresholds are depicted as yellow spheres. The sidechain of Cys67 is depicted as green stick, and the GSH molecule is depicted as CPK mode in gray.

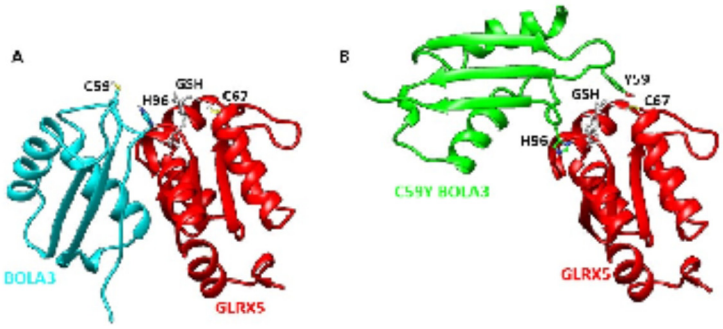

Figure 5. Visualizing the structure of the aberrant protein–protein complex by data-driven biomolecular docking. Structural models of apo BOLA3–GLRX5 (**A**) and C59Y BOLA3–GLRX5 (**B**) complexes. Ribbon diagrams of GLRX5, BOLA3, and C59Y BOLA3 structures are in red, cyan, and green, respectively. Sidechains of His96 and Cys59 in BOLA3, His96 and Tyr59 in C59Y BOLA3, Cys67 in GLRX5, and the GSH molecule bound to GLRX5 are shown as sticks.

In conclusion, the NMR data indicate that the Cys59Tyr mutation did not abolish the formation of an apo hetero-complex between BOLA3 and GLRX5, but it significantly modified the interaction between the two proteins, promoting the formation of a hetero-complex structurally different from that formed by the wild-type protein.

2.3. C59Y BOLA3–GLRX5 Complex Bound a $[2Fe–2S]^{2+}$ Cluster

In light of the different interaction properties of the C59Y BOLA3 mutant with apo GLRX5 in comparison with those of wild-type BOLA3, we investigated whether the C59Y BOLA3–GLRX5 complex is still able to bind a $[2Fe–2S]^{2+}$ cluster, as the BOLA3–GLRX5 complex does [22,23]. To address this question, we chemically reconstituted the apo C59Y BOLA3–GLRX5 complex, obtained by mixing equimolar amounts of apo GLRX5 and C59Y BOLA3, and then analyzed the chemically reconstituted mixture by UV–VIS, UV–VIS circular dichroism (CD), and paramagnetic 1D ^{1}H NMR spectroscopies.

The data showed that the C59Y BOLA3–GLRX5 complex was still able to bind a $[2Fe–2S]^{2+}$ cluster: indeed, the UV–VIS spectrum had absorption bands between 300 and 600 nm, typical of biological oxidized $[2Fe–2S]^{2+}$ centers [36,37] (Figure 6A); the UV–VIS CD spectrum showed well-structured, intense bands typical of protein-bound [2Fe–2S] cluster [38,39] (Figure 6B); and paramagnetic 1D ^{1}H NMR spectrum showed broad signals in the 35–20 ppm range and of a sharper one at 13 ppm, all of them typical of residues bound to an oxidized $[2Fe–2S]^{2+}$ cluster [40–42] (Figure 6C).

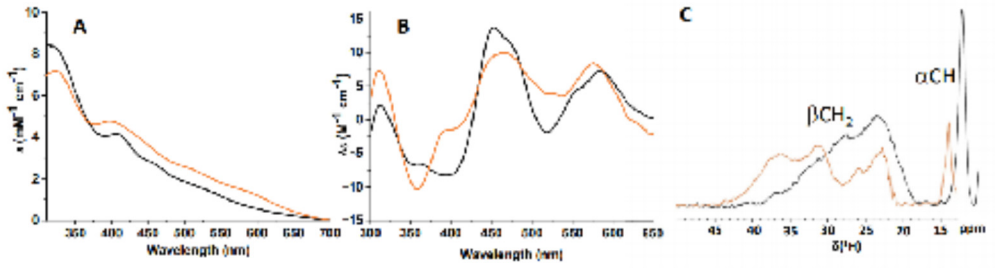

Figure 6. C59Y BOLA3–GLRX5 complex bound a $[2Fe–2S]^{2+}$ cluster. UV–VIS (**A**), UV–VIS CD (**B**), and paramagnetic 1D ^{1}H NMR spectra (**C**) of chemically reconstituted C59Y BOLA3–GLRX5 (black) and BOLA3–GLRX5 (orange) apo complexes.

Comparing the UV–VIS, UV–VIS CD, and paramagnetic 1D ^{1}H NMR spectra of the $[2Fe–2S]^{2+}$ C59Y BOLA3–GLRX5 complex with the corresponding spectra obtained on the $[2Fe–2S]^{2+}$ BOLA3–GLRX5 complex, we observed significant differences, indicating that the Cys-to-Tyr mutation perturbed the cluster-binding environment. Specifically, the absorption bands at 398, 440, 512, and 593 nm in the $[2Fe–2S]^{2+}$ BOLA3–GLRX5 complex were shifted to 407, 459, 507, and 540 nm in the $[2Fe–2S]^{2+}$ C59Y BOLA3–GLRX5 (Figure 6A). Considering that it has previously been shown that the UV–VIS absorption spectra of $[2Fe–2S]^{2+}$ ferredoxins display hypsochromic shifts in the 400–500 nm region upon the replacement of a sulfur by an oxygen ligand [43,44], the bathochromic shifts observed in the UV–VIS spectrum of the C59Y BOLA3–GLRX5 complex, as compared to the spectrum of the wild-type hetero-complex, suggests that the tyrosine did not coordinate the cluster. This is consistent with the fact that the coordination of a Tyr to an Fe–S cluster is extremely rare and previously detected only for a [4Fe–4S] cluster of the hydrogenase maturase HydE from *Thermotoga maritima* and for the P-cluster in *G. diazotrophicus* nitrogenase [45,46], but never for a [2Fe–2S] cluster. Moreover, the UV–VIS CD and paramagnetic 1D ^{1}H NMR spectra indicated that the Cys-to-Tyr mutation affected the cluster-binding environment. Indeed, the UV–VIS CD spectrum of the $[2Fe–2S]^{2+}$ C59Y BOLA3–GLRX5 complex differed from that of the $[2Fe–2S]^{2+}$ BOLA3–GLRX5 complex, showing an opposite trend of the intensities of the two bands in the region 350–425 nm (Figure 6B), as well as the hyperfine-

shifted NMR signals, which are typical of βCH_2 and αCH protons of the residues bound to a $[2Fe–2S]^{2+}$ cluster, show changes in the chemical shift values when comparing the paramagnetic 1D ^1H NMR spectra of the two $[2Fe–2S]^{2+}$ hetero-complexes (Figure 6C).

In order to further examine the potential involvement of Tyr59 in cluster-binding in place of Cys59, we performed fluorescence emission spectroscopy, which has been extensively applied to discriminate between a tyrosine having a protonated or a deprotonated phenolic side-chain group (i.e., phenol- or phenoxide-tyrosine hereafter, respectively) in proteins [47–50], with the phenoxide state of the tyrosine being the only one able to coordinate a metal cofactor. A phenoxide-tyrosine has an emission maximum at 345 nm [51] while a phenol-tyrosine has an emission maximum at 303 nm [52]. Fluorescence emission spectra of native proteins containing Trp, Tyr, and Phe residues (as it occurs in the BOLA3–GLRX5 complex) typically show an emission maximum in the range of 331 to 343 nm [53] as a consequence of the predominant contribution of fluorescence emission of Trp [54] over that of Tyr and Phe residues [55]. The fluorescence emission spectrum of apo C59Y BOLA3–GLRX5 complex shows a band with a maximum at 335 nm (Figure 7) due to the presence of a Trp in GLRX5, while the fluorescence emission spectrum of $[2Fe–2S]^{2+}$ C59Y BOLA3–GLRX5 is significantly different, showing, in addition to the band at 335 nm due to the Trp, an intense band at 308 nm in the fluorescence region typical of a phenol-tyrosine (Figure 7). On the contrary, no apparent changes were observed in the fluorescence region typical of a phenoxide-tyrosine at 345 nm. This is better visualized by the difference of the two fluorescence emission spectra (Figure 7, inset), which resulted in a positive band with a maximum at 303 nm, typical of a phenol-tyrosine, and with no positive band with a maximum centered at 345 nm, typical of a phenoxide-tyrosine. Therefore, the fluorescence emission data strongly support the idea that Tyr59 is not involved in cluster coordination. A possible alternative Fe–S cluster ligand in place of Cys59 might be the cysteine of a GSH molecule additionally bound to the hetero-complex. However, it is highly unlikely considering that we previously showed that the C59A mutation, which provides structural perturbations on BOLA3 quite similar to those determined by the C59Y mutation (see Section 2.1), do not promote the binding of a second GSH molecule to the [2Fe–2S] cluster bound to the hetero-complex [22].

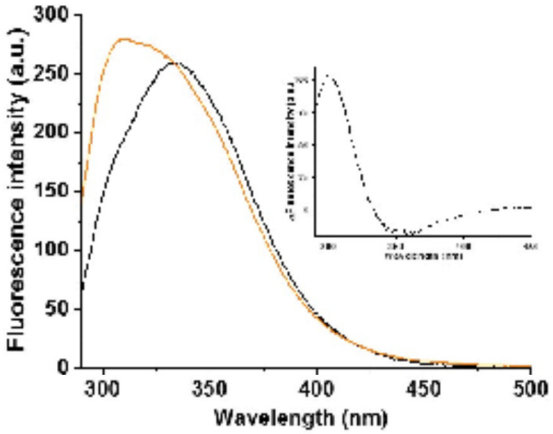

Figure 7. Fluorescence emission spectroscopy indicated that tyrosine 59 was not involved in cluster coordination in the C59Y BOLA3–GLRX5 complex. Fluorescence emission spectra of apo C59Y BOLA3–GLRX5 complex before (black) and after (orange) chemical reconstitution recorded upon excitation at 280 nm. In the inset, fluorescence emission difference spectrum (Δ) obtained by subtracting the spectrum of the chemically reconstituted hetero-complex from that of the apo hetero-complex.

Finally, considering that we have recently shown the transfer of [2Fe–2S] clusters bound to BOLA3–GLRX5 to apo NFU1 to form a $[4Fe–4S]^{2+}$ cluster-bound NFU1 dimer [26], we investigated by NMR the effect of the Cys59Tyr mutation on this process. Specifically, by replicating on the Cys59Tyr mutant the $^{1}H–^{15}N$ HSQC NMR experiments previously performed on the wild-type protein [26] (see the Materials and Methods section for details), we found that, although the [4Fe–4S] cluster assembly on NFU1 was not abolished, a significant lower efficiency was observed for the mutant with respect to the wild-type protein. Specifically, the amount of [4Fe–4S] NFU1 that was formed in the final mixture was 25% (C59Y mutant) vs. 65% (wild-type).

In conclusion, all the observed spectroscopic data were consistent with the presence of a $[2Fe–2S]^{2+}$ cluster bound to the C59Y BOLA3–GLRX5 complex, as it occurred in the wild-type hetero-complex. However, they also showed that (1)the Cys59Tyr mutation determined a perturbation in the chemical environment of the $[2Fe–2S]^{2+}$ cluster due to the absence of the Cys59 Fe–S cluster ligand, (2) Tyr 59 did not replace Cys59 as Fe-S cluster ligand, and (3) the Cys59Tyr mutation reduced the efficiency of [4Fe–4S] cluster assembly on NFU1.

3. Discussion

BOLA3 is a protein required in human cells for the assembly of mitochondrial [4Fe–4S] cluster-binding target proteins that are involved in central pathways of mitochondrial energy production and carbon metabolism [5,11,23,28]. As a result of this, the impairment of BOLA3 function causes severe cellular defects, which are associated with a mitochondrial human disease identified as MMDS2 [1,5,7,15]. The number of disease-causing variants found in BOLA3 has recently increased and, among them, a novel phenotype for MMDS2, with complete clinical recovery after 8 years old, was observed in a patient [18]. This patient was characterized by heterozygous variants in BOLA3, i.e., c.136C > T, p.Arg46* (paternally inherited) and c.176G > A, p.Cys59Tyr (maternally inherited). The peculiarity of these heterozygous variants is that they determine a much milder phenotype with respect to homozygous c.136C > T (p.Arg46*) variants reported by Baker et al. in three unrelated patients [7]. The latter variant resulted, indeed, incompatible with life, due to the fact that the absence of BOLA3 cannot be compensated by other systems in the metabolic cell request. This suggested us that Cys59Tyr BOLA3 variant might, on the contrary, maintain some functional activity and thus might compensate, at least partially, the effect of the other p.Arg46* BOLA3 heterozygous variant. In order to characterize at the molecular level this novel and unique heterozygous phenotype never documented in MMDS2, we here investigated the impact of the Cys59Tyr mutation on BOLA3 structure, on the hetero-complex formation between BOLA3 and its partner protein GLRX5 and on the Fe–S cluster binding and transfer properties of the hetero-complex.

We showed that the Cys59Tyr mutation did not have severe effects on the overall protein fold of BOLA3. C59Y BOLA3 resulted indeed as a well-structured protein with the same fold of the wild-type protein. These data suggest that the pathogenic effects of the mutation did not promote increased folding instability and thus the protein turnover in cells is expected to not be altered with respect to that of the wild-type protein. We also found that the mutation did not impair apo protein–protein interaction between BOLA3 and GLRX5 and did not significantly affect the affinity constant for the hetero-complex formation. C59Y BOLA3 indeed maintained the same ability to interact with GLRX5 as wild-type BOLA3. However, NMR protein–protein interaction data showed that tyrosine 59 promoted the formation of an aberrant interaction with GLRX5, which was not present in wild-type BOLA3. This effect can be structurally rationalized considering both the high solvent exposure of the mutated position and that the mutation did not dramatically modify the protein surface between the two proteins. Indeed, Cys59 is highly solvent-exposed, being located in at the edge of an extended loop of BOLA3 [23]. When substituted by a tyrosine, the latter residue, which remained still solvent-exposed in the C59Y BOLA3 structure (Supplementary Figure S3), had the ability, thanks to its aromatic

ring, to trigger, in the apo C59Y BOLA3–GLRX5 complex, an intermolecular protein–protein interaction not occurring in the wild-type hetero-complex. The structural model of the apo C59Y BOLA3–GLRX5 complex showed, indeed, that Tyr59 closely interacted with the glutathione molecule bound to the hetero-complex as well as with the Cys67 Fe–S cluster ligand of GLRX5, causing a structural conformation of the apo hetero-complex different from that observed when Cys59 was present. The formation of this aberrant hetero-complex might represent the cause of the pathogenic effects induced by the Cys59Tyr mutation. NMR data also showed that the formation of this Tyr59-driven interaction depended on protein concentration, thus indicating the presence of an equilibrium between a native-like hetero-complex conformation and an aberrant hetero-complex conformation. Specifically, the NMR data support that this equilibrium occurred involving multiple binding states of comparable energy. Indeed, the majority of the backbone NHs of the residues at the protein–protein interface of the apo C59Y BOLA3–GLRX5 complex showed line broadening beyond detection on both interacting proteins that was not recovered by adding an excess of the protein titrant, as it would be expected in the case of a single-mode binding [56]. This effect was accompanied by a higher number of signals being involved at the interacting interfaces of the two proteins, when the Cys59Tyr mutation was present (Figure 3B,D and Figure 4), suggesting that the mutation had the following effect: the interacting proteins in their associated state sampled each other's surfaces, increasing the number of contacts to find optimal binding geometry, which is, however, prevented by the mutation, thus mimicking a condition commonly known as encounter complex [57]. Overall, our data suggested that the Cys59Tyr mutation does not impair the formation of a native-like hetero-complex, but it can substantially modify it. This model allows the "reversible" phenotype observed in the patient affected by the p.Arg46*/Cys59Tyr heterozygous variants to be explained [18]. We can suggest, indeed, that the Cys59Tyr mutation does not completely abolish the physiological function performed by wild-type BOLA3–GLRX5 complex, in such a way partially compensating the complete lack of function of the other p.Arg46* BOLA3 heterozygous variant [7]. In the early human development phases during which the functional processes performed by BOLA3 are much more critical, the performance of the native-like hetero-complex formed by C59Y BOLA3 might not be sufficient to sustain the correct human development in that period of life, as the aberrant non-functional complex is also formed. Once a less metabolic demand of the hetero-complex is needed after the early stages of human development, such as it occurs at the age of eight years, a complete clinical recovery can occur as the levels of native-like hetero-complex formed by C59Y BOLA3 can fully satisfy the BOLA3-dependent physiological processes.

It has been proposed, on the basis of a combination of in vitro and in vivo studies [23,28], that the BOLA3–GLRX5 complex transfers its $[2Fe–2S]^{2+}$ cluster to protein partners, such as NFU1 [26], which are involved in the final steps of the maturation of mitochondrial [4Fe–4S] cluster-binding target proteins [28,58]. On this respect, it is also relevant to investigate how the Cys59Tyr mutation affects the Fe–S cluster-binding properties of the hetero-complex, as Cys59 is a ligand of the $[2Fe–2S]^{2+}$ cluster in the hetero-complex [22]. Spectroscopic data showed that the C59Y BOLA3–GLRX5 complex maintained its ability to bind a $[2Fe–2S]^{2+}$ cluster even if the tyrosine did not substitute the cysteine in [2Fe–2S] cluster-binding. Thus, the Cys59Tyr mutation, in addition of altering the apo BOLA3–GLRX5 complex conformation, modified the coordination mode of the cluster with respect to the wild-type hetero-complex. This aspect might also play a key role in the pathogenic effects of the Cys59Tyr mutation. Specifically, the ability of the BOLA3–GLRX5 complex in transferring its $[2Fe–2S]^{2+}$ cluster to protein partners might be altered in the Cys59Tyr mutant, as well as the cluster stability towards its degradation in the cellular environment might be affected. In agreement with this view, NMR data showed a lower efficiency of [4Fe–4S] cluster assembly on NFU1 by [2Fe–2S] C59Y BOLA3–GLRX5 with respect to the wild-type hetero-complex, suggesting that the BOLA3–GLRX5–NFU1 cellular pathway might be negatively perturbed by the Cys59Tyr mutation. The fact that

[2Fe–2S] cluster-binding is not abolished by the Cys59Tyr mutation, but it is only modified, again agrees with the MMDS2 phenotype: indeed, the modified coordination properties of the hetero-complex might reduce the BOLA3 function in a period of the human body development with a high BOLA3-dependent metabolic demand. However, the ability of the hetero-complex to still coordinate the cluster guarantees a certain level of cellular functionality of the hetero-complex, which can thus rationalize the observed complete clinical recovery when the BOLA3-dependent metabolic requirements are less demanding.

In conclusion, our in vitro study investigating the effects of the Cys59Tyr mutation on the structural, protein–protein interaction, and cluster-binding and -transfer properties of BOLA3/BOLA3–GLRX5 complex sheds light on the molecular grounds of the Cys59Tyr variant-dependent MMDS2, explaining its novel phenotype associated with a complete clinical recovery.

4. Materials and Methods

4.1. Protein Expression and Purification

Site-directed mutagenesis (QuickChange Site-directed Mutagenesis Kit, Agilent Technologies, Milan, Italy) was applied on the pETG20A/wild-type BOLA3 expression vector, already available in the lab [22], to produce recombinant C59Y BOLA3 mutant.

Escherichia coli BL21(DE3)-Gold (Agilent Technologies, Milan, Italy) competent cells were transformed with pETG20A plasmid containing N-terminal-tagged (N-terminal TRX-6His-tag) C59Y BOLA3. Cells were cultivated at 37 °C in 1 L of Luria–Bertani (LB) media adding ampicillin (100 µg/mL) until the OD_{600} reached 0.6–0.8. The protein expression was induced by adding 0.5 mM of isopropyl β-D-1-thiogalactopyranoside and shaking for 5 h at 30 °C, 200 rpm. The cells were harvested by centrifugation at 5000 rpm for 20 min (JA-10, Beckman Coulter, Milan, Italy). The cell pellet was resuspended in the binding buffer (50 mM phosphate buffer, 300 mM NaCl, 20 mM imidazole (pH 8.0)), and the cells were lysed by sonication (30 min, 2″ ON and 9.9″ OFF). The N-terminal TRX-6His-tag C59Y BOLA3 protein was purified from the lysate using a HisTrap HP column (GE Healthcare, Milan, Italy). The TRX-6His-tag was cleaved by tobacco etch virus protease overnight at room temperature in 50 mM phosphate buffer, 300 mM NaCl, and 20 mM imidazole (pH 8.0). HisTrap HP column was then performed to separate C59Y BOLA3 cleaved by the TRX-6His-tag from uncleaved TRX-6His-tag C59Y BOLA3. The final yield of C59Y BOLA3 was ≈40 mg per liter of LB culture. Recovered C59Y BOLA3 was pure enough to be used for spectroscopic and biochemical studies. All the expression and purification steps were performed in aerobic conditions. ^{15}N-labelled C59Y BOLA3 was produced in M9 minimal medium supplemented with $^{15}NH_4Cl$ following the same procedure described for *E. coli* cells grown in LB medium. The expression and purification of wild-type BOLA3, apo GLRX5, and apo NFU1 were obtained as previously described [23,26,59].

4.2. In Vitro Chemical Reconstitution of the Hetero-Complexes

The apo BOLA3–GLRX5 and apo C59Y BOLA3–GLRX5 hetero-complexes were chemically reconstituted in anaerobic conditions in 50 mM Tris-HCl, 100 mM NaCl, and 5 mM DTT buffer at pH 8.0 with eightfold $FeCl_3$ and Na_2S for 16 h at room temperature. Fe–S cluster chemical reconstitution was performed with hetero-complex concentrations of ≈40–80 µM. Excess of $FeCl_3$ and Na_2S was anaerobically removed by passing the mixture on a PD-10 desalting column, and the holo hetero-complex was recovered. Anaerobic conditions were obtained performing the chemical reconstitution in an anaerobic chamber (O_2 < 1 ppm) and by using all buffers degassed.

4.3. NMR Spectroscopy to Characterize Proteins and Hetero-Complexes in Their Apo Forms

Diamagnetic NMR experiments were acquired at 298 K in 150 mM NaCl, 5 mM GSH, 5 mM DTT, 50 mM phosphate buffer (pH 7.0), and 10% (*v*/*v*) D_2O. Diamagnetic NMR spectra were recorded on Bruker AVANCE 700 and 950 MHz spectrometers, processed using the standard Bruker software (Topspin), and analyzed with CARA program. Back-

bone weighted chemical shift differences ($\Delta\delta_{avg}$(HN)) were calculated by the equation $\Delta\delta_{avg}(HN) = (((\Delta H)^2 + (\Delta N/5)^2)/2)^{1/2}$. The estimation of a chemical shift threshold value to define meaningful chemical shift differences was obtained by averaging $\Delta\delta_{avg}$(HN) values plus 1σ.

The formation of the apo C59Y BOLA3–GLRX5 complex was monitored by running ^{1}H–^{15}N HSQC NMR experiments. ^{15}N-labelled C59Y BOLA3 at 100 or 800 µM starting protein concentration or ^{15}N-labelled apo GLRX5 at 800 µM starting protein concentration was titrated with increasing amounts of unlabeled partner until the 1:2 protein ratio was reached. Spectral changes were monitored upon the addition of increasing amounts of the unlabeled partner. NMR data were analyzed following standard procedures [60,61]. The same set of NMR data were collected to monitor the formation of the apo BOLA3–GLRX5 complex. A 1:1 ^{15}N-labelled BOLA3-^{15}N-labelled C59Y BOLA3 mixture was also titrated with unlabeled apo GLRX5 up to a 1:1:2 ^{15}N-labelled BOLA3-^{15}N-labelled C59Y BOLA3–GLRX5 ratio to compare the relative affinity of GLRX5 versus the two BOLA3 proteins.

The experimental procedure followed in each NMR titration and the relative data analysis are reported hereinafter. In a first step, the ^{15}N-labelled protein was titrated with the unlabeled protein partner in the absence of GSH but in the presence of 5 mM DTT, so as to avoid oxidative processes potentially occurring during the titration experiment. This allowed for exclusively following the effects of the protein–protein interaction on the backbone chemical shifts, avoiding chemical shift perturbations due to GSH–protein interaction. Indeed, while GSH does not interact with both wild-type and C59Y BOLA3 (Supplementary Figure S4), GSH additions at millimolar concentration largely affects the chemical shifts of backbone NHs of apo GLRX5 [59], indicating a specific binding of GSH for GLRX5 and not for BOLA3. Once the end of the titration was reached, i.e., when no further chemical shifts were observed upon titrant additions indicating full hetero-complex formation, 5 mM GSH was added to the final mixture. The chemical shift perturbations that were observed comparing the ^{1}H–^{15}N HSQC maps before and after the addition of 5 mM GSH exclusively monitored the interaction of GSH with the ^{15}N-labelled protein in the final mixture. The ^{1}H–^{15}N HSQC spectrum of the final mixture (i.e., with 5 mM GSH) was also compared with the ^{1}H–^{15}N HSQC spectrum of the starting ^{15}N-labelled protein containing 5 mM GSH. The ^{1}H–^{15}N HSQC spectra showed 1) chemical shift changes exclusively due to the protein–protein interaction in the absence of GSH, and 2) further chemical shift changes upon 5 mM GSH addition. Moreover, when we compared the ^{1}H–^{15}N HSQC NMR spectrum of the final mixture (i.e., with 5 mM GSH) with the ^{1}H–^{15}N HSQC spectrum of the starting ^{15}N-labelled protein containing 5 mM GSH, we found that they did not overlap. Collectively, all the NMR data indicated the formation of an apo hetero-complex in the absence of GSH and that GSH, which binds to the GLRX5 subunit of the hetero-complex, interacts at the protein–protein interface without promoting the releasing of the free proteins. The data reported in Figures 3 and 4 were obtained through comparing the NMR spectra of the final mixtures with the starting ^{15}N-labelled proteins, all containing 5 mM DTT and 5 mM GSH. These data thus included chemical shift changes due to two contributions, i.e., protein–protein and GSH–hetero-complex interactions.

4.4. Spectroscopic Methods to Characterize Fe–S Cluster-Binding and Transfer

All the spectroscopic experiments were performed under anaerobic conditions, preparing the samples in an anaerobic chamber (O_2 < 1 ppm) and using degassed buffers, gas-tight cuvette, and gas-tight NMR tubes.

UV–VIS and UV–VIS CD spectra were performed at room temperature in 150 mM NaCl, 5 mM GSH, 5 mM DTT, and 50 mM phosphate buffer (pH 7.0) on a Cary 50 Eclipse spectrophotometer and JASCO J-810 spectropolarimeter, respectively.

Fluorescence emission measurements were performed at 298 K in 150 mM NaCl, 5 mM GSH, 5 mM DTT, and 50 mM phosphate buffer (pH 7.0) on a Cary 50 Eclipse spectrophotometer supplied with a single-cell Peltier thermostatic cell holder. After excitation at

280 nm, an emission scan was recorded between 200 and 600 nm. The emission spectra were corrected for the buffer baseline.

Paramagnetic 1D ^{1}H NMR experiments were performed at 400 MHz with a ^{1}H optimized 5 mm probe at 298 K in 150 mM NaCl, 5 mM GSH, 5 mM DTT, 50 mM phosphate buffer (pH 7.0), and 99% (*v*/*v*) D_2O. These spectra were acquired by means of the superWEFT sequence with a recycle time of 65 ms [62].

$^{1}H-^{15}N$ HSQC NMR experiments were performed to follow the formation of [4Fe–4S]$^{2+}$ NFU1 by mixing unlabeled [2Fe–2S]$^{2+}$ C59Y BOLA3–GLRX5 and apo ^{15}N-labelled NFU1 at a 1:1 ratio in the presence of 5 mM DTT and 5 mM GSH using the same experimental conditions previously applied to the wild-type hetero-complex [26].

4.5. Data-Driven Biomolecular Docking

Structural models of the apo BOLA3–GLRX5 and apo C59Y BOLA3–GLRX5 complexes were calculated using the protein–protein docking program HADDOCK 2.2 by following the standard HADDOCK procedure and employing the HADDOCK2.2 Web Server (https://alcazar.science.uu.nl/services/HADDOCK2.2/) [34,63]. Specifically, the structural models of the apo hetero-dimers were built from the structures of individual proteins (monomeric apo GLRX5 with a bound GSH molecule obtained from PDB entry 2WUL [64] and BOLA3 from PDB entry 2NCL [23]). The structure of the C59Y BOLA3 was obtained with Modeller 9.20 (https://salilab.org/modeller/) [65], using as template the existing NMR solution structure of BOLA3. The C59Y BOLA3 structure obtained by Modeller 9.20 was then energy minimized in explicit water using an AMBER 12.0 molecular dynamics program [66]. The NMR chemical shift mapping data obtained for the two hetero-complexes in the titrations performed at 800 µM starting protein concentration were used to define ambiguous interaction restraints for the residues at the interface. The "active" residues were defined as those having a chemical shift perturbation upon hetero-complex formation larger than the average of $\Delta\delta_{av\beta}$(HN) plus 1σ, as well as those residues whose backbone NHs broaden beyond detection upon the interaction with the protein partner, and all having a solvent accessibility higher than 50%; the "passive" residues were defined as those being surface neighbors to the active residues and having a solvent accessibility higher than 50%. NACCESS is the program used to calculate the atomic and residue accessibilities from the PDB file. GSH molecule was also included as active residue on the basis of the NMR data described in Section 4.3. The ensemble of 200 solutions was analyzed and clustered on the basis of the pairwise RMSD matrix calculated over the backbone atoms of the interface residues of GLRX5 after fitting on the interface residues of BOLA3 or C59Y BOLA3. This way of calculating RMSD values in HADDOCK resulted in high values that emphasized the differences between docking solutions. For this reason, we performed clustering using a 7.5 Å cut-off. The water-refined models were clustered on the basis of the default fraction of common contacts, FCC = 0.75, with the minimum number of elements in a cluster of 4. The clusters were ranked on the basis of the averaged HADDOCK score of their top 10 members and plotted against RMSD from lowest energy structure (Supplementary Figure S2, Tables S1 and S2).

Supplementary Materials: The following are available online at https://www.mdpi.com/article/10.3390/ijms22094848/s1, Figure S1: Estimating the relative affinity of apo GLRX5 versus BOLA3 and C59Y BOLA3 by NMR. Figure S2: Clustering the HADDOCK-generated hetero-complex structural models. Figure S3: Structural changes of the loop containing the C59Y mutation. Figure S4: GSH did not interact with C59Y BOLA3 and BOLA3. Table S1: Cluster statistics of the HADDOCK docking run for the apo BOLA3–GLRX5 complex. Table S2: Cluster statistics of the HADDOCK docking run for the apo C59Y BOLA3–GLRX5 complex.

Author Contributions: Conceptualization, L.B. and V.N.; methodology, S.C.-B. and V.N.; validation, G.S. and D.S.; investigation, V.N., G.S., and D.S.; writing—original draft preparation, V.N.; writing—review and editing, S.C.-B. and L.B.; visualization, V.N. and S.C.-B.; supervision, S.C.-B.; project administration, L.B. and S.C.-B.; funding acquisition, L.B. and S.C.-B. All authors have read and agreed to the published version of the manuscript.

Funding: This research was funded by iNEXT-Discovery, grant agreement no. 871037, funded by the Horizon 2020 research and innovation program of the European Commission (to L.B.) and in part by grant no. CRF2018.0920 (to S.C.-B.) from the Fondazione Cassa di Risparmio di Firenze. The article processing charge was funded by Fondi per la ricerca scientifica d'Ateneo Budget 2021.

Institutional Review Board Statement: Not applicable.

Informed Consent Statement: Not applicable.

Data Availability Statement: The data presented in this study are available within the article text, figures, and supplementary materials.

Acknowledgments: The authors acknowledge the support by the Italian Ministry for University and Research (FOE funding) to the CERM/CIRMMP Italian Centre of Instruct-ERIC, a landmark ESFRI project.

Conflicts of Interest: The authors declare no conflict of interest.

References

1. Seyda, A.; Newbold, R.F.; Hudson, T.J.; Verner, A.; MacKay, N.; Winter, S.; Feigenbaum, A.; Malaney, S.; Gonzalez-Halphen, D.; Cuthbert, A.P.; et al. A novel syndrome affecting multiple mitochondrial functions, located by microcell-mediated transfer to chromosome 2p14–2p13. *Am. J. Hum. Genet.* **2001**, *68*, 386–396. [CrossRef] [PubMed]
2. Lill, R.; Freibert, S.A. Mechanisms of Mitochondrial Iron-Sulfur Protein Biogenesis. *Annu. Rev. Biochem.* **2020**, *89*, 471–499. [CrossRef] [PubMed]
3. Maio, N.; Rouault, T.A. Outlining the Complex Pathway of Mammalian Fe-S Cluster Biogenesis. *Trends Biochem. Sci.* **2020**, *45*, 411–426. [CrossRef] [PubMed]
4. Wachnowsky, C.; Fidai, I.; Cowan, J.A. Iron-sulfur cluster biosynthesis and trafficking—Impact on human disease conditions. *Metallomics* **2018**, *10*, 9–29. [CrossRef] [PubMed]
5. Cameron, J.M.; Janer, A.; Levandovskiy, V.; MacKay, N.; Rouault, T.A.; Tong, W.H.; Ogilvie, I.; Shoubridge, E.A.; Robinson, B.H. Mutations in iron-sulfur cluster scaffold genes NFU1 and BOLA3 cause a fatal deficiency of multiple respiratory chain and 2-oxoacid dehydrogenase enzymes. *Am. J. Hum. Genet.* **2011**, *89*, 486–495. [CrossRef]
6. Navarro-Sastre, A.; Tort, F.; Stehling, O.; Uzarska, M.A.; Arranz, J.A.; Del, T.M.; Labayru, M.T.; Landa, J.; Font, A.; Garcia-Villoria, J.; et al. A fatal mitochondrial disease is associated with defective NFU1 function in the maturation of a subset of mitochondrial Fe-S proteins. *Am. J. Hum. Genet.* **2011**, *89*, 656–667. [CrossRef]
7. Baker, P.R.; Friederich, M.W.; Swanson, M.A.; Shaikh, T.; Bhattacharya, K.; Scharer, G.H.; Aicher, J.; Creadon-Swindell, G.; Geiger, E.; MacLean, K.N.; et al. Variant non ketotic hyperglycinemia is caused by mutations in LIAS, BOLA3 and the novel gene GLRX5. *Brain* **2014**, *137*, 366–379. [CrossRef] [PubMed]
8. Ajit, B.N.; Vanlander, A.V.; Wilbrecht, C.; Van der Aa, N.; Smet, J.; De, P.B.; Vandeweyer, G.; Kooy, F.; Eyskens, F.; De, L.E.; et al. Mutation of the iron-sulfur cluster assembly gene IBA57 causes severe myopathy and encephalopathy. *Hum. Mol. Genet.* **2013**, *22*, 2590–2602. [CrossRef]
9. Shukla, A.; Hebbar, M.; Srivastava, A.; Kadavigere, R.; Upadhyai, P.; Kanthi, A.; Brandau, O.; Bielas, S.; Girisha, K.M. Homozygous p.(Glu87Lys) variant in ISCA1 is associated with a multiple mitochondrial dysfunctions syndrome. *J. Hum. Genet.* **2017**, *62*, 723–727. [CrossRef]
10. Alfadhel, M. Multiple Mitochondrial Dysfunctions Syndrome 4 Due to ISCA2 Gene Defects: A Review. *Child. Neurol. Open* **2019**, *6*. [CrossRef]
11. Haack, T.B.; Rolinski, B.; Haberberger, B.; Zimmermann, F.; Schum, J.; Strecker, V.; Graf, E.; Athing, U.; Hoppen, T.; Wittig, I.; et al. Homozygous missense mutation in BOLA3 causes multiple mitochondrial dysfunctions syndrome in two siblings. *J. Inherit. Metab. Dis.* **2013**, *36*, 55–62. [CrossRef] [PubMed]
12. Lebigot, E.; Gaignard, P.; Dorboz, I.; Slama, A.; Rio, M.; de Lonlay, P.; Heron, B.; Sabourdy, F.; Boespflug-Tanguy, O.; Cardoso, A.; et al. Impact of mutations within the [Fe-S] cluster or the lipoic acid biosynthesis pathways on mitochondrial protein expression profiles in fibroblasts from patients. *Mol. Genet. Metab.* **2017**, *122*, 85–94. [CrossRef] [PubMed]
13. Bindu, P.S.; Sonam, K.; Chiplunkar, S.; Govindaraj, P.; Nagappa, M.; Vekhande, C.C.; Aravinda, H.R.; Ponmalar, J.J.; Mahadevan, A.; Gayathri, N.; et al. Mitochondrial leukoencephalopathies: A border zone between acquired and inherited white matter disorders in children? *Mult. Scler. Relat. Disord.* **2018**, *20*, 84–92. [CrossRef]
14. Kohda, M.; Tokuzawa, Y.; Kishita, Y.; Nyuzuki, H.; Moriyama, Y.; Mizuno, Y.; Hirata, T.; Yatsuka, Y.; Yamashita-Sugahara, Y.; Nakachi, Y.; et al. A Comprehensive Genomic Analysis Reveals the Genetic Landscape of Mitochondrial Respiratory Chain Complex Deficiencies. *PLoS Genet.* **2016**, *12*, e1005679. [CrossRef] [PubMed]
15. Nikam, R.M.; Gripp, K.W.; Choudhary, A.K.; Kandula, V. Imaging phenotype of multiple mitochondrial dysfunction syndrome 2, a rare BOLA3-associated leukodystrophy. *Am. J. Med. Genet. A* **2018**, *176*, 2787–2790. [CrossRef]
16. Khoza, S.; Ngqaneka, T.; Magwebu, Z.E.; Chauke, C.G. Nonketotic hyperglycinemia in captive-bred Vervet monkeys (*Chlorocebus aethiops*) with cataracts. *J. Med. Primatol.* **2019**, *48*, 161–165. [CrossRef] [PubMed]

17. Meldau, S.; Fratter, C.; Bhengu, L.N.; Sergeant, K.; Khan, K.; Riordan, G.T.; Berman, P.A.M. Pitfalls of relying on genetic testing only to diagnose inherited metabolic disorders in non-western populations—5 cases of pyruvate dehydrogenase deficiency from South Africa. *Mol. Genet. Metab. Rep.* **2020**, *24*, 100629. [CrossRef]
18. Stutterd, C.A.; Lake, N.J.; Peters, H.; Lockhart, P.J.; Taft, R.J.; van der Knaap, M.S.; Vanderver, A.; Thorburn, D.R.; Simons, C.; Leventer, R.J. Severe Leukoencephalopathy with Clinical Recovery Caused by Recessive BOLA3 Mutations. *JIMD Rep.* **2019**, *43*, 63–70.
19. Nishioka, M.; Inaba, Y.; Motobayashi, M.; Hara, Y.; Numata, R.; Amano, Y.; Shingu, K.; Yamamoto, Y.; Murayama, K.; Ohtake, A.; et al. An infant case of diffuse cerebrospinal lesions and cardiomyopathy caused by a BOLA3 mutation. *Brain Dev.* **2018**, *40*, 484–488. [CrossRef]
20. Imai-Okazaki, A.; Kishita, Y.; Kohda, M.; Mizuno, Y.; Fushimi, T.; Matsunaga, A.; Yatsuka, Y.; Hirata, T.; Harashima, H.; Takeda, A.; et al. Cardiomyopathy in children with mitochondrial disease: Prognosis and genetic background. *Int. J. Cardiol.* **2019**, *279*, 115–121. [CrossRef] [PubMed]
21. Meldau, S.; Owen, E.P.; Khan, K.; Riordan, G.T. Mitochondrial molecular genetic results in a South African cohort: Divergent mitochondrial and nuclear DNA findings. *J. Clin. Pathol.* **2020**. [CrossRef] [PubMed]
22. Nasta, V.; Giachetti, A.; Ciofi-Baffoni, S.; Banci, L. Structural insights into the molecular function of human (2Fe-2S) BOLA1-GRX5 and (2Fe-2S) BOLA3-GRX5 complexes. *Biochim. Biophys. Acta* **2017**, *1861*, 2119–2131. [CrossRef]
23. Uzarska, M.A.; Nasta, V.; Weiler, B.D.; Spantgar, F.; Ciofi-Baffoni, S.; Saviello, M.; Gonnelli, L.; Muhlenhoff, U.; Banci, L.; Lill, R. Mitochondrial Bol1 and Bol3 function as assembly factors for specific iron-sulfur proteins. *Elife* **2016**, *5*, e16673. [CrossRef] [PubMed]
24. Sen, S.; Rao, B.; Wachnowsky, C.; Cowan, J.A. Cluster exchange reactivity of [2Fe-2S] cluster-bridged complexes of BOLA3 with monothiol glutaredoxins. *Metallomics* **2018**, *10*, 1282–1290. [CrossRef]
25. Jia, M.; Sen, S.; Wachnowsky, C.; Fidai, I.; Cowan, J.A.; Wysocki, V. Characterization of [2Fe-2S]-Cluster-Bridged Protein Complexes and Reaction Intermediates by use of Robust Native Mass Spectrometric Methods. *Angew. Chem. Int. Ed. (Engl.)* **2020**, *59*, 6724–6728. [CrossRef]
26. Nasta, V.; Suraci, D.; Gourdoupis, S.; Ciofi-Baffoni, S.; Banci, L. A pathway for assembling [4Fe-4S]2+ clusters in mitochondrial iron-sulfur protein biogenesis. *FEBS J.* **2020**, *287*, 2312–2327. [CrossRef]
27. Tong, W.H.; Jameson, G.N.; Huynh, B.H.; Rouault, T.A. Subcellular compartmentalization of human Nfu, an iron-sulfur cluster scaffold protein, and its ability to assemble a [4Fe-4S] cluster. *Proc. Natl. Acad. Sci. USA* **2003**, *100*, 9762–9767. [CrossRef] [PubMed]
28. Melber, A.; Na, U.; Vashisht, A.; Weiler, B.D.; Lill, R.; Wohlschlegel, J.A.; Winge, D.R. Role of Nfu1 and Bol3 in iron-sulfur cluster transfer to mitochondrial clients. *Elife* **2016**, *5*, e15991. [CrossRef]
29. Suraci, D.; Saudino, G.; Nasta, V.; Ciofi-Baffoni, S.; Banci, L. ISCA1 orchestrates ISCA2 and NFU1 in the maturation of human mitochondrial [4Fe-4S] proteins. *J. Mol. Biol.* **2021**, *433*, 166924. [CrossRef] [PubMed]
30. Ahting, U.; Mayr, J.A.; Vanlander, A.V.; Hardy, S.A.; Santra, S.; Makowski, C.; Alston, C.L.; Zimmermann, F.A.; Abela, L.; Plecko, B.; et al. Clinical, biochemical, and genetic spectrum of seven patients with NFU1 deficiency. *Front. Genet.* **2015**, *6*, 123. [CrossRef] [PubMed]
31. Tonduti, D.; Dorboz, I.; Imbard, A.; Slama, A.; Boutron, A.; Pichard, S.; Elmaleh, M.; Vallee, L.; Benoist, J.F.; Ogier, H.; et al. New spastic paraplegia phenotype associated to mutation of NFU1. *Orphanet J. Rare Dis* **2015**, *10*, 13. [CrossRef] [PubMed]
32. Invernizzi, F.; Ardissone, A.; Lamantea, E.; Garavaglia, B.; Zeviani, M.; Farina, L.; Ghezzi, D.; Moroni, I. Cavitating leukoencephalopathy with multiple mitochondrial dysfunction syndrome and NFU1 mutations. *Front. Genet.* **2014**, *5*, 412. [CrossRef] [PubMed]
33. de Vries, S.J.; van Dijk, M.; Bonvin, A.M. The HADDOCK web server for data-driven biomolecular docking. *Nat. Protoc.* **2010**, *5*, 883–897. [CrossRef]
34. Dominguez, C.; Boelens, R.; Bonvin, A.M. HADDOCK: A protein-protein docking approach based on biochemical or biophysical information. *J. Am. Chem. Soc.* **2003**, *125*, 1731–1737. [CrossRef] [PubMed]
35. Rodrigues, J.P.; Trellet, M.; Schmitz, C.; Kastritis, P.; Karaca, E.; Melquiond, A.S.; Bonvin, A.M. Clustering biomolecular complexes by residue contacts similarity. *Proteins* **2012**, *80*, 1810–1817. [CrossRef]
36. Noodleman, L.; Baerends, E.J. Electronic structure, magnetic properties, ESR and optical spectra for 2-Fe ferredoxin models by LCAO-Xa valence bond theory. *J. Am. Chem. Soc.* **1984**, *106*, 2316–2327. [CrossRef]
37. Dailey, H.A.; Finnegan, M.G.; Johnson, M.K. Human ferrochelatase is an iron-sulfur protein. *Biochemistry* **1994**, *33*, 403–407. [CrossRef]
38. Freibert, S.A.; Weiler, B.D.; Bill, E.; Pierik, A.J.; Muhlenhoff, U.; Lill, R. Biochemical Reconstitution and Spectroscopic Analysis of Iron-Sulfur Proteins. *Methods Enzym.* **2018**, *599*, 197–226.
39. Mapolelo, D.T.; Zhang, B.; Naik, S.G.; Huynh, B.H.; Johnson, M.K. Spectroscopic and functional characterization of iron-sulfur cluster-bound forms of Azotobacter vinelandii (Nif)IscA. *Biochemistry* **2012**, *51*, 8071–8084. [CrossRef]
40. Banci, L.; Camponeschi, F.; Ciofi-Baffoni, S.; Piccioli, M. The NMR contribution to protein-protein networking in Fe-S protein maturation. *J. Biol. Inorg. Chem.* **2018**, *23*, 687. [CrossRef]

41. Xia, B.; Jenk, D.; LeMaster, D.M.; Westler, W.M.; Markley, J.L. Electron-nuclear interactions in two prototypical [2Fe-2S] proteins: Selective (chiral) deuteration and analysis of ^{1}H and ^{2}H NMR signals from the alpha and beta hydrogens of cysteinyl residues that ligate the iron in the active sites of human ferredoxin and Anabaena 7120 vegetative ferredoxin. *Arch. Biochem. Biophys.* **2000**, *373*, 328–334.
42. Banci, L.; Bertini, I.; Luchinat, C. The ^{1}H NMR parameters of magnetically coupled dimers—The Fe_2S_2 proteins as an example. *Bioinorg. Chem.* **1990**, *72*, 113–136.
43. Cleland, W.E.J.; Averill, B.A. Effects of phenoxide ligation on iron-sulfur clusters. 2. Preparation and properties of [Fe2S2(OAr)4]2- ions. *Inorg. Chem.* **1984**, *23*, 4192–4197. [CrossRef]
44. Fujinaga, J.; Gaillard, J.; Meyer, J. Mutated forms of a [2Fe-2S] ferredoxin with serine ligands to the iron-sulfur cluster. *Biochem. Biophys. Res. Commun.* **1993**, *194*, 104–111. [CrossRef]
45. Nicolet, Y.; Rohac, R.; Martin, L.; Fontecilla-Camps, J.C. X-ray snapshots of possible intermediates in the time course of synthesis and degradation of protein-bound Fe4S4 clusters. *Proc. Natl. Acad. Sci. USA* **2013**, *110*, 7188–7192. [CrossRef]
46. Owens, C.P.; Katz, F.E.; Carter, C.H.; Oswald, V.E.; Tezcan, F.A. Tyrosine-Coordinated P-Cluster in G. diazotrophicus Nitrogenase: Evidence for the Importance of O-Based Ligands in Conformationally Gated Electron Transfer. *J. Am. Chem. Soc.* **2016**, *138*, 10124–10127. [CrossRef]
47. O'Neil, J.D.; Hofmann, T. Tyrosine and tyrosinate fluorescence of pig intestinal Ca2+-binding protein. *Biochem. J.* **1987**, *243*, 611–615. [CrossRef]
48. Szabo, A.G.; Lynn, K.R.; Krajcarski, D.T.; Rayner, D.M. Tyrosinate fluorescence maxima at 345 nm in proteins lacking tryptophan at pH 7. *FEBS Lett.* **1978**, *94*, 249–252. [CrossRef]
49. Kierdaszuk, B. Fluorescence anisotropy of tyrosinate anion using one-, two- and three-photon excitation: Tyrosinate anion fluorescence. *J. Fluoresc.* **2013**, *23*, 339–347. [CrossRef] [PubMed]
50. Pundak, S.; Roche, R.S. Tyrosine and tyrosinate fluorescence of bovine testes calmodulin: Calcium and pH dependence. *Biochemistry* **1984**, *23*, 1549–1555. [CrossRef] [PubMed]
51. Cornog, J.L., Jr.; Adams, W.R. The fluorescence of tyrosine in alkaline solution. *Biochim. Biophys. Acta* **1963**, *66*, 356–365. [CrossRef]
52. Teale, F.W.; Weber, G. Ultraviolet fluorescence of the aromatic amino acids. *Biochem. J.* **1957**, *65*, 476–482. [CrossRef] [PubMed]
53. Pokalsky, C.; Wick, P.; Harms, E.; Lytle, F.E.; Van Etten, R.L. Fluorescence resolution of the intrinsic tryptophan residues of bovine protein tyrosyl phosphatase. *J. Biol. Chem.* **1995**, *270*, 3809–3815. [CrossRef] [PubMed]
54. Ghisaidoobe, A.B.; Chung, S.J. Intrinsic tryptophan fluorescence in the detection and analysis of proteins: A focus on Förster resonance energy transfer techniques. *Int. J. Mol. Sci.* **2014**, *15*, 22518–22538. [CrossRef] [PubMed]
55. Lakowicz, J.R. Principles of frequency-domain fluorescence spectroscopy and applications to cell membranes. *Sub-Cell. Biochem.* **1988**, *13*, 89–126.
56. Reibarkh, M.; Malia, T.J.; Wagner, G. NMR distinction of single- and multiple-mode binding of small-molecule protein ligands. *J. Am. Chem. Soc.* **2006**, *128*, 2160–2161. [CrossRef] [PubMed]
57. Schilder, J.; Ubbink, M. Formation of transient protein complexes. *Curr. Opin. Struct. Biol.* **2013**, *23*, 911–918. [CrossRef]
58. Jain, A.; Singh, A.; Maio, N.; Rouault, T.A. Assembly of the [4Fe-4S] cluster of NFU1 requires the coordinated donation of two [2Fe-2S] clusters from the scaffold proteins, ISCU2 and ISCA1. *Hum. Mol. Genet.* **2020**, *29*, 3165–3182. [CrossRef]
59. Banci, L.; Brancaccio, D.; Ciofi-Baffoni, S.; Del Conte, R.; Gadepalli, R.; Mikolajczyk, M.; Neri, S.; Piccioli, M.; Winkelmann, J. [2Fe-2S] cluster transfer in iron-sulfur protein biogenesis. *Proc. Natl. Acad. Sci. USA* **2014**, *111*, 6203–6208. [CrossRef] [PubMed]
60. Banci, L.; Camponeschi, F.; Ciofi-Baffoni, S.; Muzzioli, R. Elucidating the molecular function of human BOLA2 in GRX3-Dependent anamorsin maturation pathway. *J. Am. Chem. Soc.* **2015**, *137*, 16133–16134. [CrossRef]
61. Gao, G.; Williams, J.G.; Campbell, S.L. Protein-protein interaction analysis by nuclear magnetic resonance spectroscopy. *Methods Mol. Biol.* **2004**, *261*, 79–92. [PubMed]
62. Inubushi, T.; Becker, E.D. Efficient detection of paramagnetically shifted NMR resonances by optimizing the WEFT pulse sequence. *J. Magn. Reson.* **1983**, *51*, 128–133. [CrossRef]
63. van Zundert, G.C.; Rodrigues, J.P.; Trellet, M.; Schmitz, C.; Kastritis, P.L.; Karaca, E.; Melquiond, A.S.; van Dijk, M.; de Vries, S.J.; Bonvin, A.M. The HADDOCK2.2 Web Server: User-Friendly Integrative Modeling of Biomolecular Complexes. *J. Mol. Biol.* **2016**, *428*, 720–725. [CrossRef] [PubMed]
64. Johansson, C.; Roos, A.K.; Montano, S.J.; Sengupta, R.; Filippakopoulos, P.; Guo, K.; von Delft, F.; Holmgren, A.; Oppermann, U.; Kavanagh, K.L. The crystal structure of human GLRX5: Iron-sulfur cluster co-ordination, tetrameric assembly and monomer activity. *Biochem. J.* **2011**, *433*, 303–311. [CrossRef] [PubMed]
65. Sali, A.; Blundell, T.L. Comparative protein modelling by satisfaction of spatial restraints. *J. Mol. Biol.* **1993**, *234*, 779–815. [CrossRef]
66. Case, D.A.; Darden, T.A.; Cheatham, T.E., III; Simmerling, C.L.; Wang, J.; Duke, R.E.; Luo, R.; Walker, R.C.; Zhang, W.; Merz, K.M.; et al. *AMBER 12*, 12th ed.; University of California: San Francisco, CA, USA, 2012.

Supplementary Materials

Molecular Basis of Multiple Mitochondrial Dysfunctions Syndrome 2 Caused by CYS59TYR BOLA3 Mutation

Giovanni Saudino [1,2,†], Dafne Suraci [1,2,†], Veronica Nasta[1,2], Simone Ciofi-Baffoni[1,2,] Lucia Banci [1,2]

[1]Magnetic Resonance Center CERM, University of Florence, Via Luigi Sacconi 6, 50019, Sesto Fiorentino, Florence, Italy.

[2]Department of Chemistry, University of Florence, Via della Lastruccia 3, 50019 Sesto Fiorentino, Florence, Italy.

[†]Equally contributed authors.

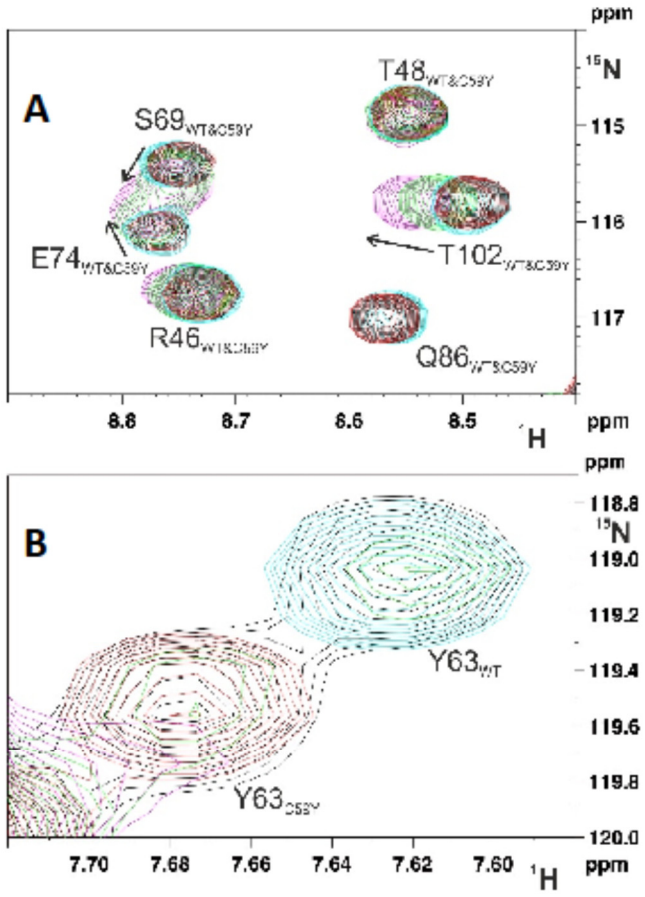

Figure S1. Estimating the relative affinity of apo GLRX5 versus BOLA3 and C59Y BOLA3 by NMR. The ^{1}H-^{15}N HSQC spectra of a 1:1 mixture of ^{15}N-labelled C59Y BOLA3 and ^{15}N-labelled BOLA3 in the presence of 0 (black), 1 (green) and 2 (purple) equivalents of unlabelled apo GLRX5. The signals of isolated ^{15}N-labelled C59Y BOLA3 and ^{15}N-labelled BOLA3 are in red and cyan, respectively. In (A) the backbone NH signals of the indicated residues of the two BOLA3 proteins are fully overlapped, while (B) the backbone NH signal of Y63 has a different chemical shift in the two BOLA3 proteins.

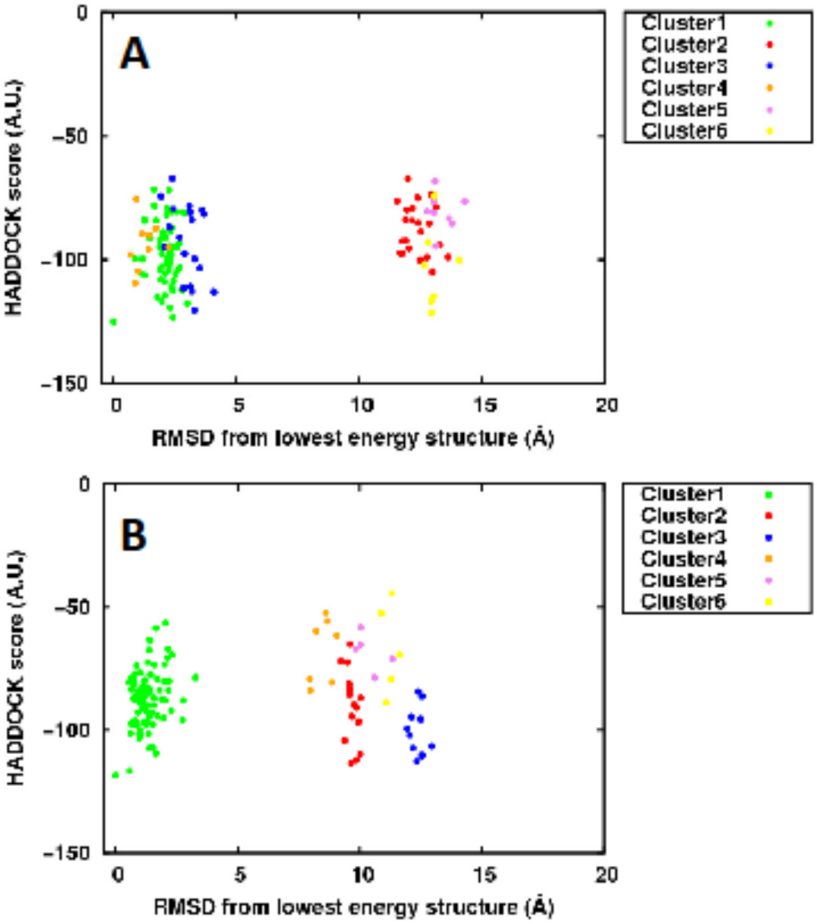

Figure S2. Clustering the HADDOCK-generated hetero-complex structural models. The plot is based on water-refined models of apo BOLA3-GLRX5 (**A**) and apo C59Y BOLA3-GLRX5 (**B**), generated by HADDOCK runs. The clusters (indicated with different colors in the plot) are plotted on the RMSD from lowest energy structure against the HADDOCK score.

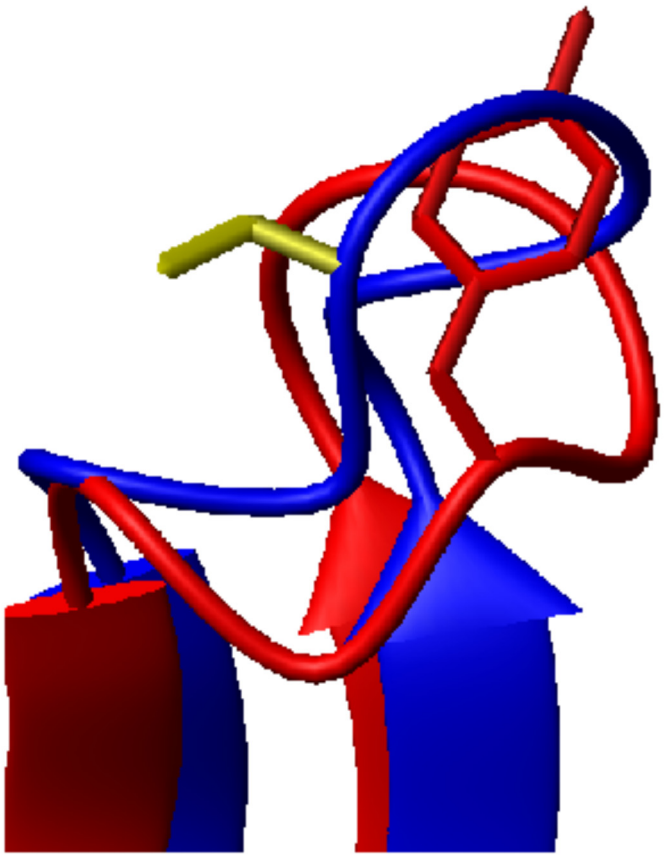

Figure S3. Structural changes of the loop containing the C59Y mutation. Ribbon diagram of the loop containing the C59Y mutation in the two structures of BOLA3 (blue) and C59Y BOLA3 (red). The side-chains of Cys 59 and Tyr 59 are shown as yellow and red sticks, respectively.

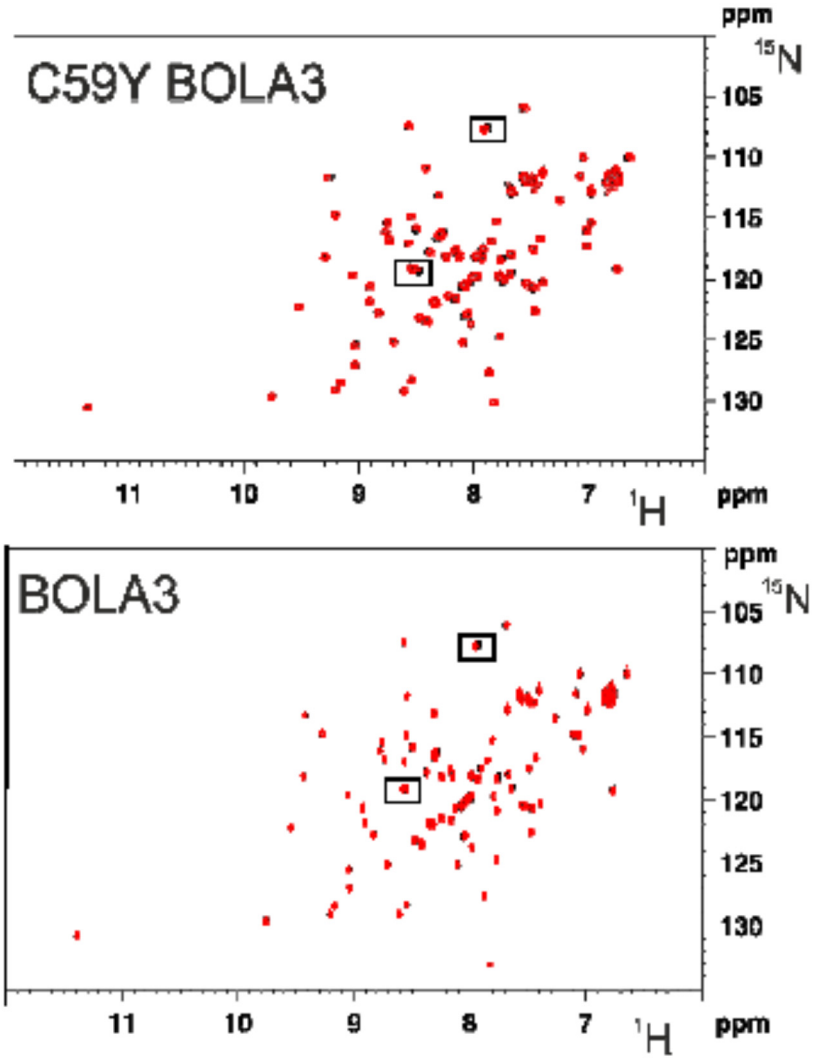

Figure S4. GSH does not interact with C59Y BOLA3 and BOLA3. ^{1}H-^{15}N HSQC NMR spectra of C59Y BOLA3 and BOLA3 with 0 mM (black) and 5 mM (red) GSH. The largest observed chemical shift differences are indicated in the boxes.

Table S1. Cluster statistics of the HADDOCK docking run for the apo BOLA3-GLRX5 complex.[a]

Cluster	HADDOCK score (a.u)	Cluster population	RMSD from the overall lowest energy structure (Å)	Van der Waals energy (Kcal mol^{-1})	Electro-static energy (Kcal mol^{-1})	Desolvation energy (Kcal mol^{-1})	Restraints violation energy (Kcal mol^{-1})	Buried Surface Area ($Å^2$)
1	-116.72 ±4.51	62	2.11 ±0.78	-85.52 ±6.91	-265.83 ±27.37	-11.75 ±8.21	71.37 ±36.87	1469.84 ±68.03
2	-97.22 ±3.65	22	12.43 ±0.67	-67.87 ±4.74	-232.85 ±30.8	-9.31 ±7.02	32.45 ±18.63	1252.01 ±60.84
3	-105.48 ±9.08	19	3.1 ±0.51	-69.04 ±4.37	-202.88 ±31.91	-25.68 ±7.19	95.27 ±36.04	1295.24 ±93.64
4	-93.91 ±9.45	9	1.27 ±0.46	-64.65 ±6.66	-188.58 ±64.62	-18.45 ±10.17	80.44 ±32.6	1349.18 ±72.93
5	-80.66 ±7.2	8	13.35 ±0.48	-59.48 ±3.99	-219.24 ±41.37	-3.7 ±5.62	44.37 ±26.26	1193.85 ±70.89
6	-103.17 ±15.15	7	13.08 ±0.43	-73.97 ±11.13	-133.24 ±42.63	-24.28 ±6.88	84.05 ±46.25	1435.05 ±105.65
7	-98.99 ±9.35	6	4.67 ±0.34	-62.03 ±5.3	-150.3 ±28.33	-26.31 ±4.81	43.78 ±25.23	1428.37 ±76.74
8	-79.98 ±15.74	5	2.12 ±0.41	-56.57 ±6.97	-118.88 ±25.63	-21.68 ±6.42	101.58 ±34.76	1260.05 ±101.64
9	-83.79 ±8.19	5	2.56 ±0.39	-64.52 ±8.66	-208.48 ±38.07	-8.43 ±3.58	100.08 ±20.84	1232.25 ±113.2
10	-98.27 ±11.4	5	2.53 ±0.24	-61.73 ±6.62	-161.13 ±14.66	-29.95 ±4.69	95.31 ±24.48	1395.96 ±72.04
11	-69.7 ±9.5	4	7.06 ±0.28	-48.26 ±5.31	-89.61 ±37.78	-28.3 ±2.53	158.18 ±28.71	1141.77 ±40.72
12	-76.34 ±12.4	4	14.66 ±0.11	-60.13 ±6.58	-100.78 ±33.1	-21.79 ±5.67	156.63 ±26.32	1142.25 ±100.47
13	-77.99 ±10.6	4	5.24 ±0.07	-56.76 ±8.26	-77.89 ±32.86	-26.34 ±3.81	128.93 ±22.28	1198.31 ±80.82

[a] All values are averages and standard deviation calculated from the best scoring ten models of each cluster.

Table S2. Cluster statistics of the HADDOCK docking run for the apo C59Y BOLA3-GLRX5 complex.[a]

Cluster	HADDOCK score (a.u)	Cluster population	RMSD from the overall lowest energy structure (Å)	Van der Waals energy (Kcal mol^{-1})	Electro-static energy (Kcal mol^{-1})	Desolvation energy (Kcal mol^{-1})	Restraints violation energy (Kcal mol^{-1})	Buried Surface Area ($Å^2$)
1	-103.56 ±6.73	60	1.75 ±0.71	-65.11 ±4.72	-296.01 ±42.13	-20.31 ±4.37	114.6 ±55.07	1010.83 ±46.1
2	-65.83 ±6.08	14	10.53 ±0.34	-40.22 ±3.71	-64.99 ±15.92	-36.01 ±6.13	168.97 ±33.77	877.72 ±57.52
3	-101.41 ±10.53	10	11.39 ±0.25	-65.92 ±9.03	-126.12 ±38.47	-32.41 ±8.26	95.33 ±33.01	1386.17 ±54.18
4	-97.32 ±15.82	9	7.38 ±0.31	-65.87 ±10.31	-150.35 ±32.03	-26.55 ±8.72	101.26 ±34.46	1482.16 ±115.73
5	-89.78 ±11.88	8	10.65 ±0.39	-58.46 ±8.78	-189.33 ±22.25	-27.02 ±7.85	146.37 ±56.88	1129.22 ±134.92
6	-62.65 ±11.14	6	8.74 ±0.45	-40.71 ±5.46	-96.36 ±26.56	-20.14 ±5.6	78.35 ±21.77	964.01 ±86.93
7	-61.16 ±11.92	6	12.04 ±0.3	-39.5 ±6.38	-84.98 ±23.88	-29.51 ±5.92	163.52 ±70.45	893.79 ±46.77
8	-81.38 ±2.49	6	6.83 ±0.16	-48.14 ±4.83	-63.54 ±15.55	-36.74 ±6.86	98.52 ±37.59	1141.8 ±41.01
9	-86.73 ±18.22	5	13.45 ±0.73	-56.49 ±8.3	-124.97 ±28.01	-33.94 ±7.74	162.03 ±55.53	1311.44 ±50.84
10	-79.07 ±8.73	4	8.72 ±0.29	-48.14 ±5	-79.42 ±17.33	-39.08 ±6	160.93 ±52	1169.44 ±46.35
11	-86.91 ±19.24	4	12.95 ±0.11	-60.26 ±5.09	-123.97 ±24.39	-25.6 ±11.89	113.38 ±52.3	1406.48 ±60.22

* All values are averages and standard deviation calculated from the best scoring ten models of each cluster.

2.3 Molecular basis of [4Fe-4S] cluster insertion in human lipoyl synthase

Giovanni Saudino[1], Simone Ciofi-Baffoni [1,2], Lucia Banci [1,2,3]

[1]Magnetic Resonance Center (CERM), University of Florence, Via L. Sacconi 6, 50019 Sesto Fiorentino, Italy.

[2]Department of Chemistry "Ugo Schiff", University of Florence, Via della Lastruccia 3, 50019 Sesto Fiorentino, Italy.

[3]Consorzio Interuniversitario Risonanze Magnetiche di Metalloproteine (CIRMMP), Via L. Sacconi 6, 50019 Sesto Fiorentino, Italy.

Submitted

Introduction

Iron-sulfur (Fe-S) proteins are required in a variety of biological processes. Biogenesis of Fe-S proteins includes assembly of Fe-S clusters (ISC) on scaffold complexes and their transfer to the recipient apo proteins with the assistance of Fe-S cluster carriers [16,73]. Among these carriers, there are the Nfu-type proteins[39,74]. They are multi-domain proteins, which are formed by a fully conserved C-terminal domain harbouring a CysXXCys sequence motif involved in Fe-S cluster binding required for the carrier function, and by one or more N-terminal domains, which show a large sequence and structural variability depending on the organism5. In some prokaryotic Nfu proteins, the functional role of the N-terminal domain was shown to be that of selecting the recipient apo protein via a specific protein-protein mediated recognition mechanism[75,76]. On the other hand, the function of the N-terminal domain in eukaryotic organisms is still not well-defined. For example, in humans the N-terminal domain of NFU1 was found to be involved in the interaction with the recipient apo protein succinate dehydrogenase but not with lipoyl synthase[49].

Recently, the mechanism of action of NFU1 in the biogenesis of mitochondrial Fe-S cluster binding proteins has been deeply investigated[32,37,48–50,77,78], but a definitive molecular model is still missing. All the data agree on the fact that NFU1 is involved in the delivery of [4Fe-4S] clusters to recipient apo proteins but two main molecular mechanisms to achieve this have been proposed. In a model, it was proposed that NFU1 receives a [4Fe-4S] cluster from a ISCA1-ISCA2 dimeric complex, which assembles it with the assistance of two other proteins IBA57 and FDX2, and then transfers it to selected recipient apo proteins[29–32,34,37,43,44,70,79–81]. Specifically, FDX2 provides two electrons to reductively couple two $[2Fe\text{-}2S]^{2+}$ clusters, donated by GLRX5, forming a $[4Fe\text{-}4S]^{2+}$ cluster on the ISCA1-ISCA2 complex[30]. IBA57 assists this process but its molecular role is still undefined. Recently, we also showed that ISCA1, thanks to its specific interaction with the C-terminal cluster-binding domain of NFU1, drives [4Fe-4S] cluster transfer from the site in the ISCA1-ISCA2 complex where it is assembled to a cluster-binding site formed by a ISCA1-NFU1 complex via the formation of a transient, ternary ISCA1-ISCA2-NFU1 complex[32]. Such process guarantees that the [4Fe-4S] cluster is safely moved from where it is assembled to NFU1, thus being available for the mitochondrial recipient apo proteins specifically requiring NFU1 for their maturation.

Another model proposed that i) the $[2Fe\text{-}2S]^{2+}$ cluster-bound forms of ISCA1 and ISCU2 donate their clusters to dimeric NFU1, which then reductively couple them to form a $[4Fe\text{-}4S]^{2+}$ cluster upon the provision of two electrons by FDX2; ii) a multi-protein complex, composed by ISCA1, ISCU2, FDX2 and dimeric [4Fe-4S] NFU1, then interacts with mitochondrial recipient apo proteins to transfer them the assembled $[4Fe\text{-}4S]^{2+}$ cluster[48–50]. It should also be considered that, since NFU1 is found in vivo

as a dimer[38], the latter species alone could be the species responsible of inserting the bound [4Fe-4S] cluster into recipient apo proteins.

In order to shed light on this still largely debated topic, we have here investigated the molecular basis of the NFU1-dependent insertion of [4Fe-4S] clusters into human lipoyl synthase (LIAS), a radical S-adenosylmethionine enzyme catalyzing the final step in the biosynthesis of the lipoyl cofactor [82].

Materials and Methods

Protein production

Human NFU1, LIAS, ISCA1 and the triple C137/C141/C144 and C106/C111/C117A LIAS variants were expressed and purified as previously described in literature[32,37,83], with the exception that, for the LIAS proteins production, no $FeCl_3$ was added in the culture in order to decrease the Fe-S cluster content. Following these procedures, NFU1 was isolated in the apo form, LIAS (both wild-type and C106/C111/C117A LIAS variant) was isolated in a [4Fe-4S] form with a partial cluster occupancy (**Table S1**, named as-isolated (AI) hereafter), C137/C141/C144 LIAS variant was isolated in a [4Fe-4S] form with a complete cluster occupancy (**Table S1**) and ISCA1 in the apo form but with 30% of [2Fe-2S] cluster occupancy per homodimer[32]. The [4Fe-4S] cluster bound forms of NFU1 and NFU1-ISCA1 complex were obtained as already reported in the literature[32,37]. Non-heme iron and acid-labile sulfide content on the as-isolated proteins was determined as described previously[84].

Analytical size exclusion chromatography and SEC-MALS

Analytical size exclusion chromatography was performed on purified samples with a Superdex 200 Increase 10/300 GL column attached to an AKTA pure chromatography unit using a continuous flow rate of 0.6 mL/min. The column was calibrated with gel filtration marker calibration kit, 6500-66000 Da (Sigma-Aldrich), to obtain the apparent molecular masses of the detected species. The column was equilibrated with degassed 50 mM phosphate buffer at pH 7.0 containing 150 mM NaCl and 5 mM DTT. SEC-MALS data were acquired by attaching a Superdex 200 Increase 10/300 GL column to a DAWN HELEOS system with a continuous flow rate of 0.6 mL/min using a filtered and degassed 50 mM phosphate buffer at pH 7.0 containing 150 mM NaCl and 5 mM DTT. Each experiment was successfully repeated at least three times.

NMR spectroscopy

^{1}H-^{15}N HSQC experiments were performed at 298 K in 50 mM phosphate buffer, 150 mM NaCl, 5 mM DTT, pH 7.0, 10% (v/v) D_2O. These NMR spectra were recorded on Bruker AVANCE 900 and 950 MHz, processed using the standard Bruker software (Topspin) and analyzed with CARA program. In order to monitor both cluster transfer and protein-protein interaction events, NMR titration experiments were performed using ^{15}N-labeled NFU1, unlabeled ISCA1 and unlabeled AI LIAS proteins (both wild-type and C106/C111/C117A LIAS variant). Specifically, ^{15}N-labeled NFU1 in its free or complexed form with ISCA1 (in both apo and [4Fe-4S] states) were stepwise titrated in anaerobic conditions with increasing amounts of unlabeled AI LIAS (both wild type and

C106/C111/C117A AI LIAS variant). The titrations were also performed in the reverse direction, i.e. adding ^{15}N-labeled NFU1 or complexed with ISCA1 to unlabeled AI LIAS. The NMR titration data were analyzed comparing the ^{1}H-^{15}N HSQC spectra recorded along the additions of the protein partner with that of the initial state as well as with ^{1}H-^{15}N HSQC spectra of the appropriate proteins and complexes in their apo and holo forms. The observed chemical shift changes were reported as backbone weighted average chemical shift differences $\Delta\delta_{avg}$(HN), i.e. $(((\Delta H)^2 + (\Delta N/5)^2)/2)^{1/2}$, where ΔH and ΔN are chemical shift differences for backbone amide ^{1}H and ^{15}N nuclei, respectively. Chemical shift assignment of full-length NFU1 was available in the Biological Magnetic Resonance Bank (under accession codes BMRB: 26801)[48]. Each titration was successfully repeated three times.

^{1}H 1D paramagnetic NMR experiments were acquired at 400 MHz with a ^{1}H optimized 5 mm probe at temperatures ranging from 283 K and 298 K, with protein samples in 50 mM phosphate buffer, 150 mM NaCl, 5 mM DTT pH 7.0, 99% or 10% (v/v) D_2O. Protein concentration was in the range of 0.3-0.6 mM. Water signal was suppressed via fast repetition experiments and water selective irradiation[85]. Experiments were typically performed using an overall recycle delay of 60 ms. Squared cosine and exponential multiplications were applied prior to Fourier transformation[86]. Manual baseline correction was performed, using polynomial functions. Each experiment was successfully repeated three times.

Results

Apo NFU1 interacts with LIAS via its C-terminal domain forming a heterodimeric complex

The interaction between apo NFU1 and LIAS was investigated by analytical gel filtration and NMR. Specifically, analytical gel filtration was applied to investigate complex formation and ^{1}H-^{15}N HSQC NMR experiments, performed on ^{15}N-labeled apo NFU1 titrated with unlabeled as-isolated LIAS (AI LIAS, hereafter) or vice versa, were used to identify the residues of NFU1 interacting with AI LIAS, which is monomeric and with a 50% of [4Fe-4S] cluster occupancy (**Table S1**).

Since apo NFU1 is a monomer with a small fraction of dimer[37] and AI LIAS is fully monomeric[83], we can easily follow complex formation between the two proteins by analytical gel filtration. In the chromatogram of a 1:1 apo NFU1-AI LIAS mixture, a peak, which contains both proteins (as detected by SDS-PAGE), is present with an elution volume smaller than those of the two isolated proteins, while the peaks of isolated apo NFU1 and AI LIAS proteins are essentially not present (**Figure S1**). Thus, the single peak containing both apo NFU1 and AI LIAS identifies a heterodimeric complex, which is fully formed at the 1:1 apo NFU1-AI LIAS ratio. SEC-MALS indicated that this single peak has a molar mass of 51 ± 0.5 kDa. This value is 10-kDa less than that expected for a heterodimeric apo NFU1-LIAS complex (61 kDa), suggesting that the two domains of NFU1 are not completely packed to LIAS to form a globular shape but they could be independently moving, possibly taking a dumbbell-like two-domain structure, as previously observed in the apo ISCA1-NFU1 complex[32].

When apo ^{15}N-labeled NFU1 was stepwise titrated with AI LIAS up to a 1:1 protein ratio, chemical shift changes were observed in the ^{1}H-^{15}N HSQC maps of apo NFU1 in intermediate/slow exchange regimes on the NMR time scale, indicating protein-protein interaction (**Figure 1A**). The majority of the resonances of apo NFU1 shift and concomitantly broaden beyond detection upon additions of AI LIAS, consistent with an intermediate exchange regime on the NMR time scale. A few residues displayed a slow exchange regime that allowed to monitor the formation of a new species, which was complete when the 1:1 NFU1-AI LIAS ratio was reached. This NMR data are in full agreement with the analytical gel filtration data. Meaningful chemical shift changes were observed only for residues of the C-domain, with the exception of residues 90-96 of the N-terminal domain (**Figure 1B**). The latter residues are the same as those affected in the apo NFU1-ISCA1 complex formation, supporting the previously proposed model[32,37], namely that these residues are likely located at an interacting region between the N- and C-domains in apo NFU1 and that complex formation (for both ISCA1-NFU1 and AI LIAS-NFU1 complexes) induces the release or modification of this intra-domain

interaction. By mapping the meaningful chemical shift changes (both broadening beyond detection effects and chemical shift changes with 1σ Δavg(HN) > 0.033 ppm) on the structure of the C-terminal domain of apo NFU1, we observed that the two helices of the C-terminal domain of apo NFU1 are completely affected by the protein-protein interaction, while the β-sheet are essentially unaffected (**Figure 1C**). The cluster binding CXXC motif of apo NFU1, encased between the two helices of the C-terminal domain, is also involved in the interaction with AI LIAS, indicating that LIAS in the complex with NFU1 is positioned close to the cluster binding region.

To more accurately follow complex formation, we have concomitantly collected ^{1}H-^{15}N HSQC spectra and analytical gel filtrations on protein mixtures containing various protein:protein ratios, obtained by adding one or more equivalents of ^{15}N-labeled apo NFU1 to unlabeled AI LIAS. On the left side of **Figure 2**, a signal in slow exchange regime on the NMR time scale, which allow efficiently monitoring the presence of apo NFU1 isolated or complexed with AI LIAS, is reported. On the right side of **Figure 2**, the analytical gel filtration chromatograms of the same mixtures analyzed by NMR are shown together with SDS-PAGEs of the fractions of the eluted peaks. Both NMR and analytical gel filtration data showed that, at the 1:1 protein ratio, apo NFU1 is fully complexed with AI LIAS. No signal of isolated apo NFU1 was indeed observed in the NMR spectrum and no peaks of isolated monomeric and dimeric apo NFU1 were observed in the analytical gel filtration chromatogram. Upon addition of two equivalents of apo NFU1, the NMR signal of isolated apo NFU1 accounts for ~40% of intensity. This result excludes the formation of a heterotrimeric complex composed by two molecules of NFU1 and one molecule of AI LIAS, thus corroborating the formation of a heterodimeric complex. This model is confirmed by the analytical gel filtration performed on the same mixture (**Figure 2**), which maintains the peak of the heterodimeric complex and additionally showed the peaks of monomeric and dimeric isolated apo NFU1. Upon addition of three and four equivalents of apo NFU1, the NMR signal of isolated apo NFU1 increases in intensity and concomitantly in the profile of the analytical gel filtration the peaks of monomeric and dimeric isolated apo NFU1 gradually increase their intensity with respect to the peak of the heterodimeric complex (**Figure 2**). In line 2 of the SDS-PAGEs (**Figure 2**), we can consistently observe the increase of the intensity of NFU1 band with respect to that of AI LIAS along the addition of more equivalents of apo NFU1.

LIAS displaces ISCA1 from the apo ISCA1-NFU1 complex to form a heterodimeric complex with apo NFU1

As we have shown that LIAS interacts with the C-domain of NFU1 similarly to what ISCA1 does in its interaction with NFU1[32], we have then investigated whether a ternary complex is formed with these three proteins or LIAS can displace ISCA1 forming a binary complex with NFU1. The binary complex between ^{15}N-labeled apo NFU1 and unlabeled ISCA1 was first formed, as previously described[32], and then AI LIAS was stepwise added to the apo ^{15}N-labeled NFU1-ISCA1 complex. The reaction mixtures were analyzed by analytical gel filtration and NMR. The ^{1}H-^{15}N HSQC map of the binary complex between apo ^{15}N-labeled NFU1 and unlabeled ISCA1 (**Figure 3A**) clearly identifies the fingerprint of the signals of the C-domain of NFU1 affected by binary complex formation with ISCA1. Upon addition of one equivalent of AI LIAS, several signals broaden beyond detection or change their chemical shifts (**Figure 3B**), indicating that apo NFU1 changes its interaction patterns. When this spectrum is compared with that of the heterodimeric complex between apo NFU1 and AI LIAS (**Figure 3C**), it results that the two spectra are essentially fully superimposable, indicating that NFU1 is now interacting with LIAS, forming a heterodimeric complex. Consistently, no NMR signals of free apo NFU1 are observed (compare black spectrum in **Figure 3A** with green spectrum in **Figure 3B**), indicating that NFU1 remains in a complexed form. The analytical gel filtration of this final mixture, containing the apo ISCA1-NFU1 complex to which AI LIAS has been added at a 1:1 ratio, showed an intense peak with an elution volume smaller than those of the three isolated monomeric proteins and of that of the heterodimeric ISCA1-NFU1 complex (**Figure 3D**), indicating that a large MW complex is formed. Its elution volume is similar to that of the apo NFU1-LIAS heterodimeric complex (**Figure S1**), indicating that no ternary complex is formed. Furthermore, a peak with the elution volume of monomeric ISCA1 (~17.7 mL) and containing ISCA1, as detected by SDS-PAGE, is formed upon addition of AI LIAS to the apo NFU1-LIAS complex (compare green, red and violet chromatograms in **Figure 3D**), indicating that ISCA1 is released in solution as a free protein. In conclusion, NMR and analytical gel filtration data indicate that LIAS displaces ISCA1 complexed with NFU1 via the competition with the same binding site, i.e. the C-domain of NFU1, thus LIAS resulting a stronger interactor with respect to ISCA1 versus the latter domain. This model also excludes ISCA1-LIAS protein-protein recognition.

[4Fe-4S] NFU1 transfers the cluster to the FeS_{RS} site of LIAS

Human NFU1 fully dimerizes upon $[4Fe\text{-}4S]^{2+}$ cluster binding[37]. The cluster is bridged between the two C-domains of the dimer and is coordinated by the CXXC motif of each subunit of the dimer[37,49].

This species has been proposed to transfer the cluster in vivo to recipient apo proteins including LIAS[38,49]that contains two [4Fe-4S] clusters that are both involved in the catalytic mechanism[82]. One of them is typical of all radical SAM enzymes (hereafter named FeS_{RS}), while the other cluster (usually defined as auxiliary cluster and named FeS_{aux} hereafter) provides the inorganic sulfides to the substrate, thus being destroyed in each turnover of the enzyme[87]. The FeS_{RS} cluster is bound to a CX3CX2C motif, i.e. three iron ions are coordinated to three Cys residues of the motif (Cys 137, Cys 141 and Cys 144 in LIAS) and the fourth iron ion is exposed for the binding of SAM[51,54]. The FeS_{aux} cluster is bound by a conserved CX4CX5C motif (Cys 106, Cys 111 and Cys 117 in LIAS) and a serine (Ser 345 in LIAS) [51,54].

In order to investigate on the [4Fe-4S] cluster transfer process between the two proteins, we have produced [4Fe-4S] NFU1 as previously reported[37] and mixed it with AI LIAS. It was not possible to directly use the apo form of LIAS, since the removal of the [4Fe-4S] clusters from AI LIAS, performed through standard protocols, resulted in protein precipitation. However, since the quantification of iron and acid-labile sulfide indicated that ~1 equivalent of [4Fe-4S] clusters are bound per monomeric LIAS (**Table S1**), we can follow the cluster transfer from dimeric [4Fe-4S] NFU1 to AI LIAS required to fully saturate the cluster binding sites of LIAS.

Unlabeled AI LIAS was added to ^{15}N-labeled [4Fe-4S] NFU1 or vice versa and ^{1}H-^{15}N HSQC and ^{1}H 1D paramagnetic NMR experiments were recorded. In the NMR spectra of the mixtures in both titrations, the signals typical of the [4Fe-4S] NFU1 species disappeared (inset of **Figure 4A**). This result indicates that the [4Fe-4S] cluster is released from NFU1 and presumably acquired by AI LIAS. On the other hand, the signals of the apo form of NFU1 were not detected (**Figure S2**), suggesting that the apo form of NFU1 become complexed to LIAS in all steps of both titrations, consistent with the interaction observed between apo NFU1 and AI LIAS (**Figure 2**). In agreement with this model, the ^{1}H-^{15}N HSQC maps of the final mixture of both titrations are well superimposable with the ^{1}H-^{15}N HSQC map of the apo NFU1-LIAS complex (**Figure 4A**). Along the steps of the titrations, the NFU1 protein is thus present in solution as two species, i.e. the [4Fe-4S] dimeric form (starting material) and the apo form complexed with LIAS (product of the cluster transfer reaction). ^{1}H 1D paramagnetic NMR spectra were then acquired on the final mixture of the titration and compared with those of [4Fe-4S] NFU1 and AI LIAS in order to monitor the cluster transfer process. The hyperfine shifted signals at 20.3 and 10.6 ppm, typical of the [4Fe-4S] NFU1[37], disappear in the final mixture, indicating that the [4Fe-4S] cluster is no more bound to NFU1. The hyperfine shifted signals at 17.9 and 13.9 ppm typical of AI LIAS, which have been assigned to βCH_2 of the ligands of both FeS_{RS} and FeS_{aux} clusters[83], change their relative intensity ratio upon addition of [4Fe-4S] NFU1 to

AI LIAS. In particular, the signal at 13.9 ppm significantly increases in intensity with respect to that of the signal at 17.9 ppm upon the addition of [4Fe-4S] NFU1. The hyperfine shifted signal at 13.9 ppm contains three proton resonances, one of a cluster ligand bound to the FeS_{aux} and two of cluster ligand(s) bound to FeS_{aux}, while the signal at 17.9 ppm contains one proton resonance due to a cluster ligand bound to the FeS_{aux}. Thus, the large increase of the 13.9 ppm signal intensity with respect to the intensity of the signal at 17.9 ppm suggests that the [4Fe-4S] cluster is predominantly transferred to the FeS_{RS} site. The data do not allow to clearly define whether NFU1 can transfer its cluster also to FeS_{aux} site, since we do not have information on the percentage of the cluster occupancy of the FeS_{aux} site vs. that of the FeS_{RS} site in AI LIAS. It would be possible indeed that, in AI LIAS, the FeS_{aux} site is largely occupied and thus, just for this reason, the cluster transfer cannot be monitored. In order to corroborate this model, a triple C137/C141/C144 LIAS variant, which lacks the cysteine ligands of the FeS_{RS} cluster and can thus bind only the FeS_{aux} cluster, was produced and its iron and acid-labile sulfide content estimated. It results 95% of [4Fe-4S] cluster occupancy (**Table S1**), suggesting that, in wild-type AI LIAS, the FeS_{aux} cluster binding site is more occupied with respect to the FeS_{RS} cluster binding site.

In conclusion, we found that dimeric [4Fe-4S] NFU1 is able to transfer its cluster to the FeS_{RS} site.

[4Fe-4S] NFU1-ISCA1 complex can transfer the cluster to the FeS_{RS} site of LIAS

We have recently showed that the NFU1-ISCA1 complex coordinates a bridged [4Fe-4S] cluster and suggested that this complex can specifically direct the [4Fe-4S] cluster to mitochondrial proteins requiring NFU1 for their maturation, such as LIAS[32]. Thus, in order to investigate the ability of the [4Fe-4S] NFU1-ISCA1 complex to transfer the cluster to LIAS, we produced the [4Fe-4S] NFU1-ISCA1 as previously reported[32] and mixed it with AI LIAS. Cluster transfer between [4Fe-4S] NFU1-ISCA1 and AI LIAS was followed by ^{1}H-^{15}N HSQC NMR experiments performing a titration in which ^{15}N labeled [4Fe-4S] NFU1-ISCA1 was added to unlabeled AI LIAS up to a 1:1 ratio was reached. In the NMR spectra acquired along the titration, we have analyzed signals that allow to monitor complex formation and/or cluster release. Some signals, such as that the two indicated in **Figure 5A**, can address whether a [4Fe-4S] NFU1-ISCA1 complex or a [4Fe-4S] NFU1-LIAS complex is formed. Two of this kind of signals having a different chemical shift depending on the formation of [4Fe-4S] NFU1-ISCA1 complex or a [4Fe-4S] NFU1-LIAS complex are shown in **Figure 5A**. In the final mixture of the titration, these signals overlay with the signals corresponding to the [4Fe-4S] NFU1-LIAS complex, thus indicating that AI LIAS displaces ISCA1 as depicted in

the cartoon of **Figure 5**. This data reproduces the same outcome that have been observed in the apo interaction (**Figure 3**). Other signals, such as that those indicated in **Figure 5B**, can allow to exclusively monitor cluster release, as their chemical shift strictly depend on the presence or absence of the [4Fe-4S] cluster bound to free or complexed NFU1. In the final mixture of the titration, these signals overlay with those corresponding to the formation of the apo form, thus supporting that the [4Fe-4S] cluster is transferred to AI LIAS, as depicted in the cartoon of **Figure 5**.

Since we showed here that [4Fe-4S] NFU1 transfers the cluster to the FeS_{RS} site of LIAS, we have investigated whether the [4Fe-4S] NFU1-ISCA1 complex can similarly work. To follow the cluster transfer to the FeS_{RS} site of LIAS, we have produced a triple C106/C111/C117A LIAS variant that lacks the cysteine ligands of the FeS_{aux} cluster and can thus bind only the FeS_{RS} cluster. The quantification of iron and acid-labile sulfide indicated that the AI LIAS variant contains ~0.5 equivalents of [4Fe-4S] clusters bound per monomeric LIAS (**Table S1**). Upon addition of one equivalent of [4Fe-4S] NFU1-ISCA1 complex to the C106/C111/C117A AI LIAS variant, the ^{1}H 1D paramagnetic NMR spectra (**Figure 5C**) showed that the intensities of the signals at 15-11 ppm, assigned to βCH_2 of the ligands of the FeS_{RS} cluster, increase in intensity, indicating that cluster transfer occurred from the NFU1-ISCA1 complex to the FeS_{RS} site. The anti-Curie temperature dependence and the chemical shifts of the signals at 15-11 ppm are consistent with the presence of an oxidized $[4Fe\text{-}4S]^{2+}$ cluster. Moreover, we observed the presence of two other signals in the 46-36 ppm region with Curie temperature dependence (inset of **Figure 5**). The Curie temperature dependence of these signals and its chemical shift are typical of protons of a cysteine residue bound to a reduced $[4Fe\text{-}4S]^{+}$ cluster, thus indicating that a fraction of the FeS_{RS} cluster is in the reduced state. The presence of protons of cysteine residues with chemical shifts typical of both reduced and oxidized [4Fe-4S] clusters indicate that the FeS_{RS} cluster can be partially reduced by 5 mM DTT present in the mixture. This result is in agreement with what previously observed in wild-type LIAS[83] and consistent with the electron transfer function of the FeS_{RS} cluster in the catalytic mechanism[88].

Discussion

The biogenesis of mitochondrial [4Fe-4S] cluster-containing proteins is governed by a complex biochemical process that comprehends up to 18 different components[73]. This high mechanistic complexity is further enhanced by the fact that the insertion of the [4Fe-4S] cluster into the recipient proteins is differently affected by the proteins involved in the biogenesis process. For example, no crucial in vivo role has been found for some late-acting mitochondrial ISC components in aconitase maturation, and this includes the [4Fe-4S] cluster carrier protein NFU1 and BOLA3[30]. On the other hand, the maturation of most other mitochondrial [4Fe-4S] proteins, especially of complex Fe-S proteins with several clusters such as respiratory complexes I and II and the radical SAM protein lipoyl synthase (LIAS) require NFU1 and BOLA3[34,38]. Furthermore, divergent models depicting how late-acting mitochondrial ISC components operate in the maturation of mitochondrial [4Fe-4S] cluster-containing proteins have been recently proposed[30,49]. As a whole, a clear picture of how [4Fe-4S] clusters are inserted into target proteins has thus far remained elusive.

Here, we have investigated the molecular mechanism of [4Fe-4S] cluster insertion in human LIAS. The latter is a member of the radical S-adenosylmethionine (SAM) superfamily, which coordinates a [4Fe-4S] cluster (FeS_{RS}) which, in its reduced state, is used to fragment SAM to methionine and a 5′-deoxyadenosin 5′-radical[82]. This radical catalyzes the last step of the biosynthesis of the lipoyl cofactor, which is the attachment of sulfur atoms at C6 and C8 of an n-octanoyl-lysyl chain on a lipoyl carrier protein. The source of these two sulfur atoms is an additional [4Fe-4S] cluster (FeS_{aux}) bound to LIAS, which has been shown to be cannibalized by the protein during catalysis to provide the sulfur atoms in the lipoyl product [82]. Recently, the E. coli homolog of human NFU1 (NfuA) was shown to restore FeS_{aux} in E. coli LIAS (LipA) after each turnover in a process that does not limit the overall rate of catalysis[17]. On the other hand, no information is available on the role of NFU1 in the insertion of the [4Fe-4S] cluster into FeS_{RS}. Our data provide the first evidence of the role of NFU1 in inserting a [4Fe-4S] cluster into the FeS_{RS} site of human LIAS.

As first finding of our study, we showed that NFU1 is a tight interactor of LIAS forming a heterodimeric complex and that the C-domain of NFU1 is in charge of specifically recognizing LIAS, while the N-domain is not directly involved in the protein-protein recognition. This result agrees with what found by yeast-two-hybrid assays that showed that the N-terminal domain of NFU1 was not found to be involved in the interaction with LIAS[49]. This result differs from what found for bacterial NfuA. Indeed, in the latter case it has been found that the N-terminal domain of NfuA tightly interacts with LipA while the C-terminal domain is unable to recognize LipA[75]. This divergent behaviour indicates that bacterial NfuA has a different mechanism of action in inserting the [4Fe-4S] clusters

into lipoyl synthase with respect to eukaryotic LIAS. In addition, LIAS by interacting with NFU1 is able of displacing the NFU1-protein partner ISCA1. LIAS replaces, indeed, ISCA1 complexed with NFU1 via the competition with the same binding site, i.e. the C-domain of NFU1. Thus, LIAS results a stronger interactor with respect to ISCA1 versus the C-domain of NFU1. In this process, ISCA1 is released as free form as no ternary complex has been observed, thus excluding that ISCA1 and LIAS recognize each other. This comprehensive protein-protein interaction network supports a model in which sequential events are involved in the [4Fe-4S] cluster insertion to LIAS with respect to a model involving a multi-protein complex, that is: i) NFU1 interacts with ISCA1 to receive the [4Fe-4S] cluster assembled on ISCA1-ISCA2 platform[32,73], and then ii) NFU1 interacts with LIAS promoting the release of ISCA1 to deliver the [4Fe-4S] cluster to LIAS. The interaction of the C-domain of NFU1 with both proteins, which increases in affinity going from ISCA1 to LIAS, is the means by which the cluster can be specifically transferred to the final target LIAS.

The second main finding of our study is that the insertion of the [4Fe-4S] cluster into the FeS_{RS} site of human LIAS occurs both when the cluster donor is homodimeric [4Fe-4S] NFU1 and when the cluster donor is heterodimeric [4Fe-4S] ISCA1-NFU1. This suggests that both the latter species can be physiological components inserting the cluster in the FeS_{RS} site of LIAS. Therefore, it is possible that two pathways might be operative in vivo in the FeS_{RS} cluster formation. One is activated once the homodimeric [4Fe-4S] NFU1 is formed, while the other works with no necessity of forming homodimeric [4Fe-4S] NFU1, but it directly involves the heterodimeric [4Fe-4S] ISCA1-NFU1 that it is formed by the transfer of the [4Fe-4S] cluster from the ISCA1-ISCA2 complex to NFU1. The existence of both pathways *in vivo* is supported by the findings that NFU1 in mitochondria is present both as homodimeric [4Fe-4S] NFU1 and as ISCA1-NFU1 complex[32,33,49]. Moreover, the two pathways can be strictly connected, as we have previously showed in vitro[32] that the addition of ISCA1 to homodimeric [4Fe-4S] NFU1 promotes the formation of the heterodimeric [4Fe-4S] ISCA1-NFU1.

In conclusion, we have showed that NFU1 is the trigging factor for the insertion of a [4Fe-4S] cluster into FeS_{RS} site of human LIAS by promoting a specific interaction with LIAS via its C-domain. The latter domain is indeed the key structural component since it is able to bind a [4Fe-4S] cluster via homo-dimerization and hetero-dimerization with ISCA1 to form [4Fe-4S] NFU1 and [4Fe-4S] ISCA1-NFU1, respectively, and then both these species, as shown here, can deliver the cluster to FeS_{RS} site of human LIAS.

Figures

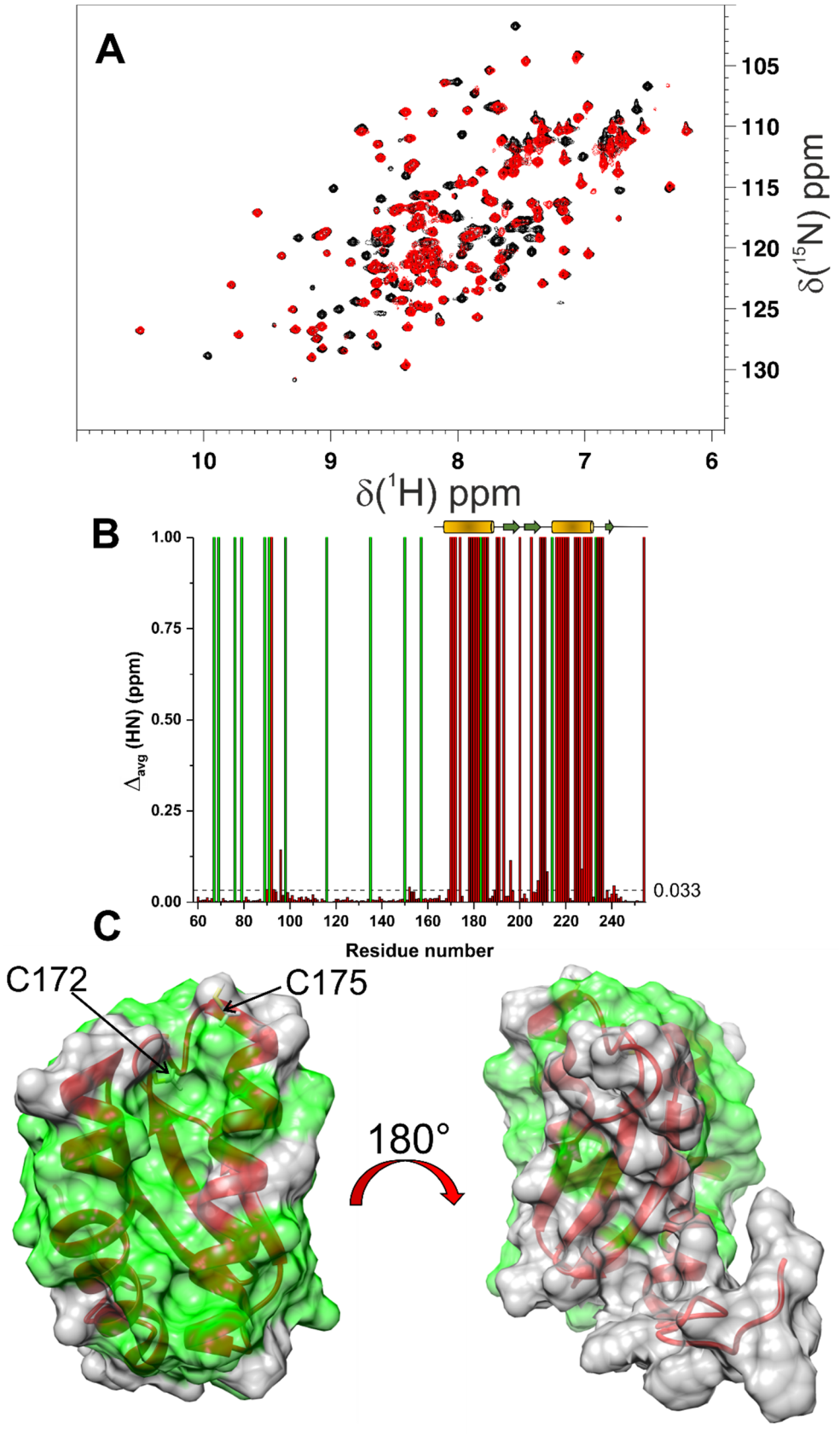
A
105
110
115
120
125
130
δ(15N) ppm
10
9
8
7
6
δ(1H) ppm
B
1.00
0.75
0.50
0.25
0.00
Δavg (HN) (ppm)
0.033
60
80
100
120
140
160
180
200
220
240
Residue number
C
C172
C175
180°

Figure 1. Apo NFU1 interacts with LIAS via its C-terminal domain. (**A**) Overlay of ^{1}H-^{15}N HSQC NMR maps of ^{15}N-labeled apo NFU1 (black) and the 1:1 ^{15}N-labeled apo NFU1-unlabeled AI LIAS mixture. (**B**) Backbone weighted average chemical shift differences $\Delta_{avg}(HN)$ (i.e., $(((\Delta H)^2 + (\Delta N/5)^2)/2)^{1/2}$) (red bars), between apo NFU1 and the 1:1 ^{15}N-labeled apo NFU1-unlabeled AI LIAS mixture. The indicated threshold values (obtained by averaging $\Delta_{avg}(HN)$ values plus 1σ) were used to define meaningful chemical shift differences. The green bars represent proline residues. The secondary structure elements of the C-domain of apo NFU1 are also shown. (**C**) The meaningful chemical shift changes are shown in green on the surface of the structure of the apo NFU1 C-domain. The cluster binding cysteines (C172 and C175) are depicted.

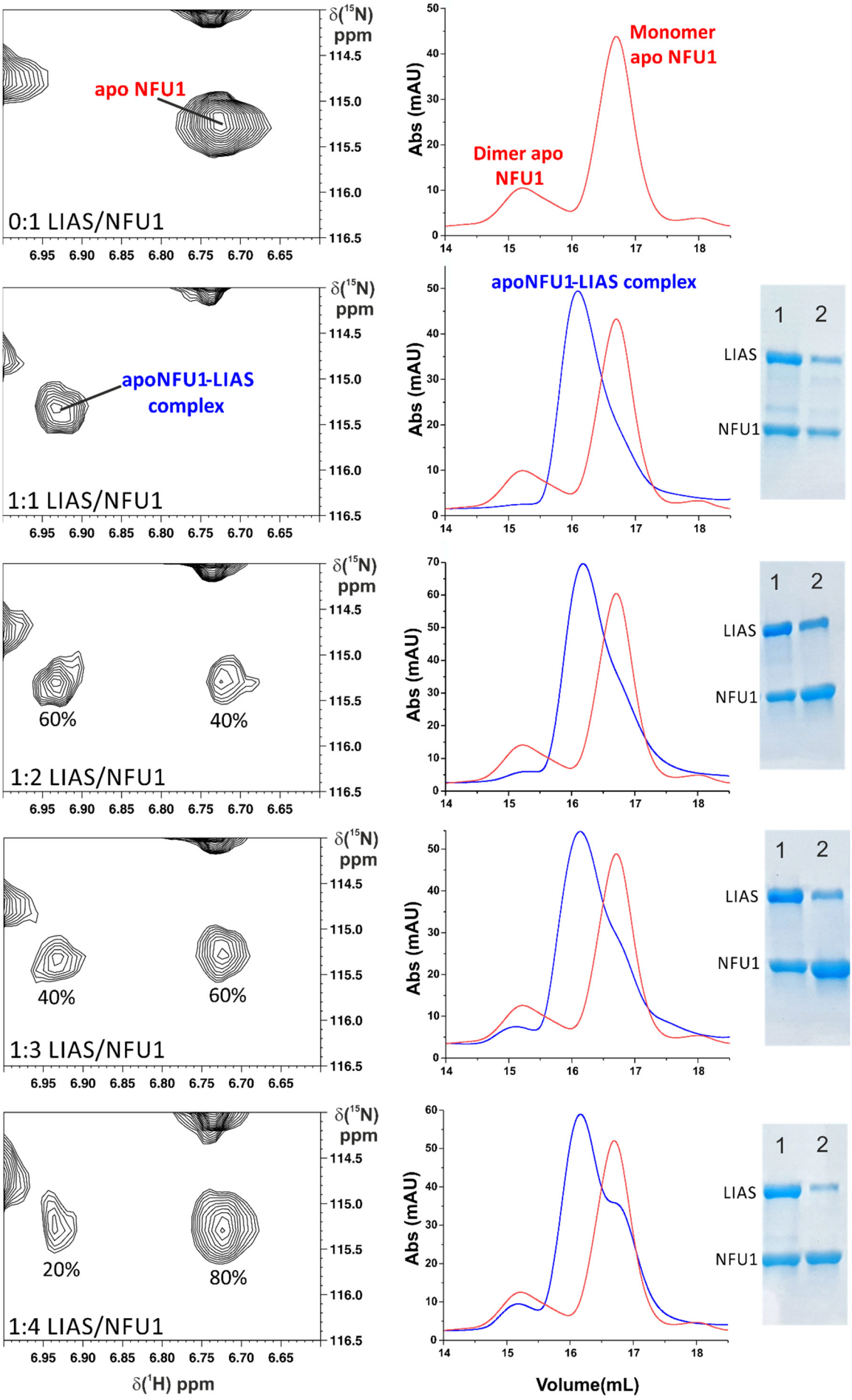
apo NFU1
0:1 LIAS/NFU1
apoNFU1-LIAS complex
1:1 LIAS/NFU1
60%
40%
1:2 LIAS/NFU1
40%
60%
1:3 LIAS/NFU1
20%
80%
1:4 LIAS/NFU1
δ(15N) ppm
δ(1H) ppm
Monomer apo NFU1
Dimer apo NFU1
apoNFU1-LIAS complex
Abs (mAU)
Volume(mL)
LIAS
NFU1
1
2

Figure 2. Apo NFU1 and LIAS form a heterodimeric complex. On the left, a region of the ^{1}H-^{15}N HSQC NMR maps at different AI LIAS/NFU1 containing a signal of ^{15}N-labeled NFU1 in slow exchange regime on the NMR time scale are shown. The relative percentages of apo NFU1 and of the heterodimeric apo NFU1-LIAS complex are indicated. On the right, the analytical gel filtration chromatograms of the same mixtures analyzed by NMR are shown. SDS-PAGEs of the fraction 1 eluted between 16.0-16.5 mL and of fraction 2 eluted at 16.5-17.0 mL are reported on the right of each chromatogram.

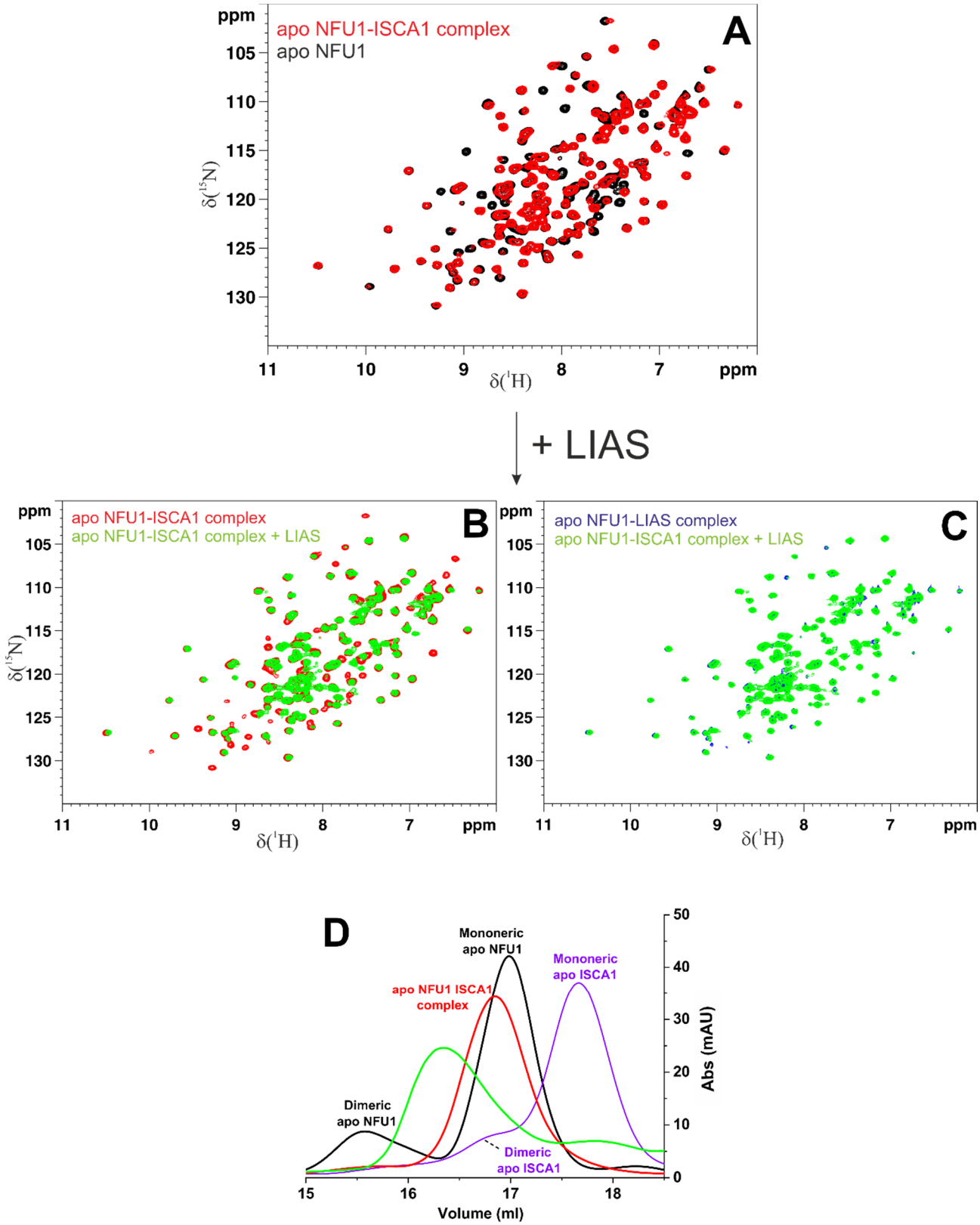
A
apo NFU1-ISCA1 complex
apo NFU1
ppm
105
110
115
120
125
130
δ(15N)
11
10
9
8
7
ppm
δ(1H)
+ LIAS
B
apo NFU1-ISCA1 complex
apo NFU1-ISCA1 complex + LIAS
C
apo NFU1-LIAS complex
apo NFU1-ISCA1 complex + LIAS
D
Mononeric
apo NFU1
Mononeric
apo ISCA1
apo NFU1 ISCA1
complex
Dimeric
apo NFU1
Dimeric
apo ISCA1
Abs (mAU)
50
40
30
20
10
0
15
16
17
18
Volume (ml)

Figure 3. LIAS displaces ISCA1 from the apo ISCA1-NFU1 complex to form a heterodimeric complex with apo NFU1. (**A**) Overlay of ^{1}H-^{15}N HSQC NMR maps of ^{15}N-labeled apo NFU1 (black) and of the apo ^{15}N-labeled NFU1-unlabeled ISCA1 complex (red). (**B**) Overlay of ^{1}H-^{15}N HSQC NMR maps of the apo ^{15}N-labeled NFU1-unlabeled ISCA1 complex (red) and of a 1:1 mixture between the apo NFU1-ISCA1 complex and unlabeled AI LIAS (green). (**C**) Overlay of ^{1}H-^{15}N HSQC NMR maps of the apo ^{15}N-labeled NFU1-unlabeled AI LIAS complex (blue) and of a 1:1 mixture between the apo NFU1-ISCA1 complex and unlabeled AI LIAS (green). (**D**) Analytical gel filtration chromatograms of apo ISCA1 (violet), apo NFU1 (black), apo NFU1-ISCA1 complex (red) and a 1:1 mixture between the apo NFU1-ISCA1 complex and unlabeled AI LIAS (green) are shown.

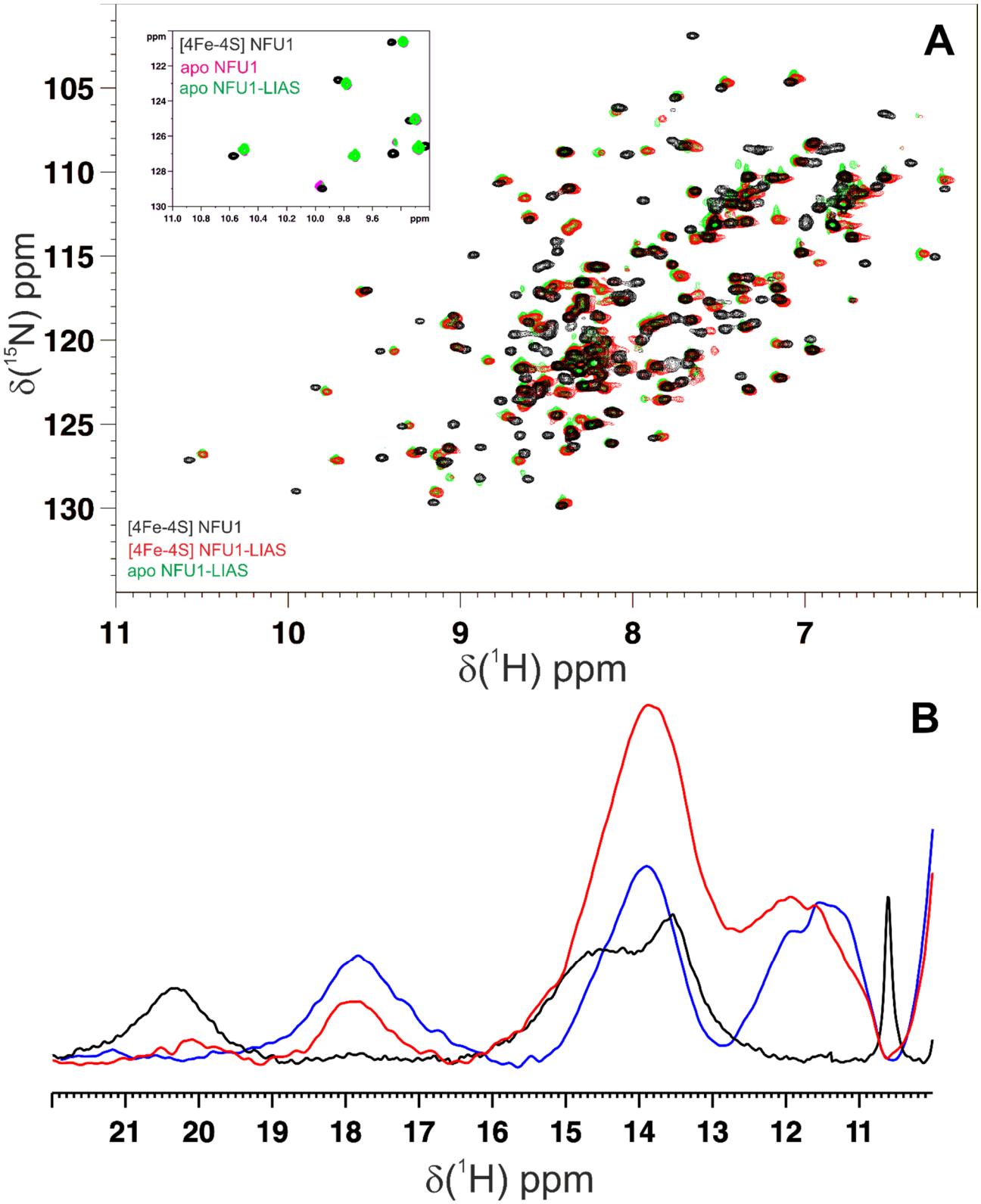
A
[4Fe-4S] NFU1
apo NFU1
apo NFU1-LIAS
[4Fe-4S] NFU1
[4Fe-4S] NFU1-LIAS
apo NFU1-LIAS
δ(15N) ppm
δ(1H) ppm
B
δ(1H) ppm

Figure 4. [4Fe-4S] NFU1 transfers the cluster to the FeS_{RS} site of LIAS. (**A**) Overlay of ^{1}H-^{15}N HSQC NMR maps of ^{15}N-labeled [4Fe-4S] NFU1 (black), of the apo ^{15}N-labeled NFU1-LIAS complex (green) and of a 1:1 mixture of ^{15}N-labeled [4Fe-4S] NFU1 and unlabeled AI LIAS (red). In the inset, a region of the ^{1}H-^{15}N HSQC NMR map that identifies signals monitoring the [4Fe-4S] cluster release from [4Fe-4S] NFU1 is shown. (**B**) 1D ^{1}H NMR spectra tailored for the detection of hyperfine-shifted signals of $[4Fe\text{-}4S]^{2+}$ NFU1 (black), AI LIAS (blue) and 1:1 mixture of ^{15}N-labeled $[4Fe\text{-}4S]^{2+}$ NFU1 and unlabeled AI LIAS (red) were acquired at 298 K in 50 mM phosphate buffer pH 7.0, 150 mM NaCl and 5 mM DTT.

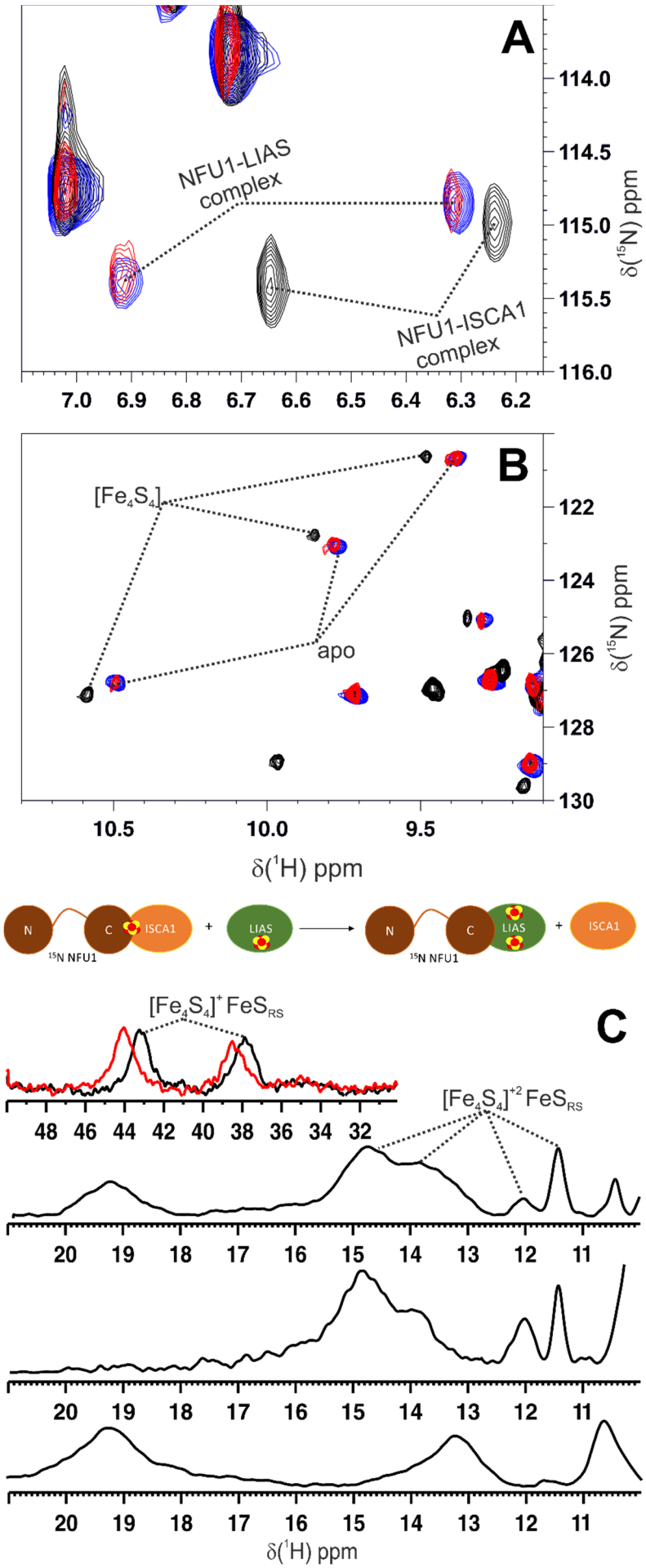
A
NFU1-LIAS complex
NFU1-ISCA1 complex
δ(15N) ppm
B
[Fe4S4]
apo
δ(15N) ppm
δ(1H) ppm
N
C
ISCA1
15N NFU1
LIAS
[Fe4S4]+ FeSRS
[Fe4S4]+2 FeSRS
C
δ(1H) ppm

Figure 5. [4Fe-4S] ISCA1-NFU1 transfers the cluster to the FeS_{RS} site of LIAS. (**A** and **B**) Overlay of two different regions of ^{1}H-^{15}N HSQC NMR maps of ^{15}N-labeled [4Fe-4S] NFU1-ISCA1 complex (black), of ^{15}N-labeled [4Fe-4S] or apo NFU1-LIAS complex (blue) and of a 1:1 mixture of ^{15}N-labeled [4Fe-4S] NFU1-ISCA1 complex and unlabeled AI LIAS (red). The signals changing their chemical shifts upon cluster transfer or different complex formation are indicated. On the bottom, a cartoon of the reaction, proposed on the basis of the NMR data, is reported. (**C**) 1D ^{1}H NMR spectra tailored for the detection of hyperfine-shifted signals of $[4Fe\text{-}4S]^{2+}$ NFU1-ISCA1 (on the bottom), C106/C111/C117A AI LIAS variant (on the middle) and 1:1 mixture of ^{15}N-labeled $[4Fe\text{-}4S]^{2+}$ NFU1-ISCA1 and unlabeled C106/C111/C117A AI LIAS variant (on the top) were acquired at 298 K in 50 mM phosphate buffer pH 7.0, 150 mM NaCl and 5 mM DTT. In the inset, a far-shifted 50-30 ppm region of the NMR spectrum is showed at two different temperatures, 298 K (black) and 290 K (red). The assignment of the signals is based on what previously reported[83].

Supplementary Materials

Molecular basis of [4Fe-4S] cluster insertion in human lipoyl synthase

Giovanni Saudino [1,2], Simone Ciofi-Baffoni[1,2,] Lucia Banci [1,2,3]

[1]Magnetic Resonance Center CERM, University of Florence, Via Luigi Sacconi 6, 50019, Sesto Fiorentino, Florence, Italy.

[2]Department of Chemistry, University of Florence, Via della Lastruccia 3, 50019 Sesto Fiorentino, Florence, Italy.

[3]Consorzio Interuniversitario Risonanze Magnetiche di Metalloproteine (CIRMMP), Via L. Sacconi 6, 50019 Sesto Fiorentino, Italy.

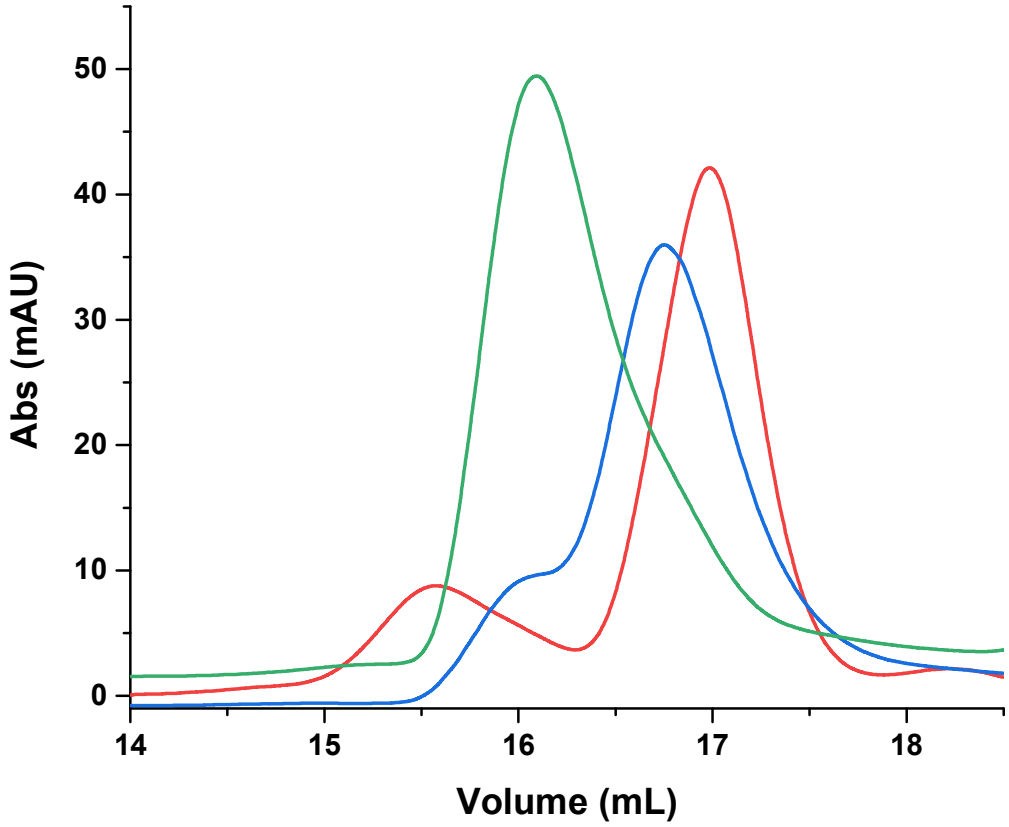

Figure S1. Analytical gel filtration of the the heterodimeric complex formed by apo NFU1 and AI LIAS. The chromatograms of a 1:1 apo NFU1-AI LIAS mixture (green), AI LIAS (blue), apo NFU1 (red) are shown.

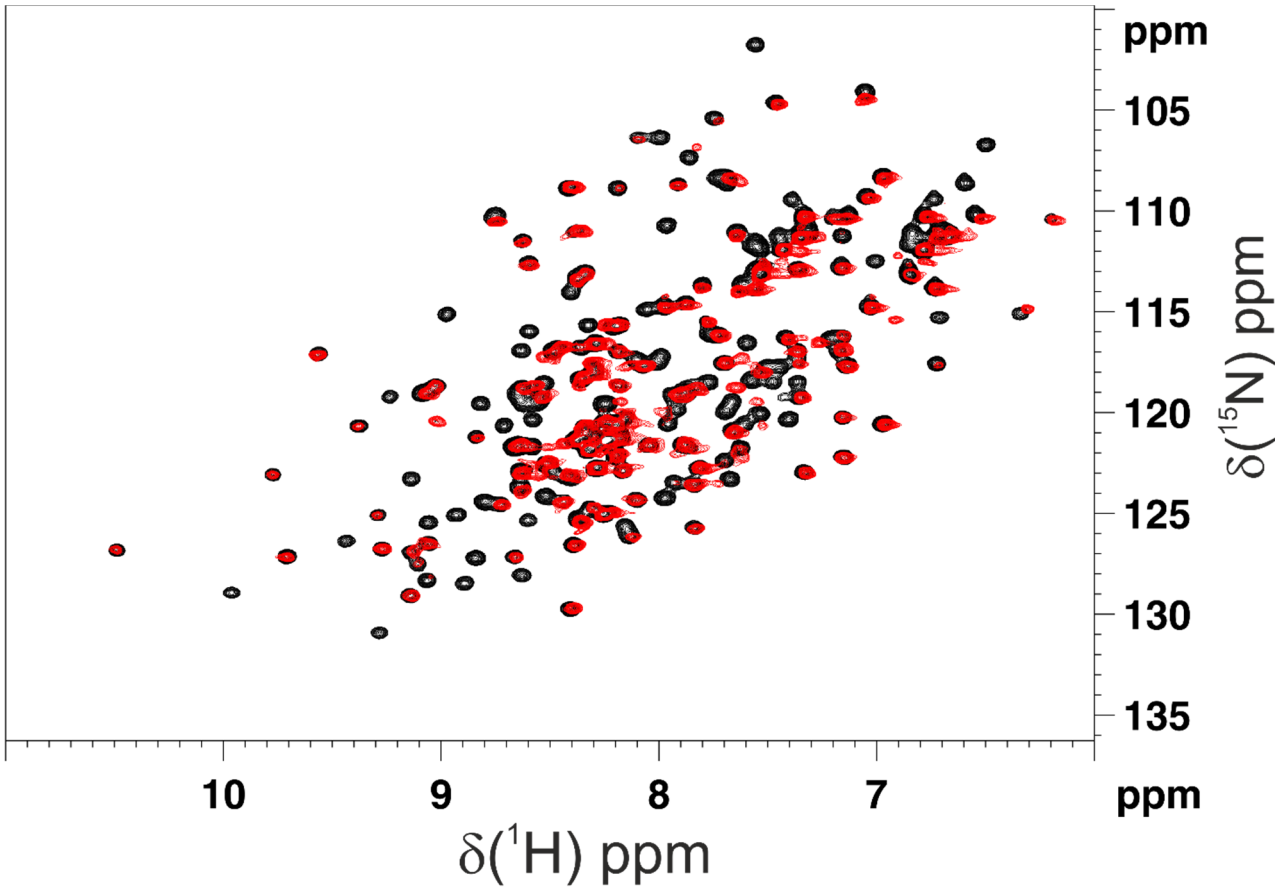

Figure S2. Apo NFU1 is not formed in the cluster transfer from [4Fe-4S] NFU1 to AI LIAS. Overlay of ^{1}H-^{15}N HSQC NMR maps of ^{15}N labeled apo NFU1(black) and of a 1:1 mixture of ^{15}N labeled NFU1 and unlabeled AI LIAS (red).

Sample	Fe[a]	S[a]	[4Fe-4S] cluster occupancy
Wild-type LIAS	3.9±0.1	4.1 ± 0.1	50%
C137/C141/C144 LIAS variant	3.3 ± 0.1	3.9 ± 0.1	95%
C106/C111/C117A LIAS variant	2.0 ± 0.1	2.1 ± 0.1	50%

[a]Fe and acid-labile S measurements are reported as mol Fe or S per mol of monomeric protein. Data are the average of three independent samples.

Table S1. Iron and acid-labile sulfide quantification of as-isolated LIAS proteins.

2.4 Structural characterization of FDX2: the electron donor of the ISC assembly machinery.

Introduction

Ferredoxins are iron sulfur proteins extensively investigated for their fundamental role as electron donors in all kingdoms of life, from bacteria to mammals. Ferredoxins provide electrons to cytochrome P450 enzymes, acting as electron shuttle between the ferredoxin reductase and P450 enzymes[47,89]. The ferredoxins are also fundamental in the mitochondrial iron sulfur cluster assembly machinery being involved in the [2Fe-2S] and [4Fe-4S] clusters de novo synthesis. Recently, in vivo studies showed that mitochondria possess two functionally independent ferredoxins with highly specific roles in distinct biochemical pathways: i) FDX1 that reduces mitochondrial cytochrome P450 enzymes that are crucial in adrenal steroidogenesis and vitamin D biosynthesis[90,91], ii) FDX2 that specifically contributes to both heme A and iron sufur clusters biosynthesis[30,45]. The mitochondrial iron sulfur cluster assembly machinery involves up to 18 different proteins and is divided in three steps. The [2Fe-2S] cluster is first assembled on the ISCU2 scaffold protein, forming a large complex with NFS1, ISD11, FXN, ACP and FDX2. The latter gives two electrons required for the [2Fe-2S] cluster assembly[23]. Then, the [2Fe-2S] cluster is released from ISCU2 to GLRX5 assisted by the HSPA9 chaperone and Hsc20 co-chaperone that are required for a safe cluster trafficking. GLRX5 can then donate two [2Fe-2S] clusters to the ISCA1-ISCA2-IBA57 hetero complex that perform the reductive coupling of two [2Fe-2S] clusters to assembles a [4Fe-4S] cluster[29,30]. It was proposed that FDX2 supplies the electrons required to reduce two [2Fe-2S] clusters to form a [4Fe-4S] cluster. Although, the FDX2 role in the ISC assembly machinery is well-known, the molecular mechanism and the interaction pattern between ISCA1, ISCA2 and FDX2 that lead to the formation of the [4Fe-4S] cluster is still unclear.

In this study, we have optimize the production protocol of the recombinant FDX2 in its apo, $[2Fe\text{-}2S]^{2+}$ and $[2Fe\text{-}2S]^{+}$ bound form. Subsequently, we structurally characterized the reduced and oxidized form of [2Fe-2S] FDX2 through diamagnetic and paramagnetic NMR and UV-visible spectroscopy. Finally, we have investigated the interaction pattern between FDX2 and ISCA1 and ISCA2 in order to elucidate protein-protein interaction network and to clarify which proteins of the ISCA1-ISCA2 hetero-complex is the preferential electron receiver. Our data provide a preliminary clue that $[2Fe\text{-}2S]^{2+}$ FDX2 does not interact with as purified ISCA1 and ISCA2 free proteins.

Materials and Methods

Protein production

We have set up and optimized a protein expression and purification protocol of FDX2 reaching a final yield of 25 mg of protein per liter of culture. pET28a plasmid containing full-length FDX2 gene (UniProt: Q4P4F2) was purchased by Twist Bioscience in order to express N-terminal 6His-tag-FDX2 protein. The latter plasmid was transformed in Escherichia coli BL21-Gold(DE3) (Agilent) competent cells. Cells were cultivated at 37 °C in LB media adding Kanamycin (50 lg/mL), 6 mL of Solution Q (40 mM HCl, 50 mg/l $FeCl_2$ $4H_2O$, 184 mg/l $CaCl_2$ $2\ H_2O$, 64 mg/l H_3BO_3, 18 mg/l $CoCl_2$ $6\ H_2O$, 4 mg/l $CuCl_2$ $2\ H_2O$, 340 mg/l $ZnCl_2$, 355 mg/l Na_2MoO_4 $2\ H_2O$, 40 mg/l $MnCl_2$ $4\ H_2O$) per liter of LB medium until OD_{600} reached 0.8. Protein expression was induced with 0.5 mM IPTG at 37 °C for 5 h. The cells were harvested by centrifugation at 5000 rpm for 20 min (JA-10, Beckman Coulter), and then resuspended in binding buffer (50 mM Tris-HCl, 500 mM NaCl, 15 mM Imidazole, pH 8.0) and were lysed by sonication at 4 °C(2'' ON, 9.9'' OFF for 40 minutes). After sonication, the cell lysate was ultracentrifuged at 40000 rpm for 40 minutes in order to remove cellular organelles and membranes. N-terminal 6His-tag-FDX2 was purified from the lysate using a HisTrap HP column (GE Healthcare) and the 6His- tag was cleaved by thrombin protease treatment over-night at room temperature in binding buffer. HisTrap column were performed to remove the 6His-tag from the digested FDX2. A mixture of apo and $[2Fe\text{-}2S]^{2+}$ FDX2 (as purified FDX2) was purified performing all the purifications steps under anaerobic conditions. The anaerobically purified FDX2 protein was characterized by UV-visible, paramagnetic and diamagnetic NMR spectroscopies and analytical size exclusion chromatography. Protein quantification was carried out with the Bradford protein assay, using BSA as a standard. The production of human ISCA2, and human full length ISCA1 in their apo and Fe-S cluster-bound forms were obtained as previously described in literature[27,29,32]. As previously reported[27], the purification under anaerobic conditions of ISCA2, named as purified ISCA2, resulted in a dimer, which is composed by a mixture of apo and $[2Fe\text{-}2S]^{2+}$ cluster-bound dimeric species with a $[2Fe\text{-}2S]^{2+}$ cluster occupancy of 0.1–0.2 cluster per homodimer. As already published[32], the purification under anaerobic conditions of ISCA1, named as purified ISCA1, resulted in a mixture of monomer and dimer in both apo and $[2Fe\text{-}2S]^{2+}$ cluster-bound state with a $[2Fe\text{-}2S]^{2+}$ cluster occupancy of 0.3 cluster per homodimer.

Analytical size exclusion chromatography

In the analytical size exclusion chromatography, purified samples were loaded on a Superdex 200. Increase 10/300 GL column attached to an AKTA pure chromatography unit with a continuous flow rate of 0.60 mL/min. The column was calibrated with gel filtration marker calibration kit, 6500–

66000 Da (Sigma-Aldrich), to obtain the apparent molecular masses of the detected species. The column was equilibrated with degassed phosphate buffer 50 mM, 150 mM NaCl, 5 mM DTT and pH 7.0. SEC-MALS data were acquired by attaching SuperdexTM 200 Increase 10/300 GL column to a DAWN HELEOS system with a continuous flow rate of 0.6 mL/min using a filtered buffer (50 mM, 150 mM NaCl, 5 mM DTT and pH 7.0). Each experiment was successfully repeated at least three times.

Chemical Reconstitution

Chemical reconstitution of as purified FDX2 was anaerobically performed in 50 mM Tris-HCl, 100 mM NaCl and 5 mM DTT buffer at pH 8.0 adding six equivalents of $FeCl_3$ and Na_2S to a protein solution of ~60-100 μM. The reaction was incubated overnight at room temperature. Anaerobic conditions were obtained performing the chemical reconstitution in glove-box (MBraun Labstar 130) with less than 2 ppm of oxygen and by using all buffers degassed. The excess of $FeCl_3$ and Na_2S as well as Fe-S precipitates were removed by PD-10 desalting column[92].

[2Fe-2S] cluster removal

As purified FDX2 was treated with ferricyanide and EDTA to totally remove the cluster from the protein and obtain apo FDX2. 100 uM of EDTA and 10 uM of ferricyanide were added to the protein solution and then incubated for 1 hour. Later, the EDTA and ferricyanide were removed by PD-10 desalting column. The apo FDX2 was stored in 50 mM phosphate buffer, 150 mM NaCl, 5 mM DTT and pH 7.0 buffer.

UV- and CD-visible spectroscopy

UV-visible spectra were acquired to characterize the cluster bound form of anaerobically purified and chemically reconstituted FDX2. The experiments were performed under anaerobic conditions, preparing the samples in glove-box with degassed buffers and using a gastight cuvette. UV-visible spectra were executed in 50 mM phosphate buffer, 150 mM NaCl, 5 mM DTT and pH 7.0 at room temperature on a Cary 50 Eclipse spectrophotometer. Each experiment was successfully repeated three times.

NMR spectroscopy

Diamagnetic NMR spectra were recorded on Bruker AVANCE 700 and 950 MHz, processed using the standard Bruker software (Topspin). ^{1}H-^{15}N HSQC spectra were performed at 298 K in 50 mM phosphate buffer, 150 mM NaCl, 5 mM DTT pH 7.0, 10% (v/v) D_2O. To characterized the structural

properties of the [2Fe-2S] FDX2, the ^{1}H-^{15}N HSQC spectra were acquired using degassed buffer and 5 mm gastight NMR tube. To monitor the possible interaction among ISCA1, ISCA2 and FDX2, ^{15}N labeled $[2Fe\text{-}2S]^{2+}$ FDX2 was stepwise titrated in anaerobic conditions with increasing amounts of unlabeled as purified ISCA2 or ISCA1. Chemical shifts of the backbone NHs observed in the ^{1}H ^{15}N HSQC spectra along the additions of the unlabeled were compared with chemical shifts of ^{15}N labeled FDX2 in the initial state. ^{1}H 1D paramagnetic NMR experiments were acquired at 400 MHz with a ^{1}H optimized 5 mm probe at temperatures ranging from 283 K and 298 K, with protein samples in 50 mM phosphate buffer, 150 mM NaCl, 5 mM DTT pH 7.0, 99% (v/v) D_2O. In the case of the cluster reduction experiments by dithionite, the protein was in 50 mM TRIS 100 mM NaCl and 5 mM DTT, pH 8, 99% (v/v) D_2O. The protein concentration was 0.5-0.6 mM. Water signal was suppressed via fast repetition experiments and water selective irradiation[85,93]. Experiments were typically performed using an overall recycle delay of 60 ms. Squared cosine and exponential multiplications were applied prior to Fourier transformation[86]. Manual baseline correction was performed, using polynomial functions. Each experiment was successfully repeated three times.

Results

Structural characterization of FDX2

FDX2 production performed under anaerobic conditions lead to a mixture of apo FDX2 and [2Fe-2S]$^{2+}$ cluster bound forms (as purified FDX2, hereafter). The anaerobically purified FDX2 were chemically reconstituted ([2Fe-2S]$^{2+}$ FDX2 hereafter) in order to increase the holo FDX2 fraction (see Material and Methods). The cluster bound species were analysed by UV-visible and paramagnetic NMR spectroscopy to explore the cluster coordination environment and oxidation state. The UV-visible spectra of the [2Fe-2S]$^{2+}$ FDX2 indicated a significant increase in the cluster-bound fraction, upon chemical reconstitution (**Figure 1A**). This is shown by the intensity of the peaks at 410 and 320 nm, that are characteristic of the [2Fe-2S]$^{2+}$ cluster bound to the proteins, which significantly increased. The ^{1}H 1D paramagnetic NMR spectrum [2Fe-2S]$^{2+}$ FDX2 showed a broad signal between 35 and 25 ppm and a sharper one at 12.5 ppm (**Figure 1B**). The chemical shift values of these signals and their linewidths are typical of βCH_2 and αCH signals of cysteine bound to a [2Fe-2S]$^{2+}$ cluster with an S = 0 electronic ground state[14,94]. In the "diamagnetic" ^{1}H 1D NMR spectrum of [2Fe-2S]$^{2+}$ FDX2 (**Figure 1C**) the backbone NH signals (10-6 ppm range) are well distributed and narrow in agreement with a folded protein. FDX2 fold was additionally investigated via ^{1}H-^{15}N HSQC NMR spectrum (**Figure 1D**, black spectrum) that is consistent with a monomeric protein having a well-folded and globular structure. In fact, the latter spectrum shows all the cross-peaks having wide dispersions and sharp linewidths. Analytical gel filtration of as purified FDX2 showed a single and symmetric peak at 17.15 ml, consistent with a globular folded protein of 16 KDa (**Figure 2**).

In order to characterize the apo form of FDX2, the as purified FDX2 species were treated with EDTA and ferricyanide (see **Material and Methods**) to remove the cluster, and the ^{1}H-^{15}N HSQC NMR spectrum was acquired (**Figure 1D**, red spectrum). In the latter NMR spectrum, all the signals are mostly concentrated on the central area within 8.6-7.8 ppm range, indicating that the tertiary protein structure of apo FDX2 is lost. This indicates that [2Fe-2S] cluster is fundamental for the correct protein folding in addition to its well-known electron transfer role.

[2Fe-2S] FDX2 redox properties

The chemically reconstituted [2Fe-2S]$^{2+}$ FDX2 was titrated with sodium dithionite, a reductant extensively used for reducing iron sulfur clusters. The reduction process was followed via UV-vis spectroscopy and ^{1}H 1D paramagnetic NMR spectroscopy. By adding two equivalents of dithionite

with respect to protein concentration, the peaks at 420 and 460nm of the UV-vis spectrum of the [2Fe-2S]$^{2+}$ FDX2 were almost totally quenched, indicating the reduction of the cluster (**Figure 3A**). Once the final mixture (light blue spectrum in **Figure 3A**) was air exposed the latter peaks reappear indicating partial re-oxidation of the [2Fe-2S] cluster (black bold spectrum in **Figure 3A**), demonstrating the chemical reduction/oxidation is possible avoiding the cluster destruction. The reduction process has been also followed via ^{1}H 1D paramagnetic NMR. The ^{1}H 1D paramagnetic NMR spectrum of [2Fe-2S]$^{2+}$ FDX2 acquired (on the top of **Figure 3B**) shows the characteristic broad peak of a oxidized [2Fe-2S]$^{2+}$ clusters. Along the dithionite addition the latter signals disappear and new sharper signals at lower ppm values appear, indicating the formation of a reduced [2Fe-2S]$^{+}$cluster species. After the reduction the electron spin relaxation rates of both iron ions increase, and consequently, the coupled nuclear spins relax slower and the NMR signals of the βCH_2 bound to the cluster became sharper than those in the oxidized cluster[14,95].

FDX2 interaction pattern in the third step of the ISC assembly machinery

In order to identify possible protein-protein interactions between [2Fe-2S]$^{2+}$ FDX2 and as purified ISCA1 or/and as purified ISCA2, which have 0.2/0.3 [2Fe-2S]$^{2+}$ cluster occupancy (see Materials and Methods), a ^{1}H-^{15}N HSQC NMR titration was performed. First, unlabeled as purified ISCA1 was stepwise added to the ^{15}N labeled chemically reconstituted [2Fe-2S]$^{2+}$ FDX2 up to 1:1 ratio, and along the as purified ISCA1 additions no chemical shift changes were observed (**Figure 4A**). The final ^{1}H-^{15}N HSQC map is totally superimposable with the ^{1}H-^{15}N HSQC map of the starting material, indicating that the two proteins do not interact each other. An analogous ^{1}H-^{15}N HSQC NMR titration was performed with unlabeled as purified ISCA2, which was stepwise added to ^{15}N labeled chemically reconstituted [2Fe-2S]$^{2+}$ FDX2. Reaching the 1:1 protein ratio, no chemical shift changes were observed in the spectrum (**Figure 4B**). The final ^{1}H-^{15}N HSQC spectrum is highly superimposable with the one of the starting material. These data lead to the conclusion that there is no protein-protein interaction between [2Fe-2S]$^{2+}$ FDX2 and as purified ISCA1 or ISCA2.

Discussion

The structural characterization of FDX2 was performed through NMR spectroscopy, UV-vis spectroscopy and analytical gel filtration. The collected data showed that $[2Fe\text{-}2S]^{2+}$ FDX2 is a well folded and globular protein. On the contrary, apo FDX2 is partially unfolded. In fact, after the cluster removal, most of its signals in the $^{1}H\text{-}^{15}N$ HSQC spectrum are overlapped and mainly grouped in the 8.5-7.5 ppm range (**Figure 1D**), indicating a loss of tertiary structure. Therefore, the [2Fe-2S] cluster is essential for FDX2 to obtain the correct folding. Paramagnetic NMR and UV-vis spectroscopy were then applied in order to explore the [2Fe-2S] redox properties. Both, ^{1}H 1D paramagnetic NMR and UV-vis spectra of [2Fe-2S] FDX2 (**Figure 1**) are typical of the oxidized $[2Fe\text{-}2S]^{2+}$ form. However, a reduced $[2Fe\text{-}2S]^{+}$ cluster of FDX2 is required to perform the electron transfer mechanism in the [4Fe-4S] cluster synthesis by ISCA1, ISCA2 and IBA57. $[2Fe\text{-}2S]^{+}$ FDX2 was thus produced through the reduction of the oxidized FDX2 by sodium dithionite. The ^{1}H 1D paramagnetic spectrum of reduced FDX2 showed the signals characteristic of the $[2Fe\text{-}2S]^{+}$ cluster (**Figure 3A**). Moreover, once reduced FDX2 is exposed to air, the UV-vis spectra showed the rea-appearance of signals at 420 and 460 nm indicating the re-oxidation of the [2Fe-2S] cluster. This data clearly indicated that the *in vitro* redox reaction on the [2Fe-2S] cluster of FDX2 is reversible. Finally, the FDX2 interaction pattern with ISCA1 and ISCA2 was analysed. We have performed two $^{1}H\text{-}^{15}N$ HSQC NMR titrations using ^{15}N labeled $[2Fe\text{-}2S]^{2+}$ FDX2 and unlabeled as purified ISCA1 or unlabeled as purified ISCA2. In both cases, no chemical shift changes were observed demonstrating that FDX2 does not interact with apo ISCA1 or apo ISCA2 suggesting that other protein partner(s) are required in the electron transfer process, for example the heterocomplex ISCA1-ISCA2 and IBA57. Further studies are thus required to investigate how FDX2 provides the electrons required to assemble a [4Fe-4S] cluster.

Conclusion

We have provided a structural characterization of human FDX2 and analysed the redox properties of the [2Fe-2S] bound to the protein. Moreover, we have set the stage for the [4Fe-4S] cluster synthesis study discovering that isolated ISCA1 and ISCA2 are not involved in the electron transfer process, and thus suggesting that they should operate in the process in a complexed form with each other and/or with IBA57. In this scenario, IBA57 could thus play an essential role in the [4Fe-4S] cluster formation acting as an electron shuttle between FDX2 and ISCA1-ISCA2 hetero-complex. However, further characterization is required to deep comprehend the [4Fe-4S] cluster formation. The following experiments are now underway:

- A ^{1}H-^{15}N HSQC titration between $[2Fe\text{-}2S]^{2+}$ FDX2 and apo ISCA1-ISCA2 hetero-complex alone or with IBA57 in order to investigate the interaction network.
- Mix the reduced $[2Fe\text{-}2S]^{+}$ FDX2 with the $[2Fe\text{-}2S]^{2+}$ ISCA1-ISCA2 hetero-complex in order to follow the electron transfer for the [4Fe-4S] synthesis. Repeating the experiments with and without IBA57 to understand its role in this process.

Figures

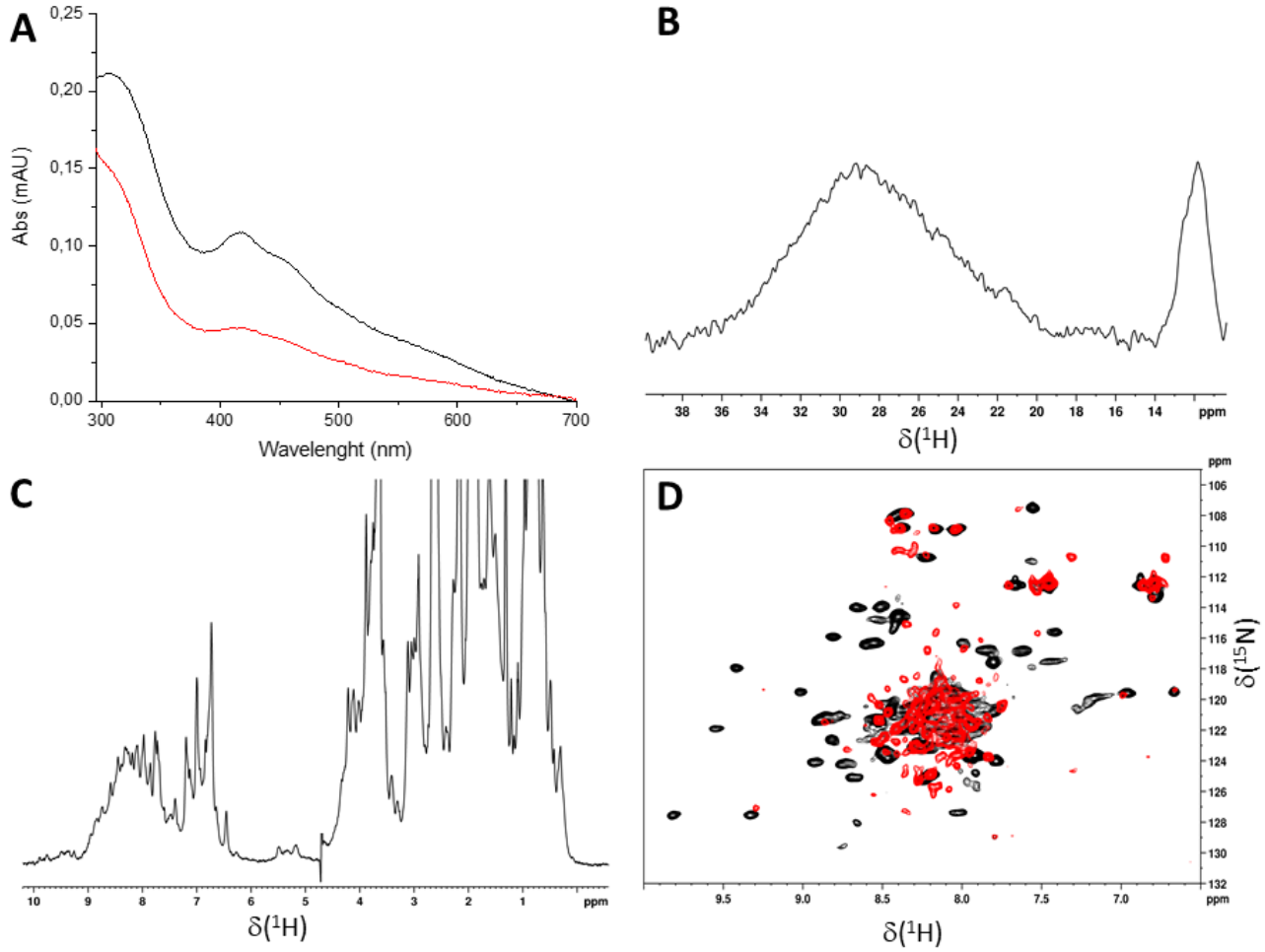

Figure 1. (**A**) UV-visible spectra of $[2Fe\text{-}2S]^{2+}$ FDX2 after (black) and before chemical reconstitution (red) (**B**) ^{1}H 1D paramagnetic NMR spectrum of $[2Fe\text{-}2S]^{2+}$ FDX2 (**C**) ^{1}H 1D NMR spectrum of $[2Fe\text{-}2S]^{2+}$ FDX2 (**D**) Overlay of the $^{1}H\text{-}^{15}N$ HSQC spectrum acquired on ^{15}N labeled $[2Fe\text{-}2S]^{2+}$ FDX2 (black) with the $^{1}H\text{-}^{15}N$ HSQC spectra acquired on ^{15}N labeled apo FDX2 after the cluster removal (red).

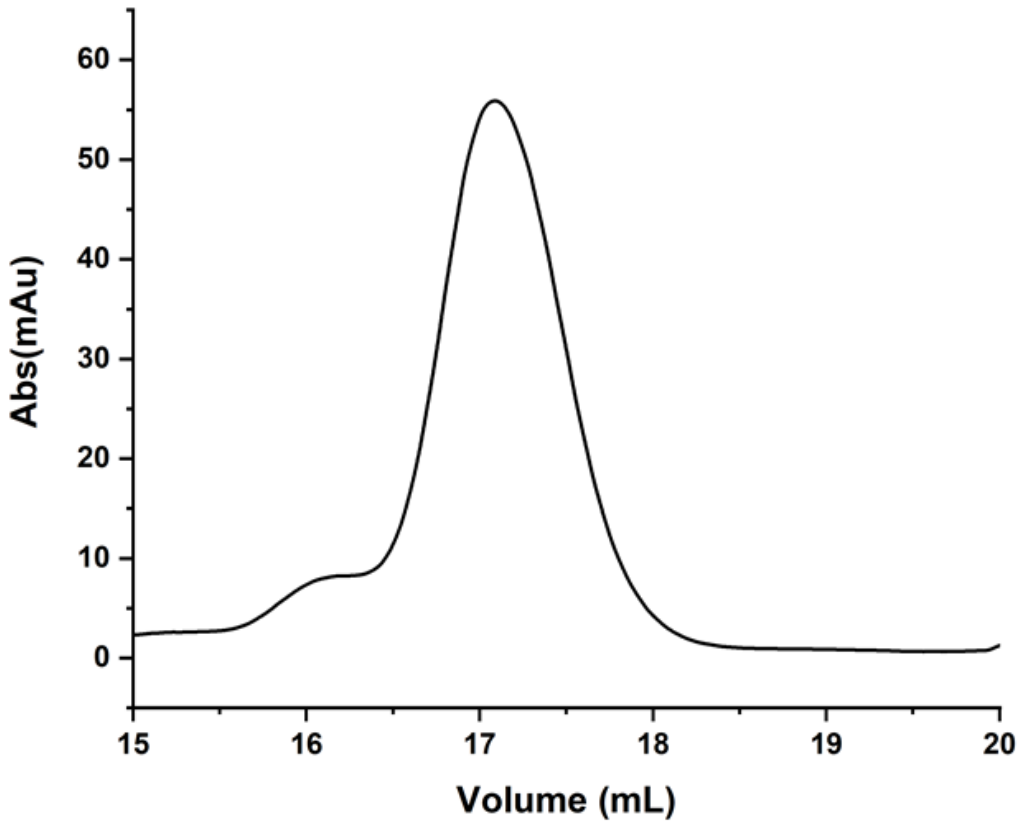

Figure 2. Analytical gel filtration profile of $[2Fe\text{-}2S]^{2+}$ FDX2 in phosphate 50 mM, 150 mM NaCl, DTT 5 mM degassed buffer at pH 7.0.

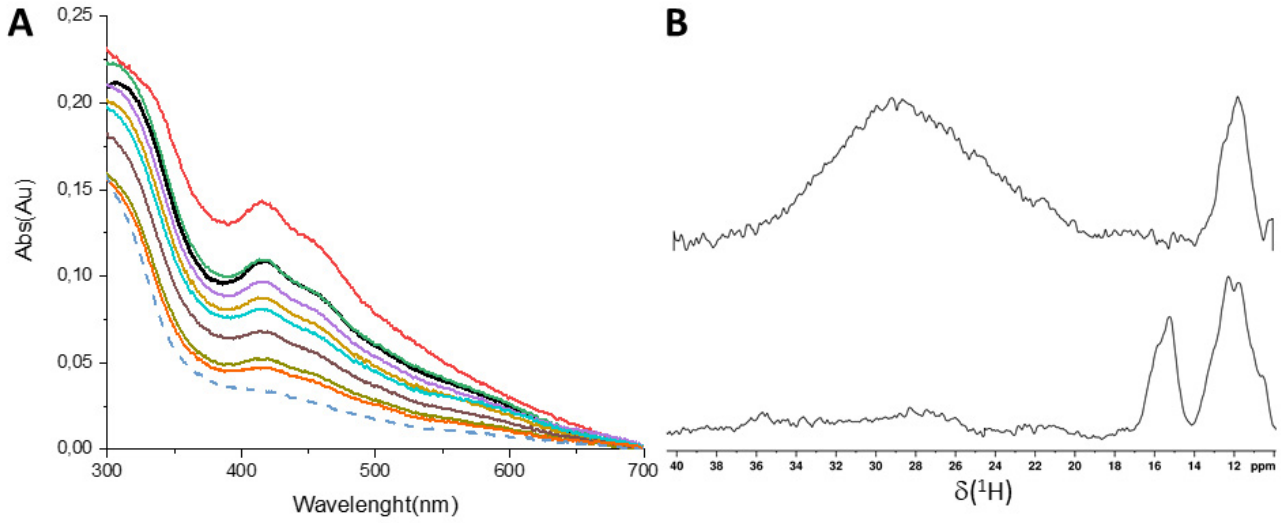

Figure 3. (**A**) UV-visible spectra of the $[2Fe\text{-}2S]^{2+}$ FDX2 titrated with sodium dithionite, the **red spectrum** is the starting $[2Fe\text{-}2S]^{2+}$ FDX2 before the sodium dithionite addition, the **light blue dash spectrum** is the $[2Fe\text{-}2S]^{+}$ FDX2 after two equivalent of sodium dithionite were added, the **black bold spectrum** is the $[2Fe\text{-}2S]^{2+}$ FDX2 after the air exposure and re-oxidation. (**B**) On the top: ^{1}H 1D paramagnetic NMR spectrum of $[2Fe\text{-}2S]^{2+}$ FDX2, on the bottom: ^{1}H 1D paramagnetic NMR spectrum of $[2Fe\text{-}2S]^{+}$ FDX2.

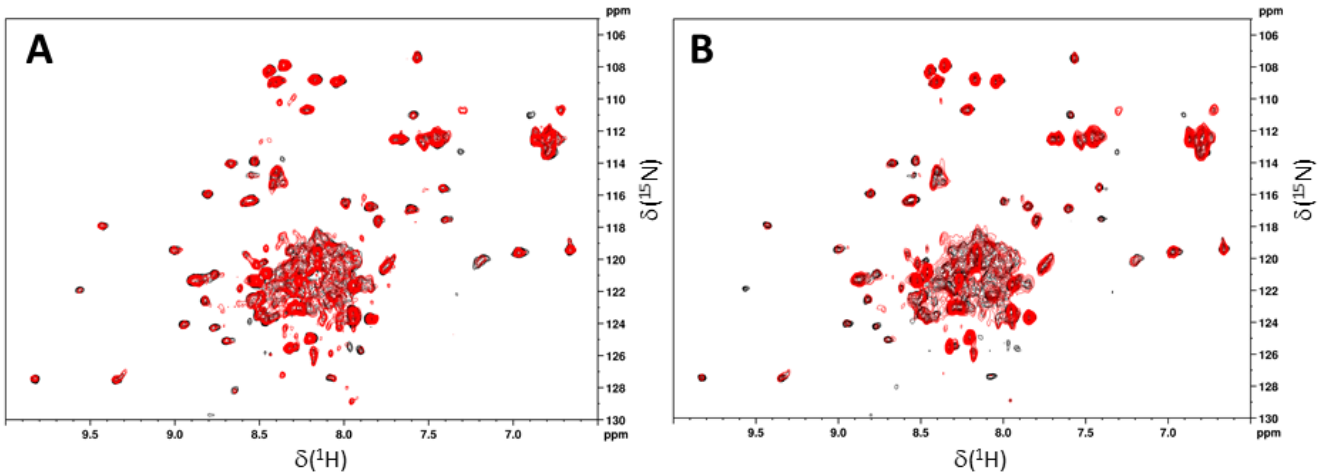

Figure 4. (**A**) Overlay of the ^{1}H-^{15}N HSQC spectrum acquired on ^{15}N labeled $[2Fe\text{-}2S]^{2+}$ FDX2 (black) with the ^{1}H-^{15}N HSQC spectrum acquired on 1:1 ^{15}N labeled $[2Fe\text{-}2S]^{2+}$ FDX2 - apo ISCA1 mixture. (**B**) Overlay of the ^{1}H-^{15}N HSQC spectrum acquired on ^{15}N labeled $[2Fe\text{-}2S]^{2+}$ FDX2 (black) with the ^{1}H-^{15}N HSQC spectrum acquired on 1:1 ^{15}N labeled $[2Fe\text{-}2S]^{2+}$ FDX2 - apo ISCA2 mixture.

2.5 Structural investigation of hetero-complexes formed by ISCA1, ISCA2 and NFU1

The late-acting step of the maturation of mitochondrial [4Fe-4S] proteins, consisting of the assembly and insertion of [4Fe-4S] clusters into mitochondrial apo proteins, are recently well characterized by NMR spectroscopy and size exclusion chromatography[32]. Our data have demonstrated that ISCA1 is the key player of the third step of the ISC assembly machinery interacting with both NFU1 and ISCA2, which are the other actors of the [4Fe-4S] cluster maturation. Specifically, ISCA1 tightly interacts with both ISCA2 and NFU1 forming a heterodimeric complexes that are required for the [4Fe-4S] cluster assembly and delivery. We have also shown that ISCA1, by its recognition with the C-terminal domain of NFU1, moves the [4Fe-4S] cluster from the ISCA1-ISCA2 heterocomplex to the NFU1-ISCA1 cluster binding site. During this process the three latter proteins act together forming a transient ternary hetero-complex. We have also newly revealed that the [4Fe-4S] ISCA1-NFU1 hetero-complex is involved in the maturation of the FeS_{RS} cluster binding site of LIAS. NMR and SEC data acquired clearly shown that both [4Fe-4S] ISCA1-NFU1 and [4Fe-4S] NFU1 are needed for the LIAS maturation.

In order to corroborate these new data on apo ISCA1-NFU1 hetero-complex and apo ISCA1-ISCA2-NFU1 transient ternary hetero-complex we have performed an integrative approach, utilizing information from small-angle X-ray scattering (SAXS) and NMR spectroscopy, to determine a low-resolution structural model of these complexes. The apo ISCA1-ISCA2, apo ISCA1-NFU1and apo ISCA1-ISCA2-NFU1 hetero-complexes were obtained through ^{1}H-^{15}N HSQC NMR titrations, and then the latter were analysed by SEC-SAXS experiments. The SEC-SAXS data achieved are now under investigation, and they require a multiple level of fitting to obtain ISCA1-NFU1 and ISCA1-ISCA2-NFU1 low resolution structures. The structural data that will be obtained through SEC-SAXS analysis would achieve new important details on the characterization of the final step of the ISC assembly machinery.

3. Methodology

3.1 Protein production

Protein production is a biotechnological process leading to the expression and isolation of recombinant proteins. This process start from the insertion of a recombinant DNA in a host/expression system, and followed by the over expression of the chosen protein and its isolation from the rest of the proteosome. The possible host systems that include insect, yeast, bacteria or mammalian cells are chosen based on the characteristic of the proteins that have to be expressed. All the proteins used for the PhD thesis work were expressed in bacteria cells.

Commonly, the starting point for the production of new proteins are the expression test, where different conditions are tested in order to define the best protein expression and purification protocol. The preliminary conditions normally tested in a small volume are:

- Cell strains: BL21 (DE3) and BL21(DE3) Gold a protease deficient strains, Rosetta (DE3) for rare codons containing genes and Origami (DE3) for disulphide containing proteins.
- Fusion proteins: the fusion proteins are required in order to increase the protein solubility (e.g.: MBP, TRX, GST and GB1)
- Expression temperatures: usually 37, 25 and 20 °C.
- IPTG concentration: normally 1, 0.5 and 0.2 mM.

Exploring this large set of conditions is possible to identify the best expression protocol for many different proteins.

In order to be analysed by spectroscopic techniques, the protein isolation from the whole host proteosome is required. Protein purification is a series of processes aimed to isolate one protein from a complex mixture. The latter protocol usually take advantage of differences in protein size, physico-chemical properties, binding affinity and biological activity. When the protein of interest is not secreted by the organism into the surrounding solution, the first step of each purification protocol is the disruption of the cells containing the protein. Commonly, are used the following techniques: i) repeated freezing and thawing, ii) sonication and iii) homogenization by high pressure (French press). Next, the cell debris can be removed by ultracentrifugation. After this separation steps the real purification process can starts. In order to simplify the latter process and increase the protein purity, affinity purification tags can be fused to the recombinant protein of interest. The most commonly used tag is the poly histidine tag (6 or 12 histidine) that relies on the affinity of histidine residues for

immobilized metals, such as nickel. The histidine tag fused with the protein can tight bound the nickel metal adsorbed on the column. The histidine tag offers several advantages such as the small size that not interfere with the protein structure and the high affinity with metals allowing the specific protein separation. In this work it was always used proteins functionalized by N-terminal 6xHistag and HisTrap column loaded with nickel.

The cDNAs coding for human LIAS, C106/C111/C117A LIAS, C137/C141/C144 LIAS, NFU1, BOLA3 and ISCA2 were already available in our laboratory and their production was performed as previously reported in literature[27,29,34,37,83], BOLA3 C59Y mutant was expressed and purified following the BOLA3 wild type protocol[96].

For the PhD work, I have developed and optimized the full length ISCA1 and FDX2 expression and purification protocol that are extensively reported below.

3.1.1 ISCA1 expression and purification protocol

Uniprot Reference code: Q9BUE6

Construct: full length 1-130

N-term tag: His-Tag MBP

C-term tag: none

Number of amino acids: 131

Molecular weight: 14,236 KDa

Theoretical pI: 9.20

Ext. coefficient at 280 nm: 4595 M^{-1} cm^{-1}, at 280 nm measured in water

Protease for tag cleavage: TEV

Final protein aminoacidic sequence:

MSASLVRATVRAVSKRKLQPTRAALTLTPSAVNKIKQLLKDKPEHVGVKVGVRTRGCNGL
SYTLEYTKTKGDSDEEVIQDGVRVFIEKKAQLTLLGTEMDYVEDKLSSEFVFNNPNIKGTC
GCGESFNI

Yield

Yield in rich medium (e.g. LB, TB, Silantes): 7-9 mg/L

Yield in chemically defined medium(e.g. M9): 7 mg/L

Growth media

LB, M9

Protocol for the production in rich medium

Material:

- *E.coli* cell strain: BL21 GOLD
- Plate for transformation or colonies propagation: LB-agar and ampicillin (100 mg/L)
- Purification column 1: His-trap
- Purification column 2: Amylose resin column
- Binding buffer: Tris 50 mM, NaCl 500 mM, Imidazole 15 mM and pH=8.

- Elution Buffer: Tris 50 mM, NaCl 500 mM, Imidazole 500 mM and pH=8.
- Buffer 3: To clean the Amylose resin column using 10 mM Maltose buffer
- Protease for tag cleavage: TEV protease
- Storage buffer: Pi 50 mM, NaCl 150 mM, DTT 5 mM and pH=7

Preculture

- 15/20 mL (falcon 50 ml) of LB fresh medium with Amp(100 mg/L), one preculture per each liter of culture. Add the colonies from a plates or glycerol stock. Growth O/N at 37 °C and 260 rpm.

Culture:

- Inoculate all the preculture volume in one liter of fresh medium. Minimum 2 L of culture per each purification. Add the antibiotic in the fresh medium. Grow at 37 °C and 160 rpm until the OD reach the value between 0.8-1. Induce the expression with 0.2 mM (final concentration) of IPTG and move the flasks at 18°C, 160 rpm, O/N. Harvest the cells at 4°C, 5000 x g, 15 min. Store the pellet at -20°C.

Lysis:

- Resuspend the pellet with 50 mL of Binding buffer (add DTT 2 mM). Sonicate 40 minutes, 2 sec ON and 9.9 sec OFF

Purification:

- Use a HisTrap FF 5mL loaded with nickel. All the purification steps are carried out at room temperature, 5mL/min system flow.
- After the sonication centrifuge the solution using a ultra-centrifuge at 40000 RPM for 40 minutes at 4°C.
- Equilibrate the His-trap column with the binding buffer.
- Load the supernatant to the column. Put in reload for at least 1 hour.
- Wash the column with at least 75 mL of binding buffer.
- Elute the protein (ISCA1-MBP-Histag) with the elution buffer, collect this fraction. Check the protein elution with the Bradford assay.
- Add TEV protease to the protein solution eluted from the HisTrap. Put all the solution in dialysis against binding buffer, O/N.
- Equilibrate the HisTrap column with the binding buffer.
- Reload the protein solution at least 30 minutes.
- Wash with binding buffer and collect this fraction that contain ISCA1 alone.

- Concentrate the proteins solution until 5/3 ml with 10 KDa centricon. Equilibrate the amylose resin column with the binding buffer.
- Load the solution in the amylose resin column(this step is not always needed, but the protein purity is increased)
- Concentrate the protein solution until 2.5 mL and change the buffer of the protein to the storage buffer with a PD10.
- Freeze the sample in liquid nitrogen and stored a -80 °C

Protein concentration:

- Usually 3.5 mL at 0.25/35 mM.

Protein storage:

- Freeze the sample in liquid nitrogen and stored a -80 °C. Is recommended to use the protein in maximum one month, after this time the protein could be unfolded and precipitate.

The expression and purification protocol is the same for M9 medium.

3.1.2 FDX2 expression and purification protocol

Uniprot Reference code: Q6P4F2

Construct: 53-183

N-term tag: His-Tag

C-term tag: none

Number of amino acids: 147

Molecular weight: 16,093 KDa

Theoretical pI: 5.20

Ext. coefficient at 280 nm: 3230 M^{-1} cm^{-1}, at 280 nm measured in water

Protease for tag cleavage: Thrombin

Final protein aminoacidic sequence:

AGEEDAGGPERPGDVVNVVFVDRSGQRIPVSGRVGDNVLHLAQRHGVDLEGACEASLAC
SCHVYVSEDHLDLLPPPEEREDDMLDMAPLLQENSRLGCQIVLTPELEGAEFTLPKITRNFY
VDGHVPKPH

Practical aspects

To obtain the holo form of the protein it is necessary perform all the purification steps in glovebox except the sonication and ultracentrifugation steps. Adding 4 ml of Solution Q and 250 uM of $FeCl_3$ per liter of LB is required to increase the expression of holo form directly from the cells.

Yield

Yield in rich medium (e.g. LB, TB, Silantes): 20-25 mg/L

Yield in chemically defined medium(e.g. M9): 12 mg/L

Growth media

LB, M9

Protocol for the production in rich medium

Material:

- *E.coli* cell strain: BL21(DE3)
- Plate for transformation or colonies propagation: LB-agar and kanamycin (50 mg/L)
- Purification column 1: His-trap
- Binding buffer: Tris 50 mM, NaCl 500 mM, Imidazole 15 mM and pH=8.
- Elution Buffer: Tris 50 mM, NaCl 500 mM, Imidazole 500 mM and pH=8.
- Protease for tag cleavage: Thrombin protease
- Storage buffer: Pi 50 mM, NaCl 150 mM, DTT 5 mM and pH=7

Preculture

- 15/20 mL (falcon 50 ml) of LB fresh medium with Kan (50 mg/L), one preculture per each liter of culture. Add the colonies from a plates or glycerol stock. Growth O/N at 37 °C and 260 rpm.

Culture:

- Inoculate all the preculture volume in one liter of fresh medium. Add the antibiotic in the fresh medium. Grow at 37 °C and 160 rpm until the OD reach the value between 0.8-1. Induce the expression with 0.5 mM (final concentration) of IPTG and wait 5 hours. Harvest the cells at 4°C, 5000 x g, 15 min. Store the pellet at -20°C.

Lysis:

- Resuspend the pellet with 50 mL of Binding buffer (add DTT 2 mM). Sonicate 40 minutes, 2 sec ON and 9.9 sec OFF

Purification:

- Use a HisTrap FF 5mL loaded with nickel. All the purification steps are carried out at room temperature, 5mL/min system flow.
- After the sonication centrifuge the solution using a ultra-centrifuge at 40000 RPM for 40 minutes at 4°C.
- Equilibrate the HisTrap column with the binding buffer.
- Load the supernatant to the column. Put in reload for at least 1 hour.
- Wash the column with at least 75 mL of binding buffer.
- Elute the protein(FDX2-6xHistag) with the elution buffer, collect this fraction. Check the protein elution with the bradford assay.
- Add Thrombin protease to the protein solution eluted from the HisTrap. Put all the solution in dialysis against binding buffer, O/N.
- Equilibrate the HisTrap column with the binding buffer.

- Reload the protein solution at least 30 minutes.
- Wash with binding buffer and collect this fraction that contain FDX2 alone.
- Concentrate the protein solution until 2.5 mL and change the buffer of the protein to the storage buffer with a PD10.
- Store at 4 °C

The expression and purification protocol is the same using M9 medium for the production of ^{15}N labeled FDX2

3.1.3 Determination of protein concentrations

Protein concentrations were estimated from measuring the absorbance at 280 nm (A280) applying the Lambert and Beer law. Theoretical molar extinction coefficients were obtained from ProtParam (Expasy tool) software.

3.1.4 Chemical reconstitution

Full length [4Fe-4S] NFU1, [4Fe-4S] NFU1-ISCA1 and [4Fe-4S] ISCA2-ISCA1 were obtained through chemically reconstitution performed under anaerobic conditions in 50 mM Tris- HCl, 100 mM NaCl, 5 mM DTT buffer at pH 8.0 adding eight-fold $FeCl_3$ and Na_2S for 16 h at room temperature. [2Fe-2S] BOLA3-GLRX5 and [2Fe-2S] BOLA3 C59Y-GLRX5 were chemically reconstituted as it is already reported for the wild type complex[66]. [2Fe-2S] FDX2 was obtained through chemically reconstitution performed under anaerobic conditions in 50 mM Tris- HCl, 100 mM NaCl, 5 mM DTT buffer at pH 8.0 adding six-fold $FeCl_3$ and Na_2S for 16 h at room temperature starting from as purified FDX2 (mixture of holo and apo species). The protein concentration used for the chemical reconstitution experiments were in the range of ~40-80 μM. Anaerobic conditions were obtained by degassing all buffers and performing the chemical reconstitution in anaerobic chamber with less than 2 ppm of oxygen.

3.2 Protein characterization

3.2.1 Analytical gel filtration

Analytical gel filtration, also called size exclusion chromatography, is a technique widely used in the biochemical studies required to separate macromolecules based on the molecular mass or hydrodynamic radius. The protein solutions are loaded in the resin (composed by porous beads). The larger the particles, the faster the elution, indeed the biggest molecules bypass the pores because those molecules are too large to enter the pores. Larger molecules consequently flow through the column more quickly than smaller molecules, the molecules are separated by their size. This technique can be used for high efficient protein purification and for the investigation of protein complexes formation. Often, size exclusion chromatography can be coupled with multi angle light scattering (MALS), named SEC-MALS, in order to better characterized the molecular weight of the proteins or the protein complexes. The MALS is used in order to determinate, both the absolute molar mass and the average size of molecules in solution, by detecting the scatter of light from a laser source. Multi angle is referred to the detection at different discrete angles.

In this PhD work, analytical gel filtration and SEC-MALS are performed in Pi 50 mM, NaCl 150 mM, DTT 5 mM and pH=7. The flow rate applied was 0.65 ml/min.

3.2.2 Uv-visible spectroscopy

UV-visible spectroscopy is a quantitative technique used to measure the quantity of chemicals detecting the intensity of light that passes through a sample with respect to the intensity of light through a reference sample or blank.

In the PhD thesis work, the UV-vis spectroscopy was widely used in order to quantify proteins and characterized the cluster type bound to the proteins. The UV-vis experiments on the holo proteins and holo complexes were performed under anaerobic conditions, preparing the samples in glove-box with degassed buffers and using a gastight cuvette. UV-visible spectra were executed in 50 mM phosphate buffer, 150 mM NaCl, 5 mM DTT and pH 7.0 at room temperature on a Cary 50 Eclipse spectrophotometer.

3.2.3 Circular Dichroism spectroscopy

Circular dichroism spectroscopy is a technique where the difference in the absorption of left and right circularly polarized light in optically active substances is measured. CD signals are observed for

optically active materials. CD in the region of 190-250 nm is typically used to investigate protein secondary structure being able to discriminate folded and unfolded proteins. Visible CD spectroscopy is a very powerful technique to study metal–protein interactions resolving individual d–d electronic and charge transfer transitions as separate bands. CD spectra in the visible light region are only produced when a metal ion is in a chiral environment.

In the PhD thesis work, the CD-vis spectroscopy was used to characterize the cluster type bound to different proteins. CD-vis analyses of holo-proteins and holo-heterocomplexes were performed in 50 mM phosphate, NaCl 150 mM, pH 7.0 on a Jasco J-810 spectropolarimeter at 298K using a 1-mm path-length cell. Spectra were recorded with an average of 5 accumulations at a scan speed of 100 nm/min and at a response time of 1 s. The proteins concentrations used are in the range of 10-70 μM.

3.2.4 NMR spectroscopy

Nuclear magnetic resonance (NMR) spectroscopy is an essential technique for structural and functional characterization of biological macromolecules. The principle behind NMR spectroscopy is that many nuclei have spin and all nuclei are electrically charged. When an external magnetic field is applied, an energy transfer is possible between the base energy to a higher energy level. The energy transfer takes place at a wavelength that corresponds to radio frequencies and when the spin returns to its base level, energy is emitted at the same frequency. The signal that matches this transfer is measured in many ways and processed in order to yield an NMR spectrum for the nucleus. Each NMR active nucleus gives rise to an individual signal in the spectrum that, proteins contain hundreds of atoms and required to be resolved through multi-dimensional NMR experiments. Developments in NMR hardware and NMR methodology, combined with the development of biochemical approaches for preparation and labelling of recombinant proteins, have radically increased the use of NMR for the functional and structural characterization of biological macromolecules.

In this PhD thesis work, it was used principally ^{1}H 1D and ^{1}H-^{15}N HSQC NMR experiments in order to structurally and functionally characterize the proteins and to explore the protein-protein interaction and hetero complexes formation. In addition, we have deeply applied ^{1}H 1D paramagnetic NMR experiments in order to explore the iron sulfur cluster coordination, environment and oxidation state.

HSQC: heteronuclear single quantum coherence

HSQC experiments determine the correlations between two different types of nuclei, generally ^{1}H with ^{13}C or ^{15}N, which are separated by one bond. Each cross-peaks of the HSQC spectrum is representative of one N-H or C-H, in fact for the ^{1}H-^{15}N HSQC spectrum each peaks are characteristic

of each aminoacidic residues (excluding the prolines) of the proteins. Thus, HSQC offers a very informative approach for signal assignments[97]. The HSQC experiment is also useful for detecting binding interface in protein-protein interaction, indeed amino acids involved in the interface will suffer residue-specific chemical shift perturbations. Comparing the HSQC spectrum of the free protein with the one bound to the ligand changes in the chemical shifts of some peaks may be observed, and this is powerful information to detect complexes formation and protein structural rearrangement.

In this thesis work, ^{1}H-^{15}N HSQC NMR experiments were widely used for the structural characterization of the proteins involved in the third step of the ISC assembly machinery and for monitoring their protein-protein interactions. Diamagnetic NMR spectra were recorded on Bruker AVANCE 700, 900 and 950 MHz, processed using the standard Bruker software (Topspin). ^{1}H-^{15}N HSQC spectra were performed at 298 K in 50 mM phosphate buffer, 150 mM NaCl, 5 mM DTT pH 7.0, 10% (v/v) D_2O. To characterize the structural properties of proteins and complexes with bound iron sulfur cluster(s), the ^{1}H-^{15}N HSQC spectra were acquired using degassed buffer and 5 mm gastight NMR tube. The ^{1}H-^{15}N HSQC spectra chemical shift perturbation occurred after the complexes formation were analysed with CARA software.

Paramagnetic NMR

Paramagnetic nuclear magnetic resonance (NMR) has been widely used to characterize metalloproteins. This spectroscopy is powerful technique for the characterization of iron sulfur clusters proteins[98]. In fact, the hyperfine shifts and the temperature dependencies of the paramagnetic signals in the NMR spectra provide an efficient fingerprint of oxidation state and of the type of iron sulfur cluster bound to the protein[83]. The magnetic coupling constants determines various electron spin energy levels for iron ions, and the coupling of the nuclear spins of the protons of the proteins with these multiple electron spin levels significantly modify the chemical shifts and the relaxation rates. For these reason, paramagnetic NMR spectra of iron sulfur proteins are different based on the cluster coordination and oxidation state. Paramagnetic NMR is unique technique to characterize the iron sulfur cluster environment at atomic level.

In this thesis work, paramagnetic NMR experiments were extensively used to investigate iron sulfur clusters bound to the protein of interest and to characterize cluster transfer among proteins/complexes. ^{1}H 1D paramagnetic NMR experiments were acquired at 400 MHz with a ^{1}H optimized 5 mm probe at temperatures ranging from 283 K and 298 K, with protein samples in 50 mM phosphate buffer, 150 mM NaCl, 5 mM DTT pH 7.0, 99% (v/v) D_2O. The protein concentration was in the range of 0.2–0.8 mM. Water signal was suppressed via fast repetition experiments and water selective

irradiation[85,93]. Experiments were typically performed using an overall recycle delay of 50-90 ms. Squared cosine and exponential multiplications were applied prior to Fourier transformation[86]. Manual baseline correction was performed, using polynomial functions. Each experiment was successfully repeated three times.

3.2.5 Molecular docking: HADDOCK 2.2

In this PhD work, molecular docking have been investigated through the program HADDOCK 2.2 that define models based on interaction data such as chemical shift perturbation from NMR titration experiments[99,100]. In this software, the docking process is driven by ambiguous interaction restraints (AIR) that include the solvent exposed residues involved in the protein-protein interaction. HADDOCK 2.2 distinguish active and passive residues in the set of residues that have significant chemical shift perturbations after the complex formation. The chosen residues are grouped by the solvent accessibility that is calculated by NACCES tool[101]. The docking protocol consists of three consecutive steps:

- Randomization of orientations and rigid body energy minimization.
- Semirigid simulated annealing in torsion angle space.
- Final refinement in Cartesian space with explicit solvent.

Successively, the best structures are grouped in cluster with a threshold of 7.5 Å of RMS each cluster contain at least 4 structures that are analysed on the basis of HADDOCK score value ($1.0*E_{vdw}+0.2*E_{elc}+0.1*E_{dist}+1.0*E_{solv}$, respectively: van der Walls energy, electrostatic energy, distance restrains energy and desolvation energy), Buried Surface Area and RMSD.

In this PhD work, the structural models of the apo BOLA3–GLRX5 and apo C59Y BOLA3–GLRX5 complexes were calculated following the standard HADDOCK procedure and employing the HADDOCK2.2 Web Server (https://alcazar.science.uu.nl/services/HADDOCK2.2/)[99,100]. Specifically, the structural models of the apo hetero-dimers were built from the structures of individual proteins (monomeric apo GLRX5 with a bound GSH molecule obtained from PDB entry 2WUL[102] and BOLA3 from PDB entry 2NCL[34]). The structure of the C59Y BOLA3 was obtained with Modeller 9.20 (https://salilab.org/modeller/)[103], using as template the existing NMR solution structure of BOLA3. The C59Y BOLA3 structure obtained by Modeller 9.20 was then energy minimized in explicit water using an AMBER 12.0 molecular dynamics program[104]. The NMR chemical shift mapping data obtained for the two hetero-complexes in the titrations performed at 0.8 mM starting protein concentration were used to define ambiguous interaction restraints for the

residues at the interface. The “active” residues were defined as those having a chemical shift perturbation upon heterocomplex formation larger than the average of Δ_{avg}(HN) plus 1σ, as well as those residues whose backbone NHs broaden beyond detection upon the interaction with the protein partner, and all having a solvent accessibility higher than 50%; the “passive” residues were defined as those being surface neighbors to the active residues and having a solvent accessibility higher than 50%. NACCESS is the program used to calculate the atomic and residue accessibilities from the PDB file. GSH molecule was also included as active residue on the basis of the NMR data. The ensemble of 200 solutions was analysed and clustered on the basis of the pairwise RMSD matrix calculated over the backbone atoms of the interface residues of GLRX5 after fitting on the interface residues of BOLA3 or C59Y BOLA3. This way of calculating RMSD values in HADDOCK resulted in high values that emphasized the differences between docking solutions. For this reason, we performed clustering using a 7.5 Å cut-off. The water-refined models were clustered on the basis of the default fraction of common contacts, FCC = 0.75, with the minimum number of elements in a cluster of 4.

4. Conclusions

The data described in this thesis provide a detailed model of the molecular snapshots driving the [4Fe-4S] cluster maturation and transfer to apo recipient proteins along the third step of ISC assembly machinery.

First, the [4Fe-4S] cluster assembly and transfer by ISCA1, ISCA2 and NFU1 was explored. It was demonstrated that ISCA1 is the key player of the [4Fe-4S] maturation process because of its ability to interact with both NFU1 and ISCA2 working as the promoter of the interaction. We also show that ISCA1, thanks to its specific recognition with the C terminal cluster-binding domain of NFU1, drives [4Fe-4S] cluster transfer guaranteeing its safely movement from where it is assembled on the ISCA1-ISCA2 complex to NFU1-ISCA1 complex. In this way, the [4Fe-4S] cluster is available for the mitochondrial apo proteins specifically requiring NFU1 for their maturation. In order to better characterize the biosynthesis of the [4Fe-4S] cluster, FDX2, the electron donor required for the reductive coupling of two $[2Fe\text{-}2S]^{2+}$ cluster performed by the ISCA1-ISCA2 hetero-complex, was produced and characterized. We have presented a structural characterization of the human FDX2 by solution NMR and analysed the redox properties of the [2Fe-2S] bound to the protein. Moreover, we have set the stage for the [4Fe-4S] cluster biosynthesis study showing that the isolated ISCA1 and ISCA2 are not involved in the electron transfer process, suggesting that they should recognize FDX2 operating as heterodimer or complexed with IBA57. In this scenario, further characterization is required in order to better explore the IBA57 role in the [4Fe-4S] cluster formation, which could act as an electron shuttle between FDX2 and ISCA1-ISCA2 hetero-complex.

Successively, we have investigated the [4Fe-4S] NFU1 and [4Fe-4S] NFU1-ISCA1 complex role in the maturation of LIAS, one of the apo recipient proteins that required NFU1 for its maturation. We have demonstrated that NFU1 tightly interacts with LIAS forming a heterodimeric complex specifically recognize the C-domain of NFU1. In addition, our data suggests that LIAS by interacting with NFU1 is able to displace the NFU1-protein partner ISCA1 that is released as a free form, no ternary complex has been observed, thus excluding that ISCA1 and LIAS recognize each other. Moreover, our study present the first evidence of the insertion of the [4Fe-4S] cluster into the FeS_{RS} site of human LIAS by the [4Fe-4S] NFU1, and we have revealed that the recently discovered hetero-dimeric [4Fe-4S] ISCA1-NFU1 complex is also able to maturate the FeS_{RS} site of human LIAS. In this way, we proved that both [4Fe-4S] NFU1 and [4Fe-4S] ISCA1-NFU1 species can act physiological inserting the cluster in the FeS_{RS} site.

Finally, we have investigated the Cys59Tyr mutation on BOLA3 protein that lead to MMDS type 2. The latter mutation shows a new interesting phenotype characterized by a full clinical recovery. In this scenario, we have demonstrated that the mutation structurally perturbed the iron-sulfur cluster-binding region of BOLA3, but without abolishing $[2Fe–2S]^{2+}$ cluster-binding on the physiologically relevant hetero-complex formed with GLRX5. We have also proved that tyrosine 59 did not replace cysteine 59 as iron-sulfur cluster ligand; and that the mutation promoted the formation of an aberrant apo C59Y BOLA3–GLRX5 complex, which could be the molecular basis of the disease. Overall, the obtained data allow us to rationalize the rare phenotype caused by Cys59Tyr mutation.

All these aspects address new fundamental molecular details of [4Fe-4S] cluster maturation, enhancing the knowledge on its characterization and contributing to the discovery of a new intriguing scenario at the basis of the third step of the ISC assembly machinery.

References:

1. González, A. & Valencia, G. Photochemical desulfurization of l-cysteine derivatives. *Tetrahedron: Asymmetry* **9**, 2761–2764 (1998).
2. Andreini, C., Rosato, A. & Banci, L. The Relationship between Environmental Dioxygen and Iron-Sulfur Proteins Explored at the Genome Level. *PLoS One* **12**, e0171279 (2017).
3. Braymer, J. J., Freibert, S. A., Rakwalska-Bange, M. & Lill, R. Mechanistic concepts of iron-sulfur protein biogenesis in Biology. *Biochim. Biophys. Acta - Mol. Cell Res.* **1868**, 118863 (2021).
4. Kuchar, J. & Hausinger, R. P. Biosynthesis of Metal Sites. *Chem. Rev.* **104**, 509–526 (2004).
5. Camponeschi, F. & Banci, L. Metal cofactors trafficking and assembly in the cell: a molecular view. *Pure Appl. Chem.* **91**, 231–245 (2019).
6. Kiley, P. J. & Beinert, H. The role of Fe–S proteins in sensing and regulation in bacteria. *Curr. Opin. Microbiol.* **6**, 181–185 (2003).
7. Chen, C.-J., Lin, Y.-H., Huang, Y.-C. & Liu, M.-Y. Crystal structure of rubredoxin from Desulfovibrio gigas to ultra-high 0.68Å resolution. *Biochem. Biophys. Res. Commun.* **349**, 79–90 (2006).
8. Watenpaugh, K. D., Sieker, L. C. & Jensen, L. H. The structure of rubredoxin at 1.2 Å resolution. *J. Mol. Biol.* **131**, 509–522 (1979).
9. Iwata, S., Saynovits, M., Link, T. A. & Michel, H. Structure of a water soluble fragment of the 'Rieske' iron–sulfur protein of the bovine heart mitochondrial cytochrome bc1 complex determined by MAD phasing at 1.5 å resolution. *Structure* **4**, 567–579 (1996).
10. Moulis, J.-M., Sieker, L. C., Wilson, K. S. & Dauter, Z. Crystal structure of the 2[4Fe-4S] ferredoxin from Chromatium vinosum : Evolutionary and mechanistic inferences for [3/4Fe-4S] ferredoxins. *Protein Sci.* **5**, 1765–1775 (1996).
11. Lu, Y. Assembly and Transfer of Iron–Sulfur Clusters in the Plastid. *Front. Plant Sci.* **9**, (2018).
12. Beinert, H. Iron-sulfur proteins: ancient structures, still full of surprises. *JBIC J. Biol. Inorg. Chem.* **5**, 2–15 (2000).
13. Johnson, D. C., Dean, D. R., Smith, A. D. & Johnson, M. K. STRUCTURE, FUNCTION, AND FORMATION OF BIOLOGICAL IRON-SULFUR CLUSTERS. *Annu. Rev. Biochem.* **74**, 247–281 (2005).
14. Banci, L., Camponeschi, F., Ciofi-Baffoni, S. & Piccioli, M. The NMR contribution to protein–protein networking in Fe–S protein maturation. *JBIC J. Biol. Inorg. Chem.* **23**, 665–685 (2018).
15. Helbig, K. J. & Beard, M. R. The role of viperin in the innate antiviral response. *J. Mol. Biol.* **426**, 1210–9 (2014).
16. Ciofi-Baffoni, S., Nasta, V. & Banci, L. Protein networks in the maturation of human iron–sulfur proteins. *Metallomics* **10**, 49–72 (2018).
17. McCarthy, E. L. & Booker, S. J. Destruction and reformation of an iron-sulfur cluster during

catalysis by lipoyl synthase. *Science (80-.).* **358**, 373–377 (2017).

18. Cicchillo, R. M. *et al.* Lipoyl Synthase Requires Two Equivalents of S -Adenosyl- l - methionine To Synthesize One Equivalent of Lipoic Acid †. *Biochemistry* **43**, 6378–6386 (2004).

19. ter Beek, J. *et al.* Structural evidence for an essential Fe–S cluster in the catalytic core domain of DNA polymerase ϵ. *Nucleic Acids Res.* **47**, 5712–5722 (2019).

20. Kispal, G., Csere, P., Prohl, C. & Lill, R. The mitochondrial proteins Atm1p and Nfs1p are essential for biogenesis of cytosolic Fe/S proteins. *EMBO J.* **18**, 3981–3989 (1999).

21. Kurland, C. G. & Andersson, S. G. E. Origin and Evolution of the Mitochondrial Proteome. *Microbiol. Mol. Biol. Rev.* **64**, 786–820 (2000).

22. Lill, R. *et al.* The role of mitochondria and the CIA machinery in the maturation of cytosolic and nuclear iron–sulfur proteins. *Eur. J. Cell Biol.* **94**, 280–291 (2015).

23. Fox, N. G. *et al.* Structure of the human frataxin-bound iron-sulfur cluster assembly complex provides insight into its activation mechanism. *Nat. Commun.* **10**, 2210 (2019).

24. Pierrel, F., Cobine, P. A. & Winge, D. R. Metal Ion availability in mitochondria. *BioMetals* **20**, 675–682 (2007).

25. Zheng, L., White, R. H., Cash, V. L. & Dean, D. R. Mechanism for the Desulfurization of L-Cysteine Catalyzed by the nifS Gene Product. *Biochemistry* **33**, 4714–4720 (1994).

26. Dutkiewicz, R. & Nowak, M. Molecular chaperones involved in mitochondrial iron–sulfur protein biogenesis. *JBIC J. Biol. Inorg. Chem.* **23**, 569–579 (2018).

27. Banci, L. *et al.* [2Fe-2S] cluster transfer in iron-sulfur protein biogenesis. *Proc. Natl. Acad. Sci.* **111**, 6203–6208 (2014).

28. Bonomi, F., Iametti, S., Morleo, A., Ta, D. & Vickery, L. E. Studies on the Mechanism of Catalysis of Iron−Sulfur Cluster Transfer from IscU[2Fe2S] by HscA/HscB Chaperones. *Biochemistry* **47**, 12795–12801 (2008).

29. Brancaccio, D. *et al.* Formation of [4Fe-4S] Clusters in the Mitochondrial Iron–Sulfur Cluster Assembly Machinery. *J. Am. Chem. Soc.* **136**, 16240–16250 (2014).

30. Weiler, B. D. *et al.* Mitochondrial [4Fe-4S] protein assembly involves reductive [2Fe-2S] cluster fusion on ISCA1–ISCA2 by electron flow from ferredoxin FDX2. *Proc. Natl. Acad. Sci.* **117**, 20555–20565 (2020).

31. Nasta, V. *et al.* Structural properties of [2Fe-2S] ISCA2-IBA57: a complex of the mitochondrial iron-sulfur cluster assembly machinery. *Sci. Rep.* **9**, 18986 (2019).

32. Suraci, D., Saudino, G., Nasta, V., Ciofi-Baffoni, S. & Banci, L. ISCA1 Orchestrates ISCA2 and NFU1 in the Maturation of Human Mitochondrial [4Fe-4S] Proteins. *J. Mol. Biol.* **433**, 166924 (2021).

33. Beilschmidt, L. K. *et al.* ISCA1 is essential for mitochondrial Fe4S4 biogenesis in vivo. *Nat. Commun.* **8**, 15124 (2017).

34. Uzarska, M. A. *et al.* Mitochondrial Bol1 and Bol3 function as assembly factors for specific iron-sulfur proteins. *Elife* **5**, (2016).

35. Jia, M. *et al.* Characterization of [2Fe–2S] Cluster Bridged Protein Complexes and

Reaction Intermediates by use of Native Mass Spectrometric Methods. *Angew. Chemie Int. Ed.* **59**, 6724–6728 (2020).

36. Sen, S., Rao, B., Wachnowsky, C. & Cowan, J. A. Cluster exchange reactivity of [2Fe–2S] cluster-bridged complexes of BOLA3 with monothiol glutaredoxins. *Metallomics* **10**, 1282–1290 (2018).

37. Nasta, V., Suraci, D., Gourdoupis, S., Ciofi□Baffoni, S. & Banci, L. A pathway for assembling [4Fe□4S] 2+ clusters in mitochondrial iron–sulfur protein biogenesis. *FEBS J.* **287**, 2312–2327 (2020).

38. Melber, A. *et al.* Role of Nfu1 and Bol3 in iron-sulfur cluster transfer to mitochondrial clients. *Elife* **5**, (2016).

39. Tong, W.-H., Jameson, G. N. L., Huynh, B. H. & Rouault, T. A. Subcellular compartmentalization of human Nfu, an iron-sulfur cluster scaffold protein, and its ability to assemble a [4Fe-4S] cluster. *Proc. Natl. Acad. Sci.* **100**, 9762–9767 (2003).

40. Jensen, L. T. & Culotta, V. C. Role of Saccharomyces cerevisiae ISA1 and ISA2 in Iron Homeostasis. *Mol. Cell. Biol.* **20**, 3918–3927 (2000).

41. DING, H. & CLARK, R. J. Characterization of iron binding in IscA, an ancient iron-sulphur cluster assembly protein. *Biochem. J.* **379**, 433–440 (2004).

42. Vinella, D., Brochier-Armanet, C., Loiseau, L., Talla, E. & Barras, F. Iron-Sulfur (Fe/S) Protein Biogenesis: Phylogenomic and Genetic Studies of A-Type Carriers. *PLoS Genet.* **5**, e1000497 (2009).

43. Mühlenhoff, U., Richter, N., Pines, O., Pierik, A. J. & Lill, R. Specialized Function of Yeast Isa1 and Isa2 Proteins in the Maturation of Mitochondrial [4Fe-4S] Proteins. *J. Biol. Chem.* **286**, 41205–41216 (2011).

44. Sheftel, A. D. *et al.* The human mitochondrial ISCA1, ISCA2, and IBA57 proteins are required for [4Fe-4S] protein maturation. *Mol. Biol. Cell* **23**, 1157–1166 (2012).

45. Cai, K., Tonelli, M., Frederick, R. O. & Markley, J. L. Human Mitochondrial Ferredoxin 1 (FDX1) and Ferredoxin 2 (FDX2) Both Bind Cysteine Desulfurase and Donate Electrons for Iron–Sulfur Cluster Biosynthesis. *Biochemistry* **56**, 487–499 (2017).

46. Seeber, F. Eukaryotic genomes contain a [2Fe□2S] ferredoxin isoform with a conserved C-terminal sequence motif. *Trends Biochem. Sci.* **27**, 545–547 (2002).

47. Ewen, K. M., Ringle, M. & Bernhardt, R. Adrenodoxin-A versatile ferredoxin. *IUBMB Life* **64**, 506–512 (2012).

48. Cai, K. *et al.* Structural/Functional Properties of Human NFU1, an Intermediate [4Fe-4S] Carrier in Human Mitochondrial Iron-Sulfur Cluster Biogenesis. *Structure* **24**, 2080–2091 (2016).

49. Jain, A., Singh, A., Maio, N. & Rouault, T. A. Assembly of the [4Fe–4S] cluster of NFU1 requires the coordinated donation of two [2Fe–2S] clusters from the scaffold proteins, ISCU2 and ISCA1. *Hum. Mol. Genet.* **29**, 3165–3182 (2020).

50. Cai, K., Frederick, R. O. & Markley, J. L. ISCU interacts with NFU1, and ISCU[4Fe-4S] transfers its Fe-S cluster to NFU1 leading to the production of holo-NFU1. *J. Struct. Biol.* **210**, 107491 (2020).

51. McLaughlin, M. I. *et al.* Crystallographic snapshots of sulfur insertion by lipoyl synthase.

Proc. Natl. Acad. Sci. **113**, 9446–9450 (2016).

52. Cicchillo, R. M. *et al.* Escherichia coli Lipoyl Synthase Binds Two Distinct [4Fe−4S] Clusters per Polypeptide †. *Biochemistry* **43**, 11770–11781 (2004).

53. Douglas, P., Kriek, M., Bryant, P. & Roach, P. L. Lipoyl Synthase Inserts Sulfur Atoms into an Octanoyl Substrate in a Stepwise Manner. *Angew. Chemie Int. Ed.* **45**, 5197–5199 (2006).

54. Harmer, J. E. *et al.* Structures of lipoyl synthase reveal a compact active site for controlling sequential sulfur insertion reactions. *Biochem. J.* **464**, 123–133 (2014).

55. Barton, J. K., Silva, R. M. B. & O'Brien, E. Redox Chemistry in the Genome: Emergence of the [4Fe4S] Cofactor in Repair and Replication. *Annu. Rev. Biochem.* **88**, 163–190 (2019).

56. Che, R., Zhang, J., Nepal, M., Han, B. & Fei, P. Multifaceted Fanconi Anemia Signaling. *Trends Genet.* **34**, 171–183 (2018).

57. Fosset, C. *et al.* RNA Silencing of Mitochondrial m-Nfs1 Reduces Fe-S Enzyme Activity Both in Mitochondria and Cytosol of Mammalian Cells. *J. Biol. Chem.* **281**, 25398–25406 (2006).

58. Stehling, O. & Lill, R. The Role of Mitochondria in Cellular Iron-Sulfur Protein Biogenesis: Mechanisms, Connected Processes, and Diseases. *Cold Spring Harb. Perspect. Biol.* **5**, a011312–a011312 (2013).

59. Maio, N. & Rouault, T. A. Outlining the Complex Pathway of Mammalian Fe-S Cluster Biogenesis. *Trends Biochem. Sci.* **45**, 411–426 (2020).

60. Wachnowsky, C., Fidai, I. & Cowan, J. A. Iron–sulfur cluster biosynthesis and trafficking – impact on human disease conditions. *Metallomics* **10**, 9–29 (2018).

61. Spiegel, R. *et al.* Deleterious mutation in FDX1L gene is associated with a novel mitochondrial muscle myopathy. *Eur. J. Hum. Genet.* **22**, 902–906 (2014).

62. Invernizzi, F. *et al.* Cavitating leukoencephalopathy with multiple mitochondrial dysfunction syndrome and NFU1 mutations. *Front. Genet.* **5**, (2014).

63. Torraco, A. *et al.* ISCA1 mutation in a patient with infantile-onset leukodystrophy causes defects in mitochondrial [4Fe–4S] proteins. *Hum. Mol. Genet.* **27**, 2739–2754 (2018).

64. Cameron, J. M. *et al.* Mutations in Iron-Sulfur Cluster Scaffold Genes NFU1 and BOLA3 Cause a Fatal Deficiency of Multiple Respiratory Chain and 2-Oxoacid Dehydrogenase Enzymes. *Am. J. Hum. Genet.* **89**, 486–495 (2011).

65. Rouault, T. A. Biogenesis of iron-sulfur clusters in mammalian cells: new insights and relevance to human disease. *Dis. Model. Mech.* **5**, 155–164 (2012).

66. Nasta, V., Giachetti, A., Ciofi-Baffoni, S. & Banci, L. Structural insights into the molecular function of human [2Fe-2S] BOLA1-GRX5 and [2Fe-2S] BOLA3-GRX5 complexes. *Biochim. Biophys. Acta - Gen. Subj.* **1861**, 2119–2131 (2017).

67. Baker, P. R. *et al.* Variant non ketotic hyperglycinemia is caused by mutations in LIAS, BOLA3 and the novel gene GLRX5. *Brain* **137**, 366–379 (2014).

68. Haack, T. B. *et al.* Homozygous missense mutation in BOLA3 causes multiple mitochondrial dysfunctions syndrome in two siblings. *J. Inherit. Metab. Dis.* **36**, 55–62 (2013).

69. Stutterd, C. A. *et al.* Severe Leukoencephalopathy with Clinical Recovery Caused by

Recessive BOLA3 Mutations. in 63–70 (2018). doi:10.1007/8904_2018_100.

70. Brancaccio, D. *et al.* [4Fe-4S] Cluster Assembly in Mitochondria and Its Impairment by Copper. *J. Am. Chem. Soc.* **139**, 719–730 (2017).

71. Lebigot, E. *et al.* Impact of mutations within the [Fe-S] cluster or the lipoic acid biosynthesis pathways on mitochondrial protein expression profiles in fibroblasts from patients. *Mol. Genet. Metab.* **122**, 85–94 (2017).

72. Navarro-Sastre, A. *et al.* A Fatal Mitochondrial Disease Is Associated with Defective NFU1 Function in the Maturation of a Subset of Mitochondrial Fe-S Proteins. *Am. J. Hum. Genet.* **89**, 656–667 (2011).

73. Lill, R. & Freibert, S.-A. Mechanisms of Mitochondrial Iron-Sulfur Protein Biogenesis. *Annu. Rev. Biochem.* **89**, 471–499 (2020).

74. Agar, J. N. *et al.* Modular organization and identification of a mononuclear iron-binding site within the NifU protein. *JBIC J. Biol. Inorg. Chem.* **5**, 167–177 (2000).

75. McCarthy, E. L., Rankin, A. N., Dill, Z. R. & Booker, S. J. The A-type domain in Escherichia coli NfuA is required for regenerating the auxiliary [4Fe–4S] cluster in Escherichia coli lipoyl synthase. *J. Biol. Chem.* **294**, 1609–1617 (2019).

76. Py, B. *et al.* Molecular organization, biochemical function, cellular role and evolution of NfuA, an atypical Fe-S carrier. *Mol. Microbiol.* **86**, 155–171 (2012).

77. Wachnowsky, C. *et al.* Understanding the Mechanism of [4Fe-4S] Cluster Assembly on Eukaryotic Mitochondrial and Cytosolic Aconitase. *Inorg. Chem.* **58**, 13686–13695 (2019).

78. Roland, M. *et al.* The plastidial Arabidopsis thaliana NFU1 protein binds and delivers [4Fe-4S] clusters to specific client proteins. *J. Biol. Chem.* **295**, 1727–1742 (2020).

79. Azam, T. *et al.* [4Fe-4S] cluster trafficking mediated by Arabidopsis mitochondrial ISCA and NFU proteins. *J. Biol. Chem.* **295**, 18367–18378 (2020).

80. Azam, T. *et al.* The Arabidopsis Mitochondrial Glutaredoxin GRXS15 Provides [2Fe-2S] Clusters for ISCA-Mediated [4Fe-4S] Cluster Maturation. *Int. J. Mol. Sci.* **21**, 9237 (2020).

81. Gourdoupis, S., Nasta, V., Calderone, V., Ciofi-Baffoni, S. & Banci, L. IBA57 Recruits ISCA2 to Form a [2Fe-2S] Cluster-Mediated Complex. *J. Am. Chem. Soc.* **140**, 14401–14412 (2018).

82. Booker, S. J., Cicchillo, R. M. & Grove, T. L. Self-sacrifice in radical S-adenosylmethionine proteins. *Curr. Opin. Chem. Biol.* **11**, 543–552 (2007).

83. Camponeschi, F., Muzzioli, R., Ciofi-Baffoni, S., Piccioli, M. & Banci, L. Paramagnetic 1H NMR Spectroscopy to Investigate the Catalytic Mechanism of Radical S-Adenosylmethionine Enzymes. *J. Mol. Biol.* **431**, 4514–4522 (2019).

84. Banci, L. *et al.* Anamorsin Is a [2Fe-2S] Cluster-Containing Substrate of the Mia40-Dependent Mitochondrial Protein Trapping Machinery. *Chem. Biol.* **18**, 794–804 (2011).

85. Inubushi, T. & Becker, E. D. Efficient detection of paramagnetically shifted NMR resonances by optimizing the WEFT pulse sequence. *J. Magn. Reson.* **51**, 128–133 (1983).

86. Ciofi-Baffoni, S., Gallo, A., Muzzioli, R. & Piccioli, M. The IR-15N-HSQC-AP experiment: a new tool for NMR spectroscopy of paramagnetic molecules. *J. Biomol. NMR* **58**, 123–128 (2014).

87. Fontecave, M., Ollagnier-de-Choudens, S. & Mulliez, E. Biological Radical Sulfur Insertion Reactions. *Chem. Rev.* **103**, 2149–2166 (2003).

88. Broderick, J. B., Duffus, B. R., Duschene, K. S. & Shepard, E. M. Radical S - Adenosylmethionine Enzymes. *Chem. Rev.* **114**, 4229–4317 (2014).

89. Ewen, K. M., Kleser, M. & Bernhardt, R. Adrenodoxin: The archetype of vertebrate-type [2Fe–2S] cluster ferredoxins. *Biochim. Biophys. Acta - Proteins Proteomics* **1814**, 111–125 (2011).

90. Sheftel, A. D. *et al.* Humans possess two mitochondrial ferredoxins, Fdx1 and Fdx2, with distinct roles in steroidogenesis, heme, and Fe/S cluster biosynthesis. *Proc. Natl. Acad. Sci.* **107**, 11775–11780 (2010).

91. Miller, W. L. Minireview: Regulation of Steroidogenesis by Electron Transfer. *Endocrinology* **146**, 2544–2550 (2005).

92. Freibert, S.-A. *et al.* Biochemical Reconstitution and Spectroscopic Analysis of Iron–Sulfur Proteins. in 197–226 (2018). doi:10.1016/bs.mie.2017.11.034.

93. Fernández, C. O. *et al.* Axial Ligand Modulation of the Electronic Structures of Binuclear Copper Sites: Analysis of Paramagnetic 1 H NMR Spectra of Met160Gln Cu A. *J. Am. Chem. Soc.* **123**, 11678–11685 (2001).

94. Xia, B., Jenk, D., LeMaster, D. M., Westler, W. M. & Markley, J. L. Electron-Nuclear Interactions in Two Prototypical [2Fe–2S] Proteins: Selective (Chiral) Deuteration and Analysis of 1H and 2H NMR Signals from the Alpha and Beta Hydrogens of Cysteinyl Residues That Ligate the Iron in the Active Sites of Human Ferredoxin. *Arch. Biochem. Biophys.* **373**, 328–334 (2000).

95. Machonkin, T. E., Westler, W. M. & Markley, J. L. Paramagnetic NMR Spectroscopy and Density Functional Calculations in the Analysis of the Geometric and Electronic Structures of Iron−Sulfur Proteins. *Inorg. Chem.* **44**, 779–797 (2005).

96. Saudino, G., Suraci, D., Nasta, V., Ciofi-Baffoni, S. & Banci, L. Molecular Basis of Multiple Mitochondrial Dysfunctions Syndrome 2 Caused by CYS59TYR BOLA3 Mutation. *Int. J. Mol. Sci.* **22**, 4848 (2021).

97. Abdul-Hamid M. Emwas, Jasmeen S. Merzaban, H. S. *Applications of NMR Spectroscopy*. (BENTHAM SCIENCE PUBLISHERS, 2015). doi:10.2174/9781608059621115010l.

98. Piccioli, M. Paramagnetic NMR Spectroscopy Is a Tool to Address Reactivity, Structure, and Protein–Protein Interactions of Metalloproteins: The Case of Iron–Sulfur Proteins. *Magnetochemistry* **6**, 46 (2020).

99. Dominguez, C., Boelens, R. & Bonvin, A. M. J. J. HADDOCK: A Protein−Protein Docking Approach Based on Biochemical or Biophysical Information. *J. Am. Chem. Soc.* **125**, 1731–1737 (2003).

100. van Zundert, G. C. P. *et al.* The HADDOCK2.2 Web Server: User-Friendly Integrative Modeling of Biomolecular Complexes. *J. Mol. Biol.* **428**, 720–725 (2016).

101. Hubbard, S. J.; Thornton, J. M. *NACCESS. Department of Biochemistry and Molecular Biology* vol. University (1993).

102. Johansson, C. *et al.* The crystal structure of human GLRX5: iron–sulfur cluster co-ordination, tetrameric assembly and monomer activity. *Biochem. J.* **433**, 303–311 (2011).

103. Šali, A. & Blundell, T. L. Comparative Protein Modelling by Satisfaction of Spatial Restraints. *J. Mol. Biol.* **234**, 779–815 (1993).

104. Case, D.A.; Darden, T.A.; Cheatham, T.E., III; Simmerling, C.L.; Wang, J.; Duke, R.E.; Luo, R.;Walker, R.C.; Zhang,W.; Merz, K. M. . AMBER 12. *Univ. Calif. San Fr. CA, USA, 2012.* **12th ed**,.